Study of hybrid FRP-FRCM superficial structural elements

TESIS DOCTORAL

Thesis by:
Amir Reza Eskenati

Directed by:
Ernest Bernat Maso

Barcelona, April 2023

Universitat Politècnica de Catalunya, BarcelonaTECH
Escola Superior d'Enginyeries Industrial, Aeroespacial i Audiovisual de Terrassa
Departament de Resistència de Materials i Estructures a l'Enginyeria
CATMech - Centre for Advanced Technologies in Mechanics

Ph.D. Thesis

Study of hybrid FRP-FRCM superficial structural elements

Author:
Amir Reza Eskenati

Directed by:
Ernest Bernant Maso

Tesi presentada per obtenir el títol de Doctor per la Universitat Politècnica de Catalunya

Programa de doctorat d'Anàlisis Estructural. Departament de Resistència de Materials i Estructures a l'Enginyeria
Escola Superior d'Enginyeries Industrial, Aeroespacial i Audiovisual de Terrassa. Universitat Politècnica de Catalunya, BarcelonaTECH

Terrassa, April 2023

Abstract

Nowadays, composite materials have been increasingly used to produce hybrid structures together with concrete. This system is commonly applied to bridges and roof structures. In parallel, the most common composite materials for strengthening building structures are divided into two different types based on the matrix's composition, organics (polymers) or inorganics (cement, lime). The hybrid structures presented herein for the first time are made of two components; fabric-reinforced cementitious matrix (FRCM) composite and pultruded fiber reinforced polymer (FRP) profiles.

The main idea of the experimental research was to characterize the individual materials and the structural behavior of FRP profiles - FRCM hybrid superficial elements. This research makes an attempt to design a hybrid element which would be able to benefit from the great advantages of FRP profiles and the adaptability of FRCM material to overcome some of the disadvantages of FRP like superficial adaptability or the flexibility to allow little terrain movements. The experimental campaigns and numerical studies consist of three parts; materials individual characterization, connection between materials (FRP-FRP, FRP-Mesh and Mesh-Mortar) and characterization of the full hybrid superficial elements using the best combination from the previous tests.

In terms of FRP-FRP connection tests, the mechanical behavior of adhesively and bolted joints for pultruded Glass FRP (GFRP) profiles has been experimentally addressed and numerically modeled. A total of nine specimens with different configurations (bolted joints, adhesive joints, web joints, web and flange joints, and two different angles between profiles) were fabricated and tested, extending the available published information. The novelty of the research is in the direct comparison of joint technologies (bolted vs. adhesive), joint configuration (web vs. flange + web) and angles between profiles in a comprehensive way. Plates for flange joints were fabricated with carbon fiber FRP. Experimental results indicate that adding the bolted flange connection allowed for a slight increase of the load bearing capacity (up to 15%) but a significant increase in the stiffness (between 2 and 7 times). Hence, it is concluded that using carbon FRP bolted flange connection should be considered when increasing the joint stiffness is sought. Adhesively connections only reached 25% of the expected shear strength according to the adhesive producer if comparing the numerically calculated shear strength at the failure time with the shear strength capacity of the adhesive. Apart from assessing adhesive connections, the implemented 3D numerical model was aimed at providing a simplified effective tool to effectively design bolted joints. Although the accurate fitting between experimental and numerical results of the mechanical response, especially the stiffness of the joint, the local failure experimentally observed was not automatically represented by the model, because of the simplified definition of the materials oriented to make the model available for a wide range of practitioners.

In FRP-Mesh connection tests part, four specimens with different materials (resin connection, bolted connection) were made and tested. Moreover, the effect of high temperature was evaluated. To sum up, the best connector is resin connection and high temperature has low effect on the resistance of the specimen with resin connector.

Regarding to the Mesh-Mortar connection tests, four specimens were made with FRCM (2 types of mortar) using glass fiber mesh and tested under tensile configuration in order to investigate the behavior of the mesh and mortar. Glass fiber mesh led to increase ultimate load and strain. Two types of mortar were used; an autolevelling one and a repair one. Axton mortar had better behavior under tensile test in comparison with Sika. Moreover, high temperature had significant effect on tested specimens.

The main idea of full hybrid panels was to extend this approach by replacing the concrete with a fabric-reinforced cementitious matrix (FRCM) composite, resulting in a combination of composite materials. The main aim was to characterize the structural behavior of fiber-reinforced polymer (FRP) profiles and FRCM hybrid superficial elements. Two different prototypes of the hybrid superficial structural typology were tested to cover bidimensional (HP1) and three-dimensional (HP2) application cases of the proposed technology. After mortar cracking, the experimental results revealed a ductile response and a high mechanical capacity. A finite element model was implemented, calibrated, and validated by comparing numerical data with experimental results of the two prototypes. The output was a validated model that correctly captured the characteristic response of the proposed technology, which consisted of changing the structural response from a stiff plate configuration to a membrane type due to cracking of the FRCM composite part of the full solution. The suggested numerical model adequately reflected the experimental response and proved valuable for understanding and explaining the resistive processes established along this complicated FRP-FRCM hybrid structure. The proposed numerical models accurately represented the experimental response with fewer than 10% difference. In HP2, the force at the end of loading reaches a value of approximately 5kN in the numerical model and experimental specimen. However, the difference in last force between the numerical model and the experimental specimen is more than 40% because experimental test stopped before due to limitations in the deformation application tooling.

Keywords: FRCM; pultruded FRP profile; hybrid element; numerical simulation; experimental tests

Resumen

Actualmente, el uso de materiales compuestos para la fabricación de estructuras híbridas junto con el hormigón se ha incrementado. Este sistema estructural es comúnmente aplicado en puentes y techados. En paralelo, los materiales compuestos para el refuerzo de estructuras más habituales se dividen en dos tipos según la composición de la matriz: orgánicos (polímeros) e inorgánicos (cemento, cal). Las estructuras híbridas que se presentan aquí por primera vez están compuestas a su vez por dos materiales compuestos: una matriz cementítica reforzada con tejidos (Fabric Reinforced Cementitious Matrix – FRCM) y perfiles pultrusionados de polímero reforzado con fibras (Fibre Reinforced POlymer – FRP).

El principal objetivo de la investigación experimental era caracterizar los materiales individualmente y el comportamiento estructural de los elementos superficiales híbridos de perfiles de FRP y FRCM. Esta investigación persigue diseñar un elemento híbrido que sea capaz de aprovechar los beneficios de las grandes ventajas de los perfiles FRP y la adaptabilidad del FRCM para superar ciertas limitaciones del FRP como la adaptabilidad superficial o la flexibilidad para asumir movimientos del terreno. Las campañas experimentales y los estudios numéricos se dividen en tres partes: caracterización individual de los materiales, estudio de la conexión entre materiales (FRP-FRP, FRP-malla y malla-mortero) y caracterización de elementos superficiales híbridos a escala real que combinen las mejores opciones resultantes de los anteriores ensayos.

Respeto a los ensayos de la conexión FRP-FRP, el comportamiento mecánico de uniones adhesivas y atornilladas de perfiles pultrusionados de FRP de vidrio (GFRP) ha sido estudiado experimentalmente y simulado numéricamente. En total, nueve especímenes con diferentes configuraciones (uniones atornilladas, uniones adhesivas, uniones del alma, uniones de alas y alma, y dos ángulos diferentes entre perfiles) fueron fabricados y ensayados, extendiendo la información publicada disponible. La novedad de la investigación en este punto está en la comparación directa de diferentes tecnologías de unión (atornillada vs. adhesiva), configuraciones de unión (alma vs. alma + alas) y ángulos entre perfiles de un modo exhaustivo. Las placas para las uniones de las alas se produjeron con FRP de fibra de carbono. Los resultados experimentales indican que añadir la unión atornillada en el ala supone un ligero aumento de la capacidad de carga (hasta un 15%) pero un gran aumento de la rigidez (de 2 a 7 veces). Por lo tanto, se concluye que usar la conexión atornillada de las alas de una placa de FRP de carbono debe considerarse cuando se busca aumentar la rigidez de la unión. Las uniones adhesivas únicamente alcanzaron un 25% de la resistencia a cortante prevista en el momento del fallo si comparamos la resistencia calculada de los ensayos con la prevista por las simulaciones. Además de para evaluar las uniones adhesivas, el modelo numérico 3D implementado estaba orientado a ser una herramienta simplificada y efectiva para el diseño de uniones atornilladas. En este sentido, a pesar de que los resultados numéricos y experimentales muestran un elevado grado de similitud, especialmente en lo relativo a la rigidez de la unión, el tipo de fallo local observado experimentalmente no es automáticamente

representado por el modelo numérico debido a la simplificación en la definición de los materiales que se planteó para hacer este modelo accesible al mayor número de usuarios posibles.

En el apartado sobre la conexión FRP-malla, cuatro espeímenes con diferentes materiales (unión adhesiva con resina y unión atornillada) se fabricaron y ensayaron. Además, el efecto de las altas temperaturas también fue estudiado. En resumen, la mejor conexión resultó ser la adhesiva mediante resina y las elevadas temperaturas probaron no tener un efecto significativo en la resistencia de los especímenes con conectores adhesivos con resina.

En relación a los ensayos de conexión malla-mortero, se fabricaron 4 especímenes con FRCM de fibra de vidrio (2 tipos de mortero) y se ensayaron bajo una configuración de tracción para investigar el comportamiento de la malla y el mortero. La malla de fibra de vidrio permitió incrementar la carga y deformación respecto la alternativa de carbono. De los dos tipos de mortero usados (autonivelante y de reparació), el Axton demostró un mejor comportamiento a tracción. En todos los casos de FRCM se detectó un efecto significativo de la exposición a elevadas temperaturas.

La principal idea de los paneles híbridos a escala real era extender la aproximación de las estructuras híbridas actuales, pero reemplazando el hormigón por la matriz cementítica reforzada con tejido (FRCM), resultando en una combinación de materiales compuestos. El principal objetivo de la investigación era caracterizar el comportamiento estructural de los elementos superficiales híbridos de FRP y FRCM. Dos prototipos de este sistema estructural híbrido fueron fabricados y ensayados para cubrir los casos de aplicación bidimensional y tridimensional. Después de la fisuración del mortero, los resultados experimentales mostraron una respuesta dúctil y una elevada capacidad mecánica. Un modelo numérico fue implementado, calibrado y validado por comparación de los datos numéricos con los experimentales de los dos prototipos. El resultado fue un modelo numérico, correctamente validado y que capturaba la respuesta característica de la tecnología propuesta, la cual consistió en cambiar el comportamiento de un tipo placa rígida a una configuración de tipo membrana debido a la fisuración del compuesto FRCM en la solución completa. El modelo numérico propuesto reflejaba la respuesta experimental de forma adecuada y demostró ser valioso para el conocimiento y la explicación de los mecanismos resistentes desarrollados por la compleja estructura híbrida de FRP-FRCM. En particular, los modelos numéricos propuestos capturan la rigidez del sistema con un error menor al 10%. En el caso del prototipo 3D (HP2) la capacidad de carga alcanzó 5kN para ambas evidencias, experimentales y numéricas representando el ensayo. No obstante, la diferencia en la capacidad de carga máxima prevista por la simulación diferió más de un 40% con la experimental que se vio limitada por la capacidad de aplicar desplazamientos durante el ensayo.

Publications

A. R. Eskenati, A. Mahboob, E. Bernat-Maso, and L. Gil, “Characterizing the Structural Behavior of FRP Profiles—FRCM Hybrid Superficial Elements: Experimental and Numerical Studies,” Polymers, vol. 14, no. 6. 2022, doi:10.3390/polym14061076.

A. R. Eskenati, A. Mahboob, E. Bernat-Maso, and L. Gil, “Experimental and Numerical Study of Adhesively and Bolted Connections of Pultruded GFRP I-Shape Profiles,” Polymers (Basel)., vol. 14, no. 5, p. 894, Feb. 2022, doi: 10.3390/polym14050894.

Acknowledgements

In the beginning, I am going to give special thanks to Dr. Ernest Bernat Maso who is my supervisor of my thesis, permitting me to work and research under his guidance and he supported and helped me over three educational years.

I am extremely thankful to the Polytechnic University of Catalonia and the Laboratory for Technical Innovation in Structures and Materials (LITEM) for providing all facilities for me to pursue my PhD.

Furthermore, I would like to thank to Prof. Lluís Gil and my colleagues Virginia, Borja, Javi, and Amir Mahboob – for their invaluable assistance in the execution of this work, as well as the great times we spent.

Ultimately, I am going to convey my heartfelt thanks to my family for their unwavering support and encouragement in helping me to achieve my goals.

Table of Contents

Table of tables

Table of figures

1

Introduction

1.1 Context and motivation

The main part of civil engineering operations, especially in developed countries, has become maintenance of a significant part of current infrastructures and structures. Over the current century, many significant studies have done to investigate durability, conservation, and environmental considerations. The usage of new and updated materials has been always considered and applied in construction and building projects in order to build structures and infrastructures with high efficiency. Fiber reinforced polymer (FRP) and fiber reinforced cementitious matrix (FRCM) are composite material. The effectiveness of these materials is proved by many civil engineers due to many benefits, including their high strength, easy installation, lower shipping costs, enhanced durability, and low maintenance needs.

Over the last decades, pultruded FRP profiles and textile reinforced mortar (also known as FRCM) have remained popular among composites due to many advantages in comparison with other materials. Nonetheless, many scientists have tried to explore for new methods that might better leverage the material's features.

The hybrid kind of element, mixing two main components, pultruded FRP profiles with cheap cost and textile reinforced mortar with high durability, is one of the unique possibilities. Hybrid FRP profile-concrete structures are normally made out of a concrete compression section that is mechanically attached or adhesively coupled to a FRP composite form that is largely in tension.

Overall, hybrid structures using pultruded FRP profiles and concrete have already been studied and have started to be applied as commercial solutions. On the other hand, the FRCM system is widely used as a strengthening solution. In addition, the FRP-concrete connection method proposed by Mahboob et al. (Mahboob *et al.*, 2021b) opened the door to future FRP-FRCM hybrid structures technology. However, as per authors knowledge, there are no published references that suggested combing pultruded FRP profiles and FRCM to produce structural superficial elements so far. The possible range of application of these hybrid structures may include urban elements, tunnel sustainment or thin roofing systems. Thus, the main objective of the current work is to

describe and to characterize the structural behavior of this new structural system composed by FRP profiles and FRCM. Experimental tests and numerical simulations have been used with this aim.

1.2 Aim and objectives

The main objective of this thesis is to characterize the structural behavior of FRP profiles - FRCM hybrid superficial elements. In particular, the first general goal is the development and study of different connection solutions: between FRP profiles and between FRP and FRCM using experimental, analytical and numerical methods. The second general goal is producing, testing and analyzing the structural response of a full hybrid panel, also including experimental and numerical models.

In order to achieve these two general aims, the following partial objectives were defined with their related activities:

1) To find, to order, to review and to present the existing information that supports the current research interest and necessity. Related activities are:

- Review FRCM strengthening solutions and FRP-concrete hybrid structures as closer existing technologies
- Review previous strengthening solutions, mostly oriented to FRCM and GFRP (Glass Fiber Reinforced Polymer) profile investigations in this field.
- Evaluate the guides and codes on the matter being aware on the recent publications.

2) To design, to execute and to analyze the results of an experimental campaign to characterize the mechanical properties of the component materials for the intended structural solution. Related activities are:

- Perform an extensive series of characterization tests on the GFRP and FRCM materials.
- Report and compare with existing literature.

3) Characterizing and simulating FRP-FRP, FRP-Mesh and Mesh-Mortar connections. Related activities are:

- To design, plan, execute and analyze experimental tests on FRP-FRP, FRP-Mesh and Mesh-Mortar interactions.
- To simulate previous interactions in detail with a finite element model in order to state the required simplifications for the modelling of full hybrid structures including all these interactions.

4) To design, to execute and to analyze the results of an experimental campaign to characterize the mechanical response of superficial structures composed by FRP profile and FRCM defined by

different connection solutions. In particular, it is intended to study the FRCM-FRP profile connection. Related activities are:

- Conduct an out-of-plane bending test to evaluate the composite response of the hybrid structure.
- Trial initial numerical models with a low level of complexity to better understand the influence of material, connection typology and geometry characteristics.
- Carry out nonlinear finite element simulations on full hybrid elements and validate the obtained results against experimental data.

The scope of the research work presented in this research is limited to the structural behavior of hybrid FRP-FRCM profiles superficial elements. The composite structure is expected to behave elastically up to the FRCM cracking when its typical nonlinear constitutive law will represent the problem. Large scale simulations or detailed micromodels on full-scale panels are discarded from the research scope.

1.3 Research methodology

The research is organized by complementary experimental and numerical researches. The main idea of the experimental research is to characterize the individual materials, their connections and the structural behavior of FRCM-FRP hybrid superficial elements. This research tries to design hybrid elements which have to be able to benefit from the great advantages of FRP profiles and the adaptability of FRCM material to overcome some of the disadvantages of FRP like superficial adaptability and excessive stiffness. Experimental tests are conducted to define the structural behavior of component materials, composites and hybrid elements are made from different composites (FRCM and FRP profiles). The experimental campaign consists of three parts; materials individual characterization, experimental study of the connection between materials (GFRP-GFRP, FRCM-FRP profile, Fabric-mortar) and characterization of the hybrid superficial elements using the best combination from the previous tests.

With the aim of enhancing the applicability of the expected results numerical simulations are carried out. In these numerical studies, several three-dimensional models including FRP-FRP connection, mesh-mortar connection and full hybrid panels are carried out by defining materials, interface contact, boundary conditions and load. To test their accuracy, the numerical models are validated with the experimental data based on simplified assumptions.

Regarding the methodology on numerical development, the following tasks are carried out:

Firstly, the existing simulation models for the calculation of hybrid structures and FRCM strengthened structures are analyzed to establish the variables to be experimentally determined through the tests according to the needs of the most widely used models.

Secondly, detailed models on components' interaction (joints between FRP profiles or FRCM-FRP connection) are defined and adjusted with experimental test.

Finally, two simplified micro-model to represent hybrid FRCM-FRP profile superficial structural elements are implemented and adjusted with the experimentally obtained data of two full scale hybrid panels.

1.4 Document outline

There are seven chapters and two appendices in this thesis; the content of each chapter is summarized in the following paragraphs.

Chapter 1. Introduction

The first chapter describes the present work subject and explains the information to contextualize the research. The specific objectives of this study, the general description of the methodology and the expected outcomes are included in this chapter.

Chapter 2. State of the art

The preliminary description of FRP and FRCM materials with details of their manufacture, characteristics and applications in civil engineering is given in the second chapter. This section also deals with the existing information regarding the application of FRP as strengthening solution and the application of FRP as hybrid system together with concrete. It also includes detailed information on FRP pultruded profiles and FRP connections. The application of FRCM as strengthening system is also considered. Finally, this second chapter gathers the experimental and numerical studies which have been published on the previously mentioned topics in recent years.

Chapter 3. Experimental characterization of materials and connections

In this chapter, the properties of all used materials in experimental study are summarized. The description of all experimental specimens which are made and tested at the laboratory has been included. This section starts with the explanation of the material definition and follows with the experimental characterization tests for FRP-FRP, FRP-Mesh and Mortar-Mesh connections. All experimental conditions, testing procedure and experimental results are discussed as main part of this chapter.

Chapter 4. Experimental characterization of full hybrid panels

This chapter describes all experimental conditions and testing procedures of full hybrid panels. Results are analyzed in terms of force-displacement curves, strength, deformability and failure modes supported by the photos of specimens before and after test.

Chapter 5. Numerical modeling of experimental characterization tests of connections

Chapter 5 represents the use of a finite element method for simulation of experimental characterization tests. To be more precise, the chapter describes several models of FRP connections and FRCM composites. The definition of all used materials, the contact between all parts, boundary condition and loads and chosen method to solve models are clearly described in appendix B of the thesis. The validation of numerical data is checked by experimental results.

Chapter 6. Numerical modeling of full hybrid panels

Chapter 6 describes the numerical modeling of two full hybrid panels. All processes and hypothesis for simulating full hybrid panels are described in details. The comparison plot between experimental results and numerical outputs for full hybrid panels and contour plots for stress distribution and displacement are analyzed in this chapter to discuss about the performance of the hybrid system.

Chapter 7. Conclusions and outlook

The final chapter summarizes the key research results and suggests various subjects for future research.

2

State of the art

2.1 Introduction

These days, novel materials are used in structure and infrastructure systems around the world and these materials can revolutionize the construction industry. New tools and updated methods are needed to sustain the structures and infrastructures incorporating these new materials.

The most common composite materials for strengthening building structures are divided in two different types based on the matrix's composition, organics (polymers) or inorganics (cement, lime). Among others, the usual types of composite material are fiber reinforced polymer (FRP) and fabric reinforced cementitious matrix (FRCM) for organic and inorganic types respectively (Estevan *et al.*, 2020). FRP materials provide many benefits over more conventional reinforcement methods, such as high strength-to-weight ratio, relative simplicity and fast installation, cost effectiveness and high durability. FRCM are sometimes favored over FRP systems depending on working conditions such as high-temperature or high-humidity environments and these are preferred for masonry applications because of their mechanical, chemical and physical compatibility (Donnini, Spagnuolo and Corinaldesi, 2019).

2.2 FRP

Fiber reinforced polymer (FRP) is a composite material. This material is made of a polymer matrix reinforced with fibers. FRPs have different applications on construction and building system. One type of FRP products is FRP profile. The most important application of FRP profile is producing new structures such as hybrid elements.

FRP has been employed to reinforce and to strengthen concrete structures and members. Low weight, high strength-to-weight ratio, high levels of stiffness, chemical resistance, fast installation and increased durability can be named as advantages of FRP products (Reichenbach *et al.*, 2021). The usage of FRP product can be useful for a long period and effective in strengthening of

structures (Ye *et al.*, 2021). Figure 1 presents several types of FRP used in structure and infrastructures system.

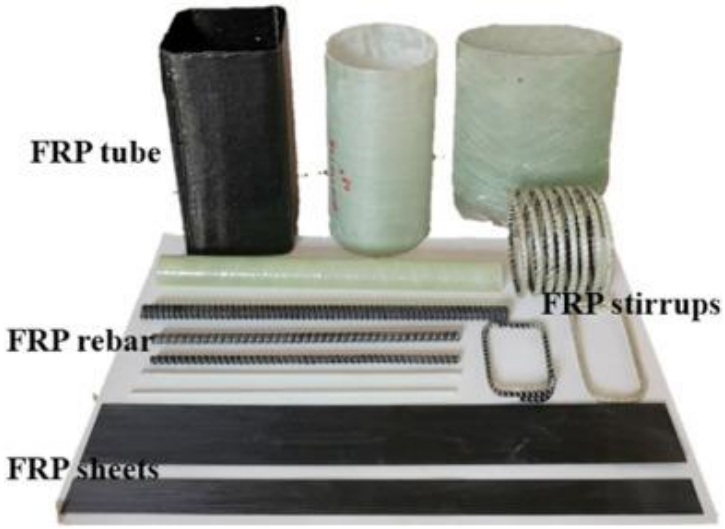

Figure 1. FRP composites used in structure and infrastructures system (Ye *et al.*, 2021)

Fiber Reinforced Polymer (FRP) profiles obtained with the pultrusion technique represent a product with interesting properties of durability and lightness, but also, economic if the glass fibers are used. On the other hand, these benefits are coupled with a structural behavior completely different from that of steel profiles traditionally used in civil engineering, making the well-known design rules and models totally invalid for the FRP profiles which are limited to the elastic response (Vedernikov *et al.*, 2020). Figure 2 shows the GFRP profile.

Figure 2. GFRP Profile (Neagoe, 2016)

FRP profiles have a lot of benefits in many terms such as strength, corrosion resistance, chemical resistance, electrical insulation, weight and lightness (Neagoe, 2016).

- Low weight: low transportation cost, easy transfer and sample installation.
- High carrying capacities: superior tensile, tilting and compressing values per weight in comparison with steel.
- Resistant to corrosion not rusting or rotting.
- Electrical conductivity: safety working.
- Low thermal conductivity: providing very good insulation.
- Dimensional stabilizations: not stretching or shrinking.
- Not magnetic: being used in sensitive places.
- Resistant to UV rays: not deforming.
- Being processed in a simple way: being cut with simple carpenter tools.
- Not requiring paint or maintenance: being cleaned easily with pressurized water.
- Being manufactured in all sorts of colors: being produced in the desired color.
- Long life: not experience deformation.
- Light transmittance properties: being used in applications where light transparency is desired.
- Increase chemical and combustion resistance: Special types of resins and chemical additives can provide improved corrosion resistance and combustion resistance.

However, these structural elements have also some drawbacks:

- high initial application costs.
- relatively high manufacturing costs.
- lack of specific national design codes.

2.1.1 FRP profile applications in civil engineering

FRP profiles have a wide range of applications due to their superior structural properties;

- Water and wastewater treatment plants.
- Chemical plants.
- Food facilities.
- General production facilities.
- Electricity distribution applications.
- Marine applications & shipyards.
- Coastal and scaffold applications.
- Architecture and building applications.
- Home and garden applications.

- Public and commercial applications and they can be used in special applications.

Example types of applications:

Figure 3 represents the example type of FRP profile applications.

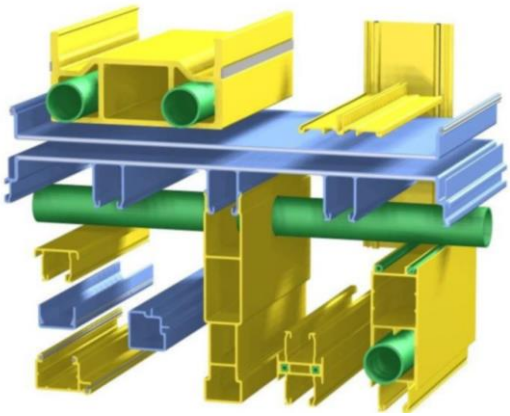

Startlink test home modular pultruded FRP concept profiles(Qureshi, 2022)

Hybrid bridge (Alocci and Valvo, 2019)

Staircase frame (PermaStruct, 2020)

Structural beams (Francesca and Salvatore, 2016)

Figure 3. The example of FRP profile applications

2.1.2 FRP-FRP Connections

In the mid-1960s, the research of FRP connections characterization (particularly mechanical connections) began in the aerospace sector in the United States, when there was a need to establish a good design for connections. The typical plastic design technique, which has been employed in bolted connections in some materials including steel, aluminum, and other ductile materials, is inapplicable to FRP connections with brittle behavior. Furthermore, utilizing linear elastic analysis

is not acceptable because to the significant strength increase caused by tiny micro failure in the intermediate area of small bolt holes (Hart-Smith, 1987). Currently, several guidelines and codes for FRPs, including design requirements for FRP connections like European standard polymeric Composites Group (EUROCOMP), BD 90/05 standard and Design guide for FRP connection written by Mosallam, are being developed based on research effort (Mosallam, 2011).

Through developing information on FRP interactions, it is anticipated that the processing and usage of FRP as a modern material with anisotropic properties would become simpler for various purposes. Most of the time, FRP elements and particularly structural pultruded appear to be similar to steel profiles and the connection between these elements appears to be similar to the steel connections. At the first glance, it can be found that FRP associations are identical to steel components as a whole through the analysis, but there are major variations between them (Khani, 2015).

Liu et al. (Liu *et al.*, 2021) evaluated the resistance and ductility of FRP composite hybrid joints; adhesively-bonded and bolted connection. There was a significant increase in joint resistance and deformation capacity due to bolted joints with multidirectional (MD) fiber architecture. The deformation capacity of bonded and bolted connection did not decrease, whereas ultimate cracking load enhance markedly in these connections.

Qureshi and Mottram (Qureshi and Mottram, 2013) carried out and investigated behavior of pultruded beam-to-column joints using steel web cleats under physical testing. Experimental results demonstrated significant increase in rotational stiffness and moment capacity on joints with FRP members. Figure 4 shows the delamination fracture at two web-flange junctions of column section.

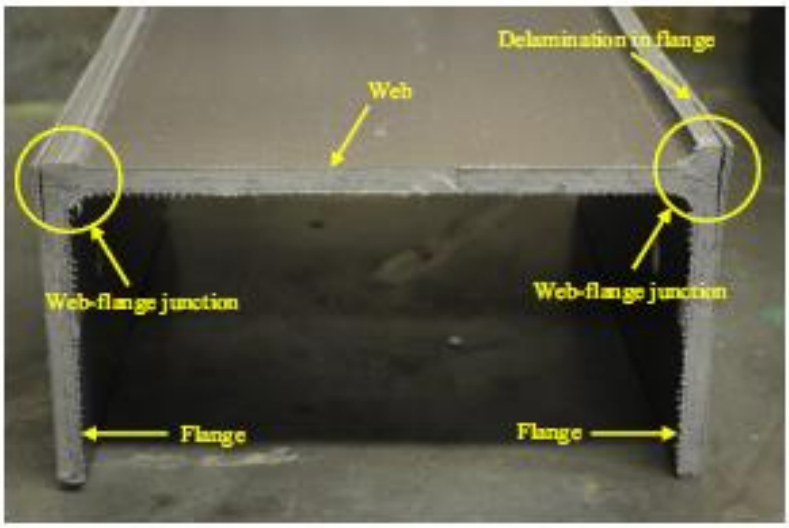

Figure 4. Internal fracture pattern in column section (Qureshi and Mottram, 2013)

Si Larbi et.al (Si Larbi *et al.*, 2007) investigated the static and instantaneous behavior of connections in composite beam bridges under push-out tests. The bonded connections reveal strong stability and strength, being equal to mechanical connectors. Additionally, they showed epoxy joints had an elastic behavior up to brittle failure.

EUROCOMP (Wood, 1996) represents the classified FRP connections which are sorted in three categories as follow (Khani, 2015):

- Primary structural connection.

- Secondary structural connection.

- Non-structural connections.

And additionally, joint categories have been separated in three groups as:

- Mechanical connection.

- Bonded or adhesive connection.

- Combined connection.

Joint categories and joint technique

A general summary of various styles of connections will be presented in this section and each typology will be described in more specifics in the following paragraphs.

As it was mentioned before, the EUROCOMP code has classified FRP connection into three groups as:

- Mechanical connection.

- Bonded or adhesive connection.

- Combined connection.

The mechanical connection such as bolts, rivets, contact strap and embedded fasteners are known as shear loaded fasteners or axially loaded fasteners (EUROCOMP). In the middle of 1960s, an study represented the types of mechanical joints in aerospace industry for the first time (Mosallam, 2011).

The most popular type of connection in FRP material is bonded connection. In general, adhesive joints transmit the load as shear force. Adhesive connections have lower stress concentration than bolted connection (Mosallam, 2011).

The third category of connections is a mixture of the first two groups depending on the EUROCOMP categorization and it was called as mixed connections. These merged joints are classified as bonded-bolted joints. It is predicted that a higher mechanical efficiency will be achieved by integrating these two processes. This kind of connection should have greater stiffness, strength and fatigue resistance in comparison with other connections. It is suggested nonlinear modelling techniques to be considered, due to analysis and design of combined joint is very complicated (Mosallam, 2011).

The Table 1 shows a comparison of three joining methods and typical joint configurations are shown in Figure 5 (Wood, 1996).

Table 1. General characterization of different connections (Wood, 1996)

Characteristic	***Mechanical***	***Adhesive***
Stress concentration at joint	*High*	*Medium*
Stress to weight ratio	*Low*	*Medium*
Use with non-rigid polymer	*Inserts required*	*Yes*
Seals assembly (water tightness)	*No*	*Yes*
Thermal or electrical insulation	*No*	*Yes*
Attractiveness	*Bad*	*Good*
Fatigue endurance	*Bad*	*Good*
Sensitive to peel loading	*No*	*Yes*
Disassembly	Possible	Impossible
Inspection	Easy	Difficult
Skill required fabricator	Low	High
Heat or pressured required	No	Yes
Tooling cost	Low	High
Time to attain ultimate strain	Instantaneously	Long

Bonded connections

Bonded connections are rarely used in civil engineering industry. The bonded connections such as adhesive bonded joints, laminated joints, molded joints, bonded insert joints and cast in joints are grouped and explained in EUROCOMP guideline. One of the most usual connections is adhesive connection in FRP material (Mosallam, 2011). Some environmental conditions, time, a heated environment, clamps, and, in certain cases, an autoclave are required to use the adhesive joining technique. As a result, employing these types of connections is uncommon and challenging in civil infrastructures. To achieve a suitable bonded connection, several aspects such as selecting the correct adhesive, surface preparation, adhesive type, adhesive thickness, proper clamping conditions, and fitting the adhesive with adherent should be taken into account (Khani, 2015)

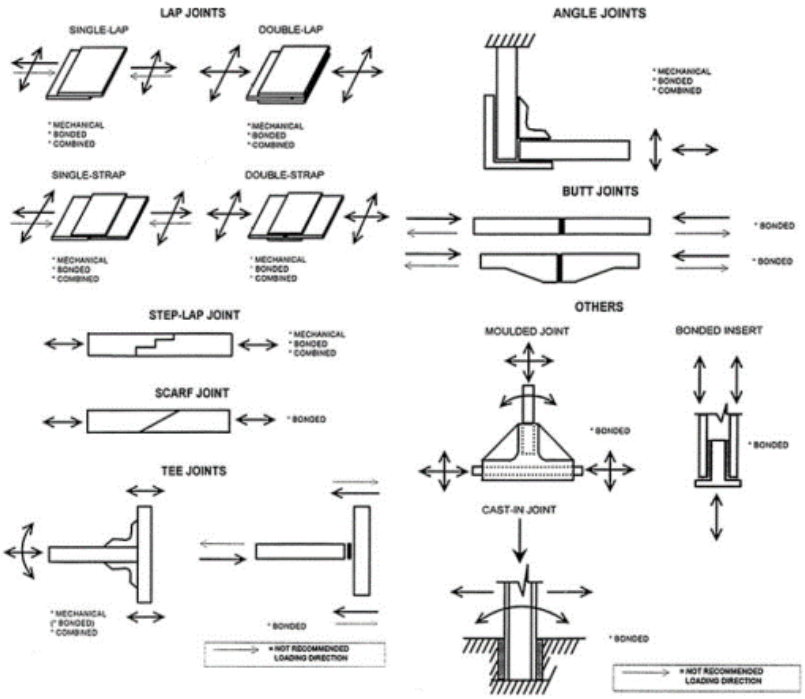

Figure 5. FPR joint configurations (Wood, 1996)

In fact, the adhesive joints transmit loads as shear forces when connecting parts. In adhesive connection, the stress concentration is less significant than in bolted and other mechanical links. When using brittle adhesives, the catastrophic failure or brittle failure is expected. Hence, a ductile adhesive is required. Adhesive bonding needs special care and is often prone to environmental factors. The system cannot be loaded immediately after the adhesive has been used, so the adhesive content requires a certain period of time for chemical reactions. These forms of interactions are often prone to temperature and humidity (Mosallam, 2011).

For the first time, Smith et al. published the results of an experimental study proving the performance of their suggested novel T-shape monolithic connection, dubbed "cuff," in the year of 1999. They resulted in a significant increase in joint stiffness (90%) and strength (330%) over standard seat angle connections used to join GFRP I-beams and columns previously (Smith, Parsons and Hjelmstad, 1999). F.Ascione et. al have carried out the experimental study of adhesively bonded connections between pultruded I-profiles in order to illustrate the structural efficiency of the epoxy adhesive. Experimental findings reveal that adhesive connections are clearly capable of performing as well as or better than bolted connections (Ascione *et al.*, 2017). The brittle failure of the epoxy attaching the parts is a significant drawback of the adhesive connection, limiting the deformability of framed GFRP constructions. To address this limitation, the authors developed a modified connection that includes enclosing some elements of the connection with carbon FRP laminate. The reinforced connection displayed a pseudo-ductile load-deflection response (Ascione *et al.*, 2018). In numerical and experimental studies, Zhang et. al recommended the bonded sleeve beam-column connection and demonstrated a ductile failure

mode under static load. Comprehensive finite element analysis and experimental research are intended to describe the effective role of bonded sleeve beam-column connection in initial rotational stiffness (Zhang, Bai and Xiao, 2018).

Bolted connection

The mechanical connection such as bolts, rivets, contact strap and embedded fasteners are known as shear loaded fasteners or axially loaded fasteners (EUROCOMP). The bolted connection is the most prevalent type of mechanical connecting for FRP materials and is one of the best types of mechanical joining for FRP materials. FRP trusses, beams, and braced frame structures, as well as multicellular FRP bridge deck systems, have all utilized this type of connection (Zoghi, 2013).

The failure modes in FRP bolted connections and steel connections are approximately the same, but the mechanisms of damage and failure initiation and propagation are fundamentally different. Even with FRP material, mechanical connection failure is not abrupt, and this is one of the goals and benefits of employing mechanical connections; in other words, mechanical connections are recognized for providing early warning of failure (Khani, 2015).

Mottram and Zheng (Mottram and Zheng, 1999) tested three full-sized beam-to-column connections including pultruded FRPs with steel flange cleat as a first approach to FRP connection technology. In another study, Qureshi and Mottram (Qureshi and Mottram, 2013) demonstrated significant increase in rotational stiffness and moment capacity on joints with FRP members. Feo et al.(Feo, Marra and Mosallam, 2012) investigated the shear behavior of bolted composites using numerical methods to evaluate the distribution of shear stress between the bolts; the number of rows and the number of bolts were variable. The numerical results showed the load was not uniformly divided in multi-bolt joints. Moreover, the pressure washers had positive effect on stress distribution. Lee et.al (Lee, Choi and Yoon, 2015) investigated the mechanical behavior of pultruded fiber reinforced polymer (PFRP) single bolted connection under tension load. They achieved the hole clearance had not significant effect. Bank (Bank, 2006) discussed FRP profile connections and considered some criteria: stress, load and resistance factor, so it was possible to define limit states. Zhang et al. (Zhang, Vassilopoulos and Keller, 2009) studied the fatigue response of adhesively-bonded pultruded connections subjected to different environmental conditions including temperature and moisture. Similarly, Wingerde et al. (Van Wingerde, Van Delft and Knudsen, 2003) investigated the fatigue behavior of pultruded FRP profiles joined with bolt connections and resin injection. Regarding Glass FRP, several experimental, analytical and numerical studies (Ascione, Feo and MacEri, 2010), (Turvey and Wang, 2008) were conducted on GFRP connections and the results showed some criteria; fiber orientation, geometric parameters, hole clearance, washer size and connection angle are effective parameters to increase the strength of GFRP connections.

Combined joints

Combined joints are made of combination of two connections; mechanical fasteners and bonded connections that have higher strength qualities than each connection type. Vinson's early study on combined connections in 1989 claimed that the combination of the two connectors can increase the strength of the joint by around 50% more than bolted connections (Khani, 2015).

Apart from these two connection bonded and bolted connections, it is theoretically feasible to mix the two and obtain a combination bolted/bonded connection, referred to as "hybrid" in research (Hart-Smith, 1985) (Kelly, 2005).

Weitzenböck and McGeorge published a chapter belonged to bolt-adhesive joints. They explained their research about this joint, including (1) The bolted and bonded parts may create a connection for forces coming from various directions, in which case each component is uniquely constructed to handle the loads corresponding to its load case; (2) Bolts may assist to assure the fire resistance of hybrid connections, but they will not bear weights during service and normal temperature conditions and (3) bolts in hybrid joints may prevent unnecessary difficulties connected to the long-term operation of bonded joints (Weitzenböck and McGeorge, 2011).

Vallée et. al have studied experimental and numerical investigations for hybrid structures including bolted, adhesively bonded between Fiber-Reinforced-Polymers (FRPs). The purpose of this work is to provide practitioners with the uniform dimensioning process for the two most common fastening systems in FRP structures, namely bolted and adhesively bonded connections. Experimental and numerical results showed adhesively bonded, bolted, and hybrid FRP connections failed in a brittle manner (Vallée *et al.*, 2013). They used surface-to-surface elements for defining the contact between bolt and FRP. Kim et. al have investigated mechanical characterization of hybrid bonded-bolted (HBB) joints by using digital image correlation (DIC) technique under the quasi-static tensile loading. The strain areas surrounding the bolt in an HBB connection and the open hole in a bonded joint were precisely compared (Kim *et al.*, 2021). Fu and Mallick have investigated the adhesive/bolted (hybrid) joints in a structural reaction injection molded composite. They resulted the usage of adhesive/bonded connection was more effective than adhesives to join random fiber composite sheets and the principal mode of failure was fiber tearing at the bonded area's ends (Fu and Mallick, 2001).

2.3 FRCM

Fiber Reinforced Cementitious Matrix (FRCM) material is a natural evolution of FRP (fiber reinforced polymer/plastic), which has become widely used as an externally bonded reinforcement of concrete and masonry structures. FRCMs like FRPs have a lot of applications in civil engineering, mostly as strengthening systems.

FRCM is composed of high strength fiber Fabric embedded into a Cementitious Matrix. This definition is shown in Figure 6.

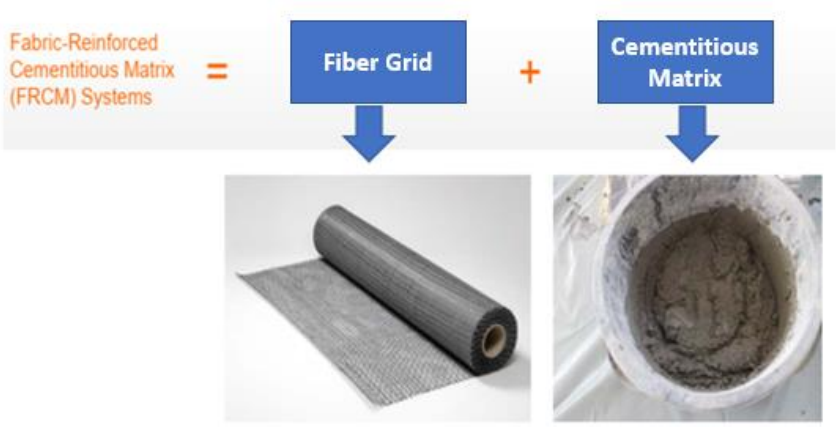

Figure 6. FRCM material

There are some benefits and drawbacks for using FRCM material in construction and building industry. Benefits are: (Sneed, 2013)

- Great stability to high temperature and fire
- UV radiation persistence
- Quick scouring and reuse of instrumentation
- Variable performance time

At the current, fiber reinforced cementitious matrix (FRCM) usage, which is based on the use of fiber reinforcements embedded in a cement-based mortar matrix, may solve the shortcomings noted for FRPs. For the mentioned reasons, FRCM systems are better than FRP systems for reinforcing existing masonry buildings, and they are the preferred choice in many projects (Carozzi *et al.*, 2017).

FRCM shows some benefits in comparison with FRP (Donnini, Spagnuolo and Corinaldesi, 2019) . These are:

- Matches substrate
- Applies on wet surfaces
- Heat resistance of matrix
- Provides protective barrier
- Easier and safer application procedure

2.3.1 FRCM characterization

Many researchers carried out mechanical characterization of FRCM material and its interaction with the strengthened substrate. D'Ambrisi et al. studied the connection between FRCM materials composed of carbon net and poliparafenilenbenzobisoxazole (PBO) net embedded in a cement

matrix (D'Ambrisi, Feo and Focacci, 2013b, 2013a). D'Antino et al. have investigated the interface between matrix-PBO fibers when debonding failure mainly happens. The friction between fiber and matrix is detected (D'Antino *et al.*, 2014). Carozzi and Poggi studies the mechanical characteristics and debonding strength of FRCM used in masonry system. Five different kinds of FRCM materials were investigated, each made up of different types of PBO, carbon and glass fibers, and three different mortars. The experimental findings showed Glass fiber had the lowest mechanical properties (Carozzi and Poggi, 2015). Carrozi et. al conducted the experimental and numerical studies on mechanical properties of Fabric Reinforced Cementitious Matrix (FRCM) systems for strengthening of masonry structures. They resulted that the ultimate strength was determined by the bonded surface and the type of mortar used (Carozzi, Milani and Poggi, 2014). Carvalho Bello et al. examined the efficiency of the Sisal-NFRCM (Natural Fiber Reinforced Cementitious Matrix) by tensile tests aim to investigate the composite's tensile response and the impact of intact mortar among some cracks. The NFRCM material characterization had a significant effect and premature failure did not occur and tensile stress-strain graph illustrated stiffening effect of the mortar between cracks (de Carvalho Bello *et al.*, 2019).

2.3.2 Applications of FRCM in civil engineering

FRCM materials are used as strengthening in concrete and masonry structures. Generally, the concrete members such as beams, slabs or unreinforced masonry walls are strengthened with FRCM in shear and flexure.

FRCM materials are applied as a reinforcement to strengthen structures under a variety of loads, including (Chellapandian and Suriya Prakash, 2021):

- Column confinement
- Flexural reinforcement
- Shear reinforcement
- Torsion and mixed loading reinforcement
- Seismic reinforcement for RC/masonry structures

In the following paragraphs, two applications and case studies of FRCM in civil engineering are mentioned (Chellapandian and Suriya Prakash, 2021):

1. Strengthening San Siro Stadium, Italy

The San Siro stadium, which is placed in Milan, Italy, was built in 1925. In 2002, the building was refurbished with new steel structures that were not linked to the previous reinforced concrete structure as shown in Figure 7. To transfer the increased load to the earth, a new foundation system was installed. A considerable degradation in the RC beam was discovered during the preliminary condition evaluation. Previously, other reinforcing techniques such as concrete coating, steel plate

bonding, and FRP reinforcement were employed. Due to a number of site restrictions and the limited time available to finish the project, such solutions were ruled out. Furthermore, FRCM jacketing was an excellent choice for this repair because no surface preparation was required.

Figure 7. Strengthening San Siro stadium (Chellapandian and Suriya Prakash, 2021)

2. Romanesque Church of San Roque, Spain

The Romanesque Church of San Roque in Spain was built during the old medieval period and was constructed of sandstone, masonry, and wooden materials. During a seismic incident, the church's exterior walls separated out of plane. Furthermore, major fractures in various points of the main vault need reinforcement. Despite the fact that the church remained solid under live loads, a few isolated areas were severely broken. To prevent the creation of additional cracks and the expansion of the existing longitudinal fracture, the FRCM system was fitted to the damaged vault.

The damaged vault was first repaired. All fine particles were cleaned prior to strengthening. Basalt fiber anchors were put first, followed by basalt fabric. The cloth was covered with cementitious mortar, which also served as a surface finish. Figure 8 shows Strengthening of corrosion damaged RC column in hot industrial area using FRCM in Romanesque Church of San Roque.

Figure 8. Strengthening of corrosion damaged RC column in hot industrial area using FRCM in Romanesque Church of San Roque (Chellapandian and Suriya Prakash, 2021)

2.3.3 FRCM used for strengthening masonry and concrete systems

In terms of FRCM components, several studies have been done to investigate the performance of this composite material and its application as a strengthening system for masonry and concrete structures combining different types of fibers and mortars. However, the most promising alternative for the construction industry is the one including glass fiber because of its lower cost. Studies about the sufficiency of glass fiber grid in different structures and infrastructures were presented by Khodaii et al. (Khodaii, Fallah and Moghadas, 2008), Meng and Khayat (Meng and Khayat, 2016) and Falliano et al. (Falliano *et al.*, 2019). Corradi et al. (Corradi *et al.*, 2014) have investigate the connection between glass fiber grids and cement mortar in shear strengthening of wall panels. Reinforced panels showed that the combination of glass fiber grids and mortar enhanced the mechanical response. Another study performed by Dalalbashi et. al (Dalalbashi *et*

al., 2018) was aimed at evaluating the bond behavior of glass fiber grids-mortar experimentally and analytically.

Ebead and El-Sherif also carried out a new FRCM Near-surface Embedded (NSE) concept to reinforce the flexural beams. The method of implementing NSE-FRCM reinforcement technique included scraping the concrete coating at beam soffit which was the most degraded. The authors indicated technique's flexural enhancing which was effective in this experimental study (Ebead and El-Sherif, 2019).

Donnini et al. have been investigated several tests, seeking to suggest a connection of three various approaches to reinforce concrete members. There were twenty compression tests which were done to investigate the mechanical properties of the most current buildings. The role of FRCM performance and failure modes have been studied. All tests illustrated FRP usage which was more efficient in comparison of FRCM material (Donnini, Spagnuolo and Corinaldesi, 2019).

Ebead and Younis have investigated concrete slabs which were reinforced with FRCM/concrete at the laboratory. After doing pull-off tests, some failure modes were seen, namely, (a) debonding at the fabric/mortar interface and (b) debonding at concrete/matrix interface, presenting in Figure 9 (Ebead and Younis, 2019).

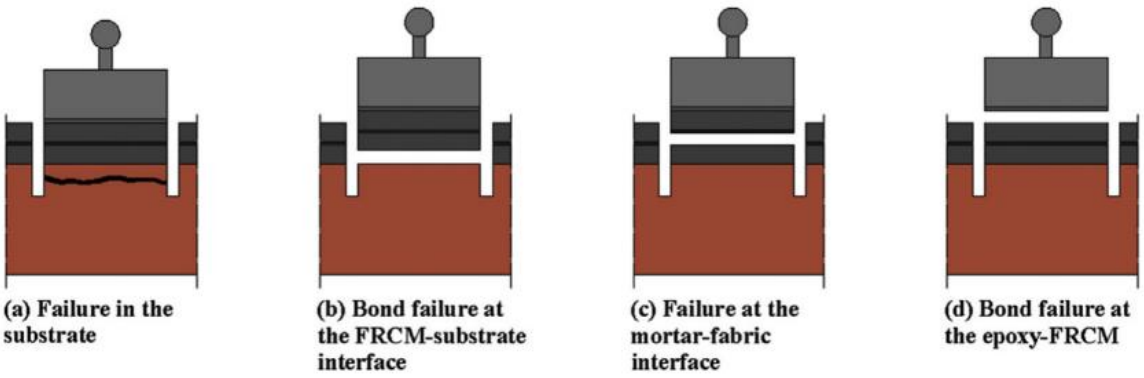

Figure 9. Possible failure modes at FRCM/concrete bond with pull-off test (Ebead and Younis, 2019)

Casacci et al. studied an experimental program in order to strengthen masonry wallets. In this study, the authors used two different methods to reinforce masonry panels; basalt bars and flexible FRCM into the mortar bed joints. After doing tests, both retrofitting methods reported a significant rise in ultimate load, shear stiffness and ductility. Figure 10 shows failure mode of specimens reinforced with FRCM. (Casacci *et al.*, 2019)

Figure 10. Failure mode of the specimens (Casacci *et al.*, 2019)

Estevan et al. have investigated the behavior of different composite materials used as a reinforcement for masonry specimens. There were several reinforcements, shown in Figure 11. The authors reached an ideal approach to reinforce masonry structures (Estevan *et al.*, 2020).

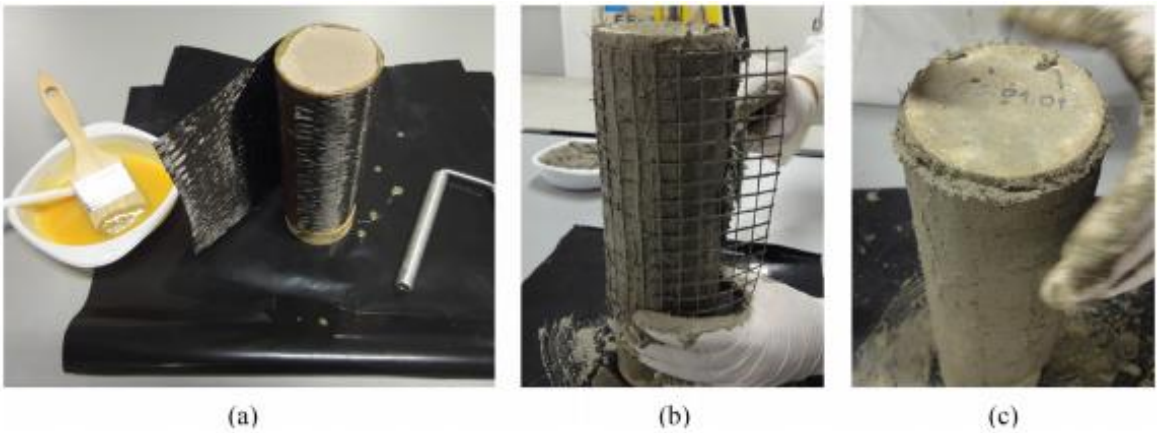

Figure 11. Reinforcement of masonry samples with composites: (a) FRP confinement; (b) mortar and fiber mesh of the FRCM confinement, and (c) end faces for a proper load application (Estevan *et al.*, 2020)

Younis et. al (Younis, Ebead and Shrestha, 2017) investigated experimental study about the usage of FRCM in concrete beams as a reinforcement. All beams were tested under three-point loading. There was a significant increase in capacity by 51% due to use FRCM. FRCM strengthening was more effective than fabric. Another experimental result was small width of crack, because of FRCM use.

Napoli and Realfonzo (Napoli and Realfonzo, 2020) have done analytical study about compressive strength of concrete reinforced with FRCM material. In this study, data of 290 concrete cylinder which reinforced, wrapping with FRCM were collected from recent literature. These data indicated the efficiency of FRCM and compared the type of FRCM; basalt, carbon, glass, PolyBenzobisOxazole (PBO) and steel composite. Analysis of data showed specimens that strengthened with glass of carbon fabrics had the lowest strength. Whereas, PBO or steel fabrics had the great performance in strengthening of specimens.

Ascione et. al (Ascione, De Felice and De Santis, 2015) introduced a qualification method for strengthening systems by externally bonded FRCM. Shear tests and tensile tests have been done in this study. Basalt, carbon, glass, and steel textiles used as a reinforcement. Maximum stress occurred through shear tests. In tensile test, qualification strain was appeared.

Domenico et. al (De Domenico *et al.*, 2020) investigated bond behavior of concrete beams reinforced with different systems; CFRP and PBO-FRCM under three-point bending tests with different environmental conditions; humidity and temperature. Experimental results different behavior of FRP and FRCM to high temperature conditions. Moreover, FRCM system was more sensitive than FRP system. Figure 12 shows the typical failure of CFRP and PBO-FRCM strengthened beams.

(a) (b)

Figure 12. Typical failure mode of (a)CFRP and (b) PBO-FRCM strengthened beams (De Domenico *et al.*, 2020)

Olivito et.al (Olivito, Codispoti and Cevallos, 2016) investigate the bond behavior of Flax-FRCM and PBO-FRCM composites applied on clay bricks. This study has done in two methods; experimental and theoretical study. The results of the test showed that flax fibers had strong mechanical property, it was the best type of FRCM material and another type PBO fiber had a poor mechanical property, this type was not suggested for a use as a reinforcement.

2.4 Hybrid structures

Research undertaken over the last 20 years into the performance of Fiber Reinforced Polymers (FRPs) in Civil Engineering applications has revealed that FRP materials have significant potential for usage in structures owing to their benefits. Recently, studies have been conducted to study the replacement of reinforced concrete components in structures with hybrid FRP-concrete members, leading to the building of many structures employing the new hybrid system.

2.4.1 Hybrid structures composed of steel profiles and concrete

Hybrid mixes of FRP and steel longitudinal reinforcement has been presented as a feasible and effective option for improving ductility, taking use of both material's advantages. FRP reinforcement offers a stronger strength, while steel reinforcement improves serviceability and ductility in addition to sharing partial load (Antonietta and Luciano, 2002) (Wenjun, Xiaoliang and Haiqun, 2009).

Lau and Pam evaluated the flexural ductility of hybrid FRP reinforced concrete beams experimentally. Adding steel rebars as reinforcement to concrete beams led to increase flexural ductility significantly (Lau and Pam, 2010). Hawileh used the combination of two materials; steel and aramid reinforcement for reinforcing hybrid concrete beams numerically. The ductility and load-carrying capacity for reinforced concrete beams improved considerably. They defined the nonlinear response of the concrete element by using tensile and compressive stress–strain relationships (Hawileh, 2015). Kara et. al proposed a numerical approach for predicting the curvature, deflection, and moment capacity of hybrid FRP/steel reinforced concrete beams. Beam ductility and stiffness are improved when steel reinforcement is added to FRP reinforced concrete beams. It is observed that steel reinforcement improved the ductility and stiffness of FRP reinforced concrete beams. The stress-strain curve for concrete, steel and FRP were used to simulate the their exact behavior in accordance with reality (Kara, Ashour and Köroğlu, 2015). Al-Sunna et. al studied the experimental study of FRP reinforced concrete beams and slabs. Experimental result showed that in FRP reinforced concrete components with moderate to high reinforcement ratios, the contribution of shear and bond induced deformations can be considerable (Al-Sunna *et al.*, 2012). Ge et al. have investigated the tensile and bond behaviors of hybrid concrete beams reinforced with Basalt FRP bars and steel bars. It was clear that when compared to steel bars, BFRP bars had a higher tensile strength but a lower elastic modulus, and their tensile destruction was sudden (Ge *et al.*, 2015). Using a basic and trustworthy 2D Finite Element (FE) model, numerical investigation on hybrid FRP-steel RC beams was performed by Bencardino et al. by specifying the post-crack behavior of tensile concrete, the tension stiffening effect was reproduced. They defined concrete damage plasticity in order to simulate the concrete behavior. (Bencardino, Condello and Ombres, 2016). Zhou et. al presented a numerical method for

estimating the flexural behavior of hybrid FRP-steel reinforced concrete beams. The stress-strain curve for compressive (unconfined) concrete was used in numerical modeling (Zhou *et al.*, 2021) and in another study, Zhou et. al have investigated crack analysis on hybrid GFRP-steel RC prisms and suggested the crack spacing model of them (Zhou *et al.*, 2020).

2.4.2 Hybrid structures composed of FRP profiles (girder) and concrete

FRP profiles have been used in recent years to produce new structures. FRP profiles are manufactured with a pultrusion technique (Vedernikov *et al.*, 2020). This product has a wide range of applications in construction and building systems. Zou et al. reported the application of pultruded GFRP profiles in the FRP-concrete hybrid section of a bridge system (Zou *et al.*, 2021). Using bolted connections and/or adhesive bonding had a positive effect on attaining the full composite section response. In another study, Zou et al. investigated the behavior of bolted shear connections placed between FRP girders and ultra-high performance concrete slabs under push-out tests. Two failure modes were observed; bolt shank shear and FRP flange shear-out (Zou, Feng and Wang, 2018). Nguyen et al. investigated the effect of adding epoxy to bolted connections in FRP-concrete hybrid slabs and they found that the combination of epoxy and steel bolts led to an improvement in ultimate load bearing capacity (Nguyen, Mutsuyoshi and Zatar, 2014).

Martins et al. have investigated the effect of GFRP profiles used on beam-to-column system in experimental and numerical method and they compared this connection with tailor-made steel connection (see Figure 13). The results represented there were some factors which were effective to strength, including the bolt edge distance, total rigidity. In addition to this, numerical models could help to estimate the connection strength (Martins *et al.*, 2017).

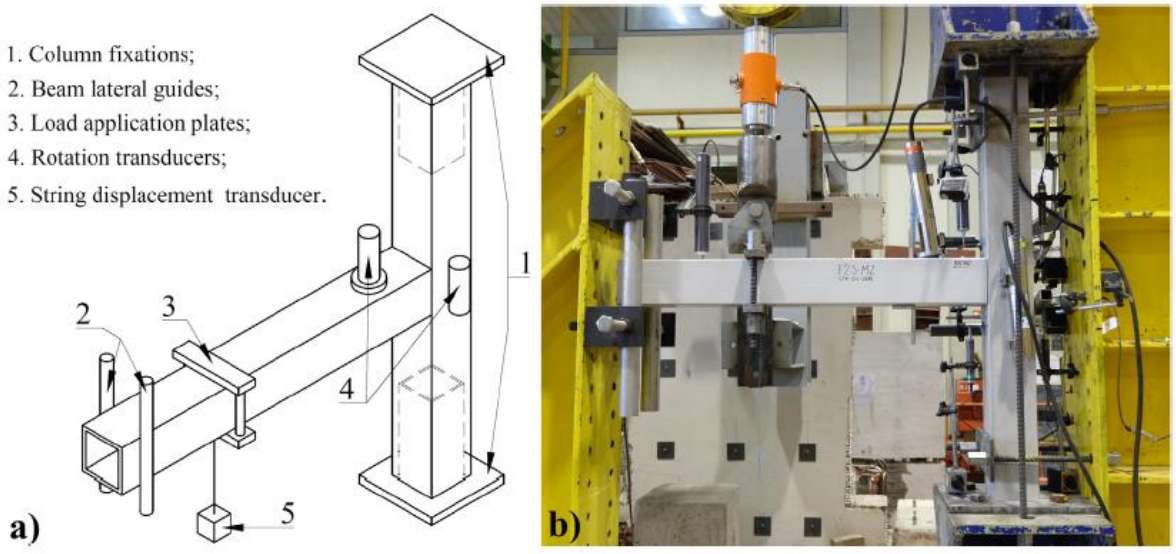

Figure 13. Test setup: a) illustrative scheme; b) frontal view (Martins *et al.*, 2017)

Hall and Mottram (Hall and Mottram, 1998) have done four-point bending tests on 12 concrete beams. All experimental specimens were fabricated from two or four T-shaped FRP profiles which adhered to FRP and attached to concrete beams. Experimental results indicated the important role of the interface between FRP profile and concrete. Moreover, bending failure did not occur and shear failure appeared in unforced beams.

Manalo et al. (Manalo *et al.*, 2012) analyzed and tested a hybrid FRP bridge girder with an overlying concrete deck. Two shear connections were used, including epoxy resin and epoxy resin with steel U-bolts.

Neagoe et.al (Neagoe, Gil and Pérez, 2015) casted and tested concrete slabs which reinforced and connected with pultruded GFRP profiles. Experimental results showed the increase in bending capacity and stiffness due to GFRP profiles. There was buckling failure modes in profile control specimen as shown in Figure 14.

Figure 14. Buckling failure modes in profile control specimens (Neagoe, Gil and Pérez, 2015)

Brózda et al have investigated the shape and cross-sectional factors in GFRP profiles. These profiles were applied to hybrid slabs in concrete structure; buildings and bridges. In this theoretical study, the results indicated the weight of these structures decreased and FRP profile was economical justifiable (Brózda, Selejdak and Koteš, 2018).

Yuan studied hybrid beams reinforced with FRP profile and steel bars to increase the ductility of these beams. Flexural tests were done on hybrid beams and the tests presented relative slip between the concrete and the I-section. Two important results conducted; 1. Tensile steel bars controlled the yield point in composite beams. 2. Composite beams had a ductile behavior during the flexural test because of the existence of the tensile steel bars (Yuan, 2017).

Huang et al. studied the behavior of fifteen composite beams which were reinforced with FRP profile, steel bar, CFRP layer and inner GFRP tube under four-point bending tests. Figure 15 shows the test setup in this study. Some studied parameters were displacement, failure modes and ductility. These were evaluated and compared with control beam. Ultimate load and ductility for all hybrid beams enhanced significantly with an increase in the thickness of hybrid FRP profile. By covering the beams with U-shape FRP, concrete cracks were not seen at the first of test. (Huang *et al.*, 2018).

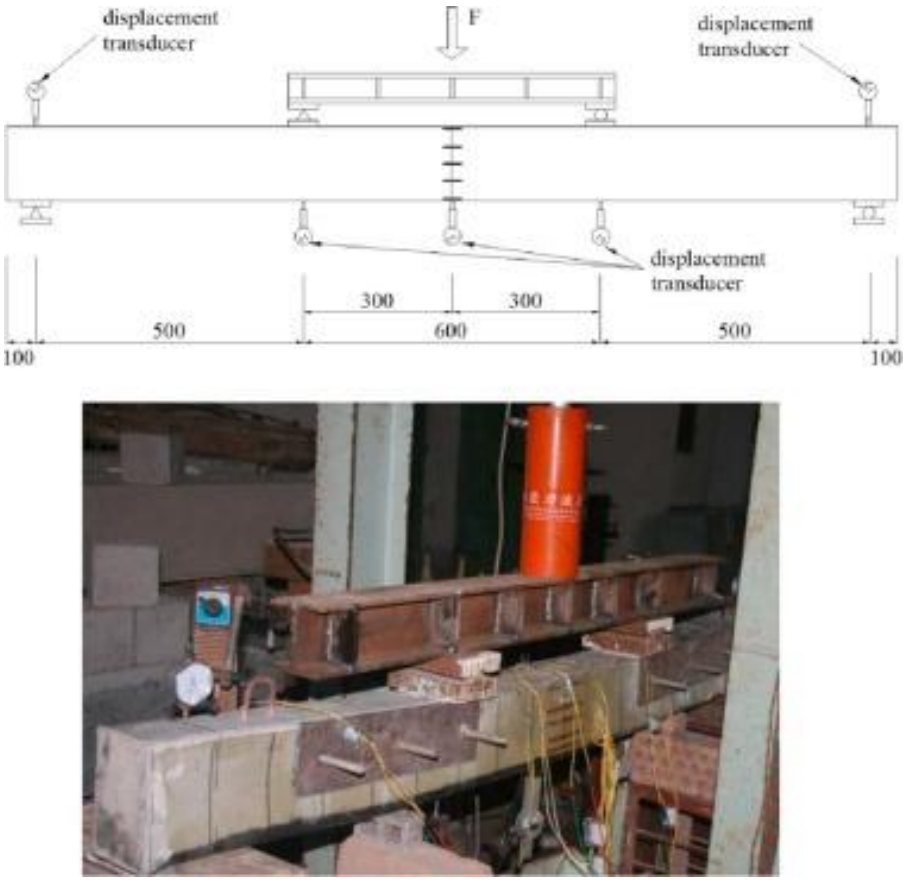

Figure 15. Setup for four-point bending test (Huang *et al.*, 2018)

Nordin and Täljstenab (Nordin and Täljsten, 2004) fabricated hybrid beams, consisting glass fiber I-shaped beam with carbon fiber. The bottom of the flange and compressive zone of concrete block were strengthened with carbon fiber. The results from bending tests showed the fabrication of FRP hybrid concrete was possible, with high stiffness and bearing heavy loads.

2.5 Conclusion

In conclusion, hybrid structures using pultruded FRP profiles and concrete have already been studied and have started to be applied as commercial solutions. On the other hand, the FRCM

system is widely used as a strengthening solution. In addition, the FRP-concrete connection method proposed by Mahboob et al. (Mahboob *et al.*, 2021b) opened the door to future FRP-FRCM hybrid structures technology. However, as per authors knowledge, there are no published references that suggested combing pultruded FRP profiles and FRCM to produce structural superficial elements so far. The possible range of application of these hybrid structures may include urban elements, tunnel sustainment or thin roofing systems. Thus, the main objective of the current work is to cover this knowledge gap. The tasks were to describe and to characterize the structural behavior of this new structural system composed by FRP profiles and FRCM. Experimental tests and numerical simulations were used with this aim.

3

Experimental characterization of materials

3.1 Introduction

The current study shows an experimental investigation of hybrid FRP-FRCM structural elements to find a solution based on producing new hybrid structure with high performance and reduced cost. Moreover, most of the studies have worked on producing hybrid FRP-concrete structures, but using FRCM composite materials and the interaction between FRP and FRCM is novel.

This chapter describes the experimental research carried out to study hybrid FRP-FRCM superficial structural elements made of arched structures of straight pultruded glass fiber-reinforced polymer (GFRP) profiles that are connected to FRCM panels to provide a thin plate solution. The developed structural system can be applied for tunneling sustainment because of benefitting from FRCM deformability capacity and GFRP durability, light-weight and reduced cost.

A previous experimental campaign about reinforced concrete beams with GFRP profiles, conducted by Neagoe (Neagoe, 2016), included different tests aimed to characterize the same GFRP profiles considered in this research. Thus, bending, tension, in-plane compression, interlaminar shear, in-plane shear and full section effective moduli have been previously determined. The current experimental tasks are divided in four phases: i. GFRP profile connections; ii. GFRP-Mesh connections; iii. Mortar-Mesh connection or FRCM characterization; and iv. Hybrid system testing.

All the tests have been performed by the author at the Laboratory for the Technological Innovation of Structures and Materials (LITEM) which is part of CATMech – TECNIO research group. It is located in Universitat Politècnica de Catalunya – Campus de Terrassa.

3.2 Materials

3.2.1 Composite profile

The application of Glass fiber-reinforced polymer (GFRP) composites is definitely increasing in construction and building system over the last decade. This material has more benefits to other

traditional materials, including the higher strength to weight ratio, the lower self-weight, the electromagnetic transparency and easier and faster performance. French company GDP S.A. produced and manufactured this material and Spanish company Composites ATE S.L. distributed it.

Following the initial study by Neagoe (Neagoe, 2016), I-shaped profiles with cross section shape similar to an IEP120 were considered. Their nominal dimensions were: 120 mm in height, 60 mm in flange widths and a thickness of the web and flanges of 8 mm and a fillet radius of 5 mm between the flanges and the web. Figure 16 shows GFRP profiles used in the current research.

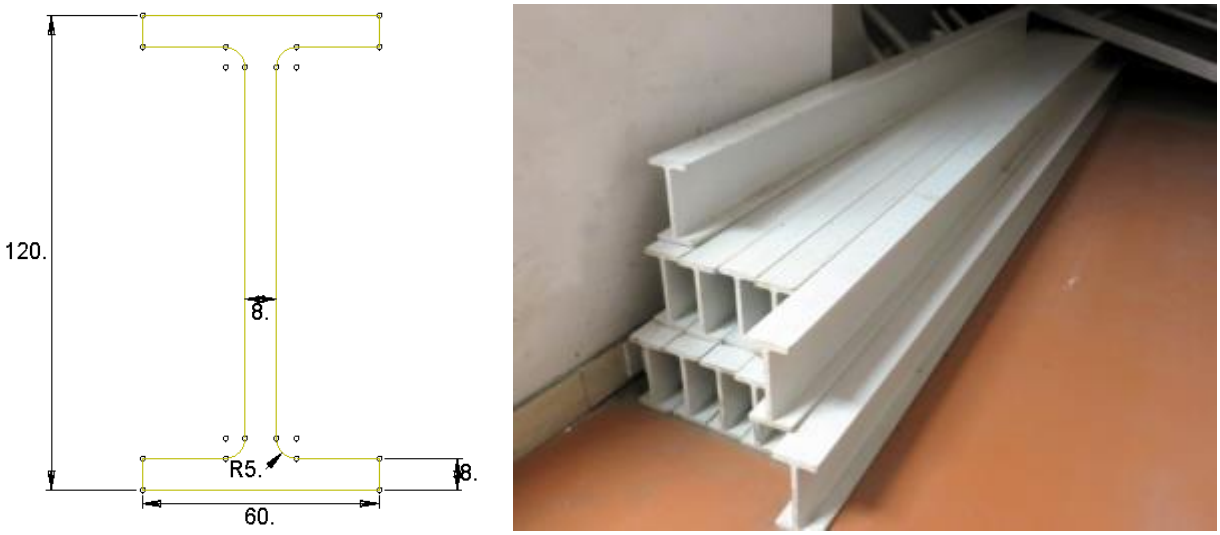

(a) **(b)**

Figure 16. (a) The geometry of the GFRP pultruded profile (dimensions in mm) (b) Storage of GFRP pultruded profiles in the laboratory

The used IPE 120 GFRP profiles were made of a thermosetting PR500 grade polyester resin reinforced with E-glass fibers. Extremely inhomogeneous pultruded profile consists of two parts; periodic layers of unidirectional fibers is served as a longitudinal reinforcement and unknitting continuous strand mats (CSM) embedded in isophthalic polyester resin which applied as shear, transverse reinforcement. Figure 17 shows the details of GFRP structural profile.

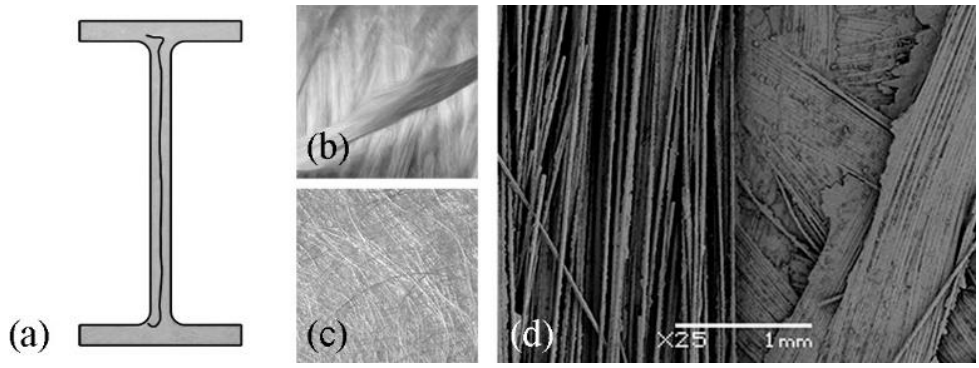

Figure 17. GFRP structural profile: (a) cross-section structure and geometry; (b) fiber roving; (c) non-woven CSM; (d) microscopic anisotropic structure of web-flange junction (Neagoe, 2016)

Table 2 presents the properties of the pultruded GFRP profiles materials in three separated parts, physical, electrical and mechanical property which were announced by the manufacturer.

Table 2. Declared properties of the pultruded GFRP profiles (Neagoe, 2016)

Property	Value	Units	Testing method
Physical			
Reinforcement ratting in weight	50-65	%	EN ISO 1172
Apparent density	1.8	kg/dm^3	EN ISO 1183-1
Barcol hardness	45/50		EN 59
Water absorption	1.50	% In weight	EN ISO 62
Coefficient of linear thermal expansion	$9 \cdot 10^{-6}$	/°C	ISO 11359-2
Thermal conductivity	0.15	W/K·m	ASTM C117
Mechanical			
Tensile strength	207	MPa	EN ISO 527-4
Modulus of elasticity	17.2	GPa	EN ISO 527-4
Flexural strength	207	MPa	EN ISO 14125
Shear strength	35	MPa	EN ISO 14130
Compressive strength	276	MPa	EN ISO 14126
Electrical			
Dielectric strength	984	kV/m	ASTM D149
Resistivity	1012	Ω·m	CEI 60093
Arc resistance	120	s	ASTM D495

Neagoe (Neagoe, 2016) did different tests: flexural, tensile, compressive, shear and full section experiments on characterization of GFRP profile material under CEN, ISO and ASTM International standards. Results are summarized in Table 3.

Table 3. The mechanical properties of the GFRP profile (Neagoe, 2016)

Property	Value	Units	Testing method
Flexural			
Ultimate strain	2.10 ± 0.05	%	
Strength	734 ± 39	MPa	EN ISO 14125:1998
Modulus of elasticity	35.0 ± 2.1	GPa	
Tensile			
Ultimate strain	1.37 ± 0.11	%	
Strength	520 ± 27	MPa	EN ISO 527-1:2012
Poisson's ratio	0.27 ± 0.02		EN ISO 527-4:1997
Modulus of elasticity	38.0 ± 1.4	GPa	
Compressive - lengthwise			
Ultimate strain	1.02 ± 0.11	%	
Strength	406 ± 30	MPa	EN ISO 14126:1999
Modulus of elasticity	40.6 ± 1.8	GPa	
Compressive - crosswise			
Ultimate strain	1.60 ± 0.13	%	
Strength	115 ± 3	MPa	EN ISO 14126:1999
Modulus of elasticity	10.8 ± 0.5	GPa	
Shear			
Apparent interlaminar strength	31.1 ± 0.7	MPa	EN ISO 14130:1997
In-plane strength	49.0 ± 4.7	MPa	ASTM D 3846-08
Full-section moduli			
Effective flexural modulus	39.1 ± 0.14	GPa	EN 13706-2:2002
Effective shear modulus	3.98 ± 0.26	GPa	

3.2.2 Mortar

To make the hybrid structure, the pultruded GFRP profiles were connected to a FRCM panel. Thus, the matrix of this panel was made of mortar. Two types of mortar were used; i. Sika Monotop 612 (repair) and ii. Pasta niveladora Axton 10mm (autoleveling).

In particular, Sika MonoTop®-612 (SIKA AG, 2018) is basically made of cement. It is a one-component structural repair mortar, reinforced with fibers and silica fume. This material is manufactured under the Class R3 of UNE-EN 1504-3 standard (Committee AEN/CTN 83, 2006) and produced by SIKA company in the UK. Water is added to the correct proportion of powder and both of them are mixed thoroughly for at least 3 minutes to the required consistency.

The second used mortar is Pasta niveladora Axton 10mm. It is manufactured and distributed by Leroy Merlin company is Spain. Pasta niveladora Axton 10 mm (PROPAMSA S.A.U., 2020) is a

self-leveling mortar made of special cements mixtures with selected aggregates, fibers and organic additives. 25kg of this powder should be mixed with 6L of water. Approximately, 1.4 of ready mortar is used per 1 square meter for one mm of thickness.

Table 4 shows the theoretical mechanical properties of the two used mortars and Figure 18 presents the two used mortars. Table 5 represents the mechanical properties of Pasta niveladora Axton.

Table 4. The mechanical properties of Sika® MonoTop-612 mortar

Property	Value	Units	Testing method
Density	2100	Kg/m^3	-
Tensile strength[1]	2.90	MPa	EN1015-11
Flexural strength[1]	6.56	MPa	EN1015-11
Modulus of Elasticity in Compression	25	GPa	EN13412
Compressive Strength[1]	39.25	MPa	EN1015-11

[1] From experimental tests published in (Mercedes, Bernat-Maso and Gil, 2020)

Table 5. The mechanical properties of Pasta niveladora Axton (Mercedes, Bernat-maso and Gil, 2020)

Material	Compressive Strength (MPa)	Modulus (GPa)	Tensile Strength (MPa)	Particles (mm)
Pasta niveladora Axton 10mm	20	9.9	5	0.5≤

Sika MonoTop 612 Pasta niveladora Axton 10mm

Figure 18. Two used mortars

Two types of standardized tests were carried out to characterize the mortars used to produce the matrix of the FRCM. To determine the flexural strength, a three-point test was performed and,

with each of the resulting parts of the specimen, a direct compression test was conducted to obtain its compressive strength. The specimens consisted of prismatic pieces with 160x40x40mm manufactured in standard molds with a capacity for three-specimen. Before pouring the mortar, the molds were smeared with oil in order to facilitate the demolding process. Once the mortar is poured, the specimen was vibrated manually and left to rest for 3 and 10 days in the molds, as shown in Figure 19, all specimens were preserved under environment condition at least 28 days.

(a) (b)

Figure 19. Preparation of mortar specimens: a) standard mold b) curing specimens in the initial phase

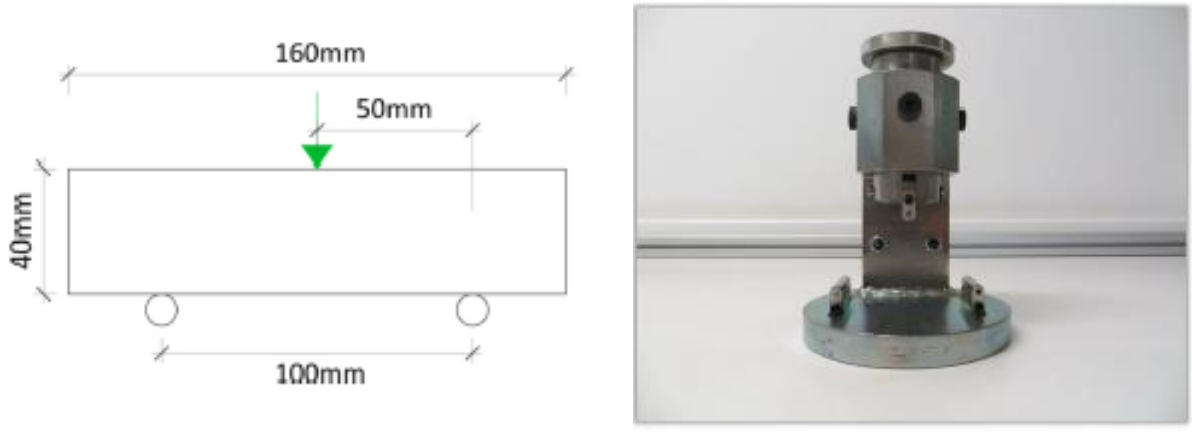

(a) (b)

Figure 20. a) Flexural test configuration, b) Standard testing tool

To determine of flexural and tensile strength, a three-point test has been done according to EN 1015-11:2000 (CEN 1999, 1999). The load was applied on the center of the specimen and the distance of two supporters was about 100 mm as shown in Figure 20a. To ensure standardization of the experimental results, the trials were run using a standard tool for this purpose as shown in Figure 20b.

The load with the range of 10N/s was applied and the load was controlled by an electromechanical test press capable with the load of 50kN. Figure 21 shows the test setup configuration for mortar characterization.

Figure 21. Test setup configuration for mortar characterization

The test procedure is described below:

- Positioning of the specimen: it had full contact with the back of the test tool. Positioning length of the specimen: it was centered with respect to the point of application of the load.
- The loading tool approximation was done by using the electromechanical press until the 1mm gap is reached with the specimen to be tested.
- Start of data acquisition and load application by control by force at a speed of 10N / s. The variables recorded were the vertical displacement of the load application tool and the force applied by the electromechanical press. These were acquired at 5Hz.
- The loading process was recorded with a high-speed camera with the objective of clearly capturing the moment of cracking of the specimen as shown in Figure 22. The test was terminated when the specimen suffered a brittle failure.
- The two parts resulting from the fractured specimen were used later for compression tests.

Figure 22. Cracking process of a mortar specimen under flexural test

The test to determine the compressive strength of the mortar specimens according to EN 1015-11: 2000 (CEN 1999, 1999), which determines the performance of a direct compression test on a cubic mortar of 40mm per side as shown in Figure 23a. Each of the halves obtained from the flexural test developed previously was used for compression test.

To ensure the correct distribution of force, the tests are executed using two 40x40x10mm metal plates on both sides of the test specimen. The applied load was carried out by force control at a speed of 350 N/s using a 100kN capacity oil-hydraulic actuator, as shown in Figure 23b.

The test procedure is described below:

- Placing of the specimen so that the two metal plates aligned and within the uncracked region of the mortar. Alignment of the system in plane with respect to the actuator.
- Controlling the oil-hydraulic actuator until it comes into contact with the upper metal plate.
- Start of data acquisition and apply the force that was controlled at a rate of 350 N/s. two outputs were recorded, including vertical displacement and applied force which were acquired at 50Hz.
- The testing process was recorded with a high-speed camera, capturing clearly the moment of the crushing of the specimen, as shown in Figure 24. The test was concluded when the specimen suffered brittle failure.

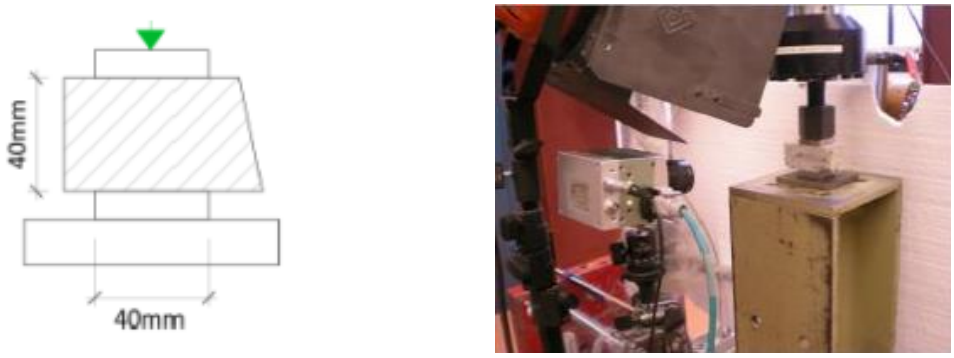

(a) ***(b)***

Figure 23. (a)Configuration of the compression test on mortar specimens (b). Installation the compression test on mortar specimens

Figure 24. Crushing process of a mortar specimen under compression test

The results of the tests carried out on mortar specimens were obtained on the following considerations:

The flexural strength of the mortar (f_{mx}) was obtained assuming a linear stress distribution in the most requested section of the specimen in the maximum load moment, as follows:

$$f_{mx} = 1.5\frac{f_{max}L}{bh^2} \quad \text{Eq 1}$$

Where F_{max} is the maximum force applied in the three-point test, L is the distance between supports and b, h are the dimensions of the cross section of the test specimen.

The compressive strength of the mortar (f_{mc}) was obtained assuming a constant stress distribution in the specimen section at the maximum load moment:

$$f_{mc} = 1.5\frac{f_{max}}{b^2} \quad \text{Eq 2}$$

Where F_{max} is the maximum applied force in the direct compression test and b is the base of the specimen.

Table 6 shows the characterizations of mortars obtained from compressive and flexural tests.

Table 6. Properties of the mortars obtained from the test

Specimen	Test tube	Flexural resistance (MPa)		Compressive resistance (MPa)	
		Individual	Media	Individual	Media
Sika Monotop 612	1	6.77	5.89 (0.16)	33.49	36.29 (0.16)
	2	6.58		34.66	
	3	5.25		44.81	
	4	4.96		32.20	
Pasta niveladora Axton 10mm	1	7.69	8.73 (0.21)	22.23	29.24 (0.25)
	2	6.92		26.98	
	3	11.01		39.5	
	4	9.29		28.23	

3.2.3 Fiber glass mesh

Three types of mesh were used in FRCM production to study which is the most suitable one for the current research. Glass, carbon and basalt were considered.

In terms of Glass, Mapegrid G220 is a two-directional fiber mesh made up of alkali-resistant glass covered by a polymeric layer, as shown in Figure 25. Depending on the direction, the strands have a width and separation different, although the quantity of fibers remains invariant. This type of fiber has been used as an external reinforcement of masonry structures, offering greater ductility and more uniform distribution of the stress on the structures. It presents an optimal tensile resistance, thus as an inalterability to chemical attacks and atmospheric agents. Mapegrid G220 is manufactured by Mapei S.p.A. and it comes distributed in 900mm of width and 45.7m of length. Technical characteristics according to manufacturer are summarized in Table 7.

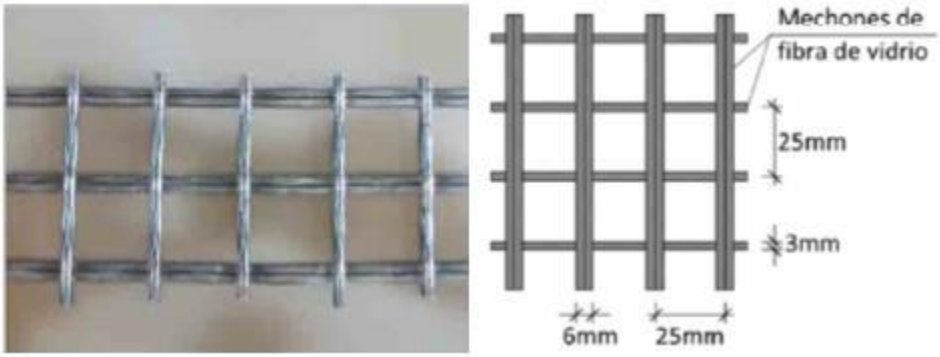

Figure 25. Mapegrid G220 mesh

Table 7. Mechanical property of Mapegrid G220 (MAPEI Spain, 2018)

Parameters	Value
Fibers	
Tensile resistance (MPa)	2600
Strand	
Strand width (mm)	6.3
Mesh	
Distribution	Bidirectional
Distance between strands (mm)	19.22
Weight (g/m^2)	225
Equivalent thickness	0.042
Tensile resistance (KN/m)	45

Regarding to another type of mesh, X Carbon Mesh (C10) (Ruredil, 2013) is a bidirectional fiber formed by tufts of carbon fiber thermo-welded to an auxiliary polyester, as shown in Figure 26. These have a width of 5 mm and are separated from each other by a distance of 5 mm. X mesh

C10 is manufactured by the company Ruredil S.p.A. and it is distributed in 1000 mm wide and 15 m long. Technical characteristics according to manufacturer are summarized in Table 8.

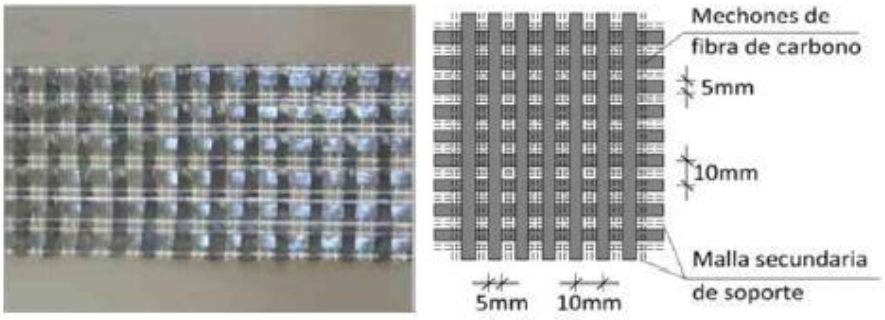

Figure 26. Carbon Mesh (C10)

Table 8. Mechanical property of X mesh C10 (Ruredil, 2013)

Parameters	Value
Fibers	
Density (g/cm^2)	1.82
Tensile resistance (MPa)	4800
Elasticity modulus (GPa)	240
Ultimate deformation (%)	1.8
Strand	
Tensile resistance (kP/m)	≥160
Strand width (mm)	5
Fabric	
Distribution	Bidirectional
Distance between strands (mm)	5
Weight (g/m^2)	168
Equivalent thickness	0.047

Regarding to basalt fiber, it is a bidirectional fabric formed by tufts of basalt fibers produced from the fusion and subsequent spinning of volcanic rocks. The strands are fixed by means of the thermo-welding of an auxiliary polyester mesh that prevents its fraying and gives consistency to the fabric. In turn, they have a width of 5mm and they are 10mm apart from each other as can be seen in Figure 27. This type of fabric is suitable to apply as a reinforcement in concrete and masonry structures, and can be impregnated with both resins and mortars. Due to its toughness, it is a suitable material to reinforce structures subjected to severe impacts or cyclical loads, as well as for mitigate seismic effects and limit crack propagation in structures. In addition, it has a high resistance to traction and fatigue, and it is not visible affected by corrosion and hydrolysis processes. The properties of the basalt fiber have been obtained from the data of the FIDIA srl group, obtained in accordance with CNR-DT (CNR-DT, 2018). Table 9 shows the mechanical property of Fidbasalt Grid 300 C95.

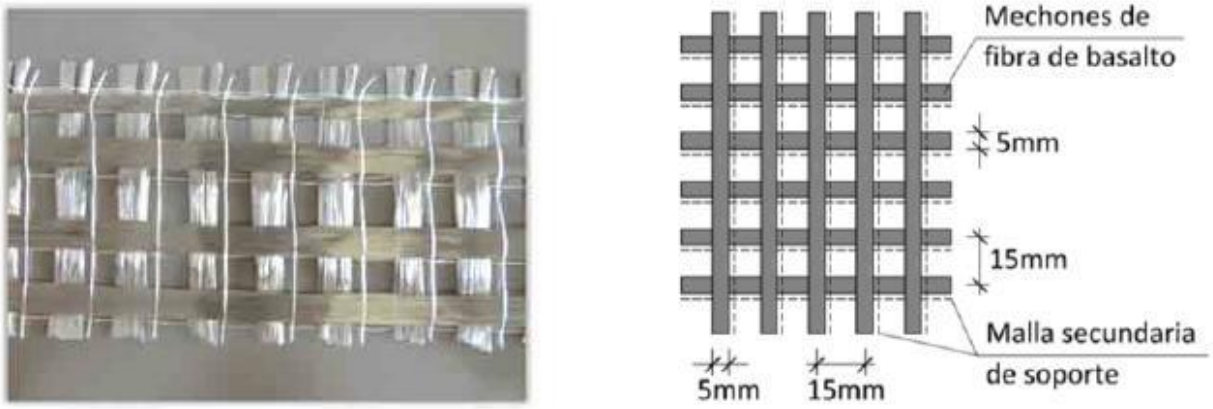

Figure 27. Fidbasalt Grid 300 C95

Table 9. Mechanical property of Fidbasalt Grid 300 C95 (FIDIA global services, 2010)

Parameters	Value
Fibers	
Density (g/cm^2)	2.8
Tensile resistance (MPa)	3080
Elasticity modulus (GPa)	95
Ultimate deformation (%)	3.15
Strand	
Tensile resistance (KN/m)	1200
Strand width (mm)	5
Fabric	
Distribution	Bidirectional
N° strands (strand/cm)	1.25
Weight (g/m^2)	168
Equivalent thickness	0.053
Tensile resistance (MPa)	1735
Elasticity modulus (GPa)	90
Ultimate deformation (%)	1.93

In order to determine the mechanical properties of the threads and tufts used in this study, it was necessary to prepare specimens of threads for tensile tests. They were tested according to the EN ISO 13934-1 / 2 code, but they were adapted to the particular requirements of this study (British Standards Institution, 1999).

For this, it was necessary to make a wooden mold with a flat surface 60 × 30 cm, on which a glass sheet was placed, with nails in the ends to align and hold the threads, as shown in Figure 28.

The method of preparation of all the samples for the tensile test was as follows:

To avoid adhesion between the resin and the mold, the surface was cleaned with acetone and moistened with two release agents (Sealer - GP and Z 6.0 Slip coat System). Then, threads were stretched and anchored on the nails at the ends of the mold. After, pieces of glass fibers (mat) were placed in the marked areas in the mold embedding the endings of the threads. Then, these were impregnated with resin Master Brace P350 epoxy resin, another sheet of fiberglass was placed and impregnated so producing an FRP. This task was performed with the purpose of consolidating the ends of the fiber and providing acceptable clamping area, with the glass fibers composites.

After one day of curing, the specimens were removed from the mold and then mechanized. Compounds at the ends were 2 cm wide and 4 cm long.

Figure 28. Preparation of yarn and tuft specimens for tensile testing

Figure 29. Traction test of a strand

The ends of the threads and tufts were held by the clamps of the testing machine shown in Figure 30(10 kN range). Once fastened, a small load of 5 N was applied to stretch the thread or strand.

The extensometer was placed on the strands with an initial opening length of 50 mm (initial length of fully closed extensometer). This extensometer was placed through rubber bands at the contact points with the thread to prevent the slippage and damage to the specimens. In the case of basalt

samples, this extensometer fixing system did not work because basalt strands were not consolidated, so it was decided to place adhesive tape on the points of contact between the specimens and the extensometer, reaching good strain compatibility.

Once the extensometer was placed, the test started at a speed of 5 mm/min acquiring. Force, displacement and opening of extensometer data was recorded at 50 Hz.

Figure 30. MTS Insight Testing Machine

Once the tests were carried out, the results were processed and analyzed. The data obtained from these tensile tests were: load-bearing capacity (force) and the displacements associated with these loading in the central area (measured by the extensometer). From these data it was possible to make the stress-strain diagram, and also to identify the stress ultimate point or breaking point, the peak strain and the modulus of elasticity of each specimen. These parameters were determined from the following equations:

$$\sigma = \frac{F_u}{A} \qquad \text{Eq 3}$$

$$\varepsilon_u = \frac{\Delta L_u}{L} \qquad \text{Eq 4}$$

$$E = \frac{\sigma_2 - \sigma_1}{\varepsilon_2 - \varepsilon_1} \qquad \text{Eq 5}$$

F_u: ultimate force reached by the thread
A: cross section of thread
ΔL: Displacement of the extensometer
L: Initial length of the extensometer
σ_1: 20% of ultimate tension

σ_2: 90% of ultimate tension
ε_1: Deformation of σ_1
ε_2: Deformation of σ_2

The modulus of elasticity was calculated, considering the linear part of the stress-strain diagrams which corresponded to the range between the 20% and 90% of the final load. Table 10 shows the properties of different threads.

Table 10. The properties of fibers

Properties	**Fibers**		
Nomenclature	**Carbon**	**Glass**	**Fidbasalt**
Thickness (mm)	0.094	0.175	0.2
Linear density (g/m)	0.8554	2.625	0.6435
Volumetric density (g/cm^3)	1.82	2.5	2.75

Table 11 shows the average values of the tensile strength ($\boldsymbol{\sigma}_{h,u}$), peak deformation ($\varepsilon_{h,peak}$) and modulus of elasticity (E_h) resulting from the threads subjected to the tensile testing. The stresses were calculated taking into account the thicknesses of the yarn supplied by the manufacturers. The modulus of elasticity was calculated with consideration of the linear part of the stress-strain diagram.

Table 11. The properties of fibers obtained from the tests. Coefficient of variation in brackets

Specimen	**NO.**	**A_h (mm^2)**	**Fu (N)**	**$\boldsymbol{\sigma}_{h,u}$ (MPa)**	**E_h (MPa)**	**$\varepsilon_{h,peak}$ (%)**
Carbon	5	0.47	900.40	1915.74 (4%)	235.69 (7%)	1.02 (9%)
Glass	5	1.05	708	674.29 (8%)	61.25 (2%)	1.32 (6%)
Fidbasalt	5	0.23	488.25	2086.54 (6%)	86.7 (2%)	2.54 (4%)

3.2.4 Steel screws, nuts and washers

Bolted connection advantages include easy installation and high strength. Bolted connection requires screws, washers and nuts. M10×40 and M10×35 screws with hexagonal head and Q12.9 quality were used. Two different lengths were required because of geometric limitations. Corresponding nuts and washers were also required. Figure 31 represents the used screws and nuts.

Figure 31. Bolts and nuts

3.2.5 Resins

Three types of epoxy resins were used. The first one was the epoxy resin MasterBrace P 3500, typically used as a primer to prepare the masonry and concrete surfaces for the later application of an epoxy adhesive. In the current research this epoxy resin was used to laminate carbon FRP flange connectors and to bond FRCM mesh to FRP profile. It is produced by BASF company, consisting of two parts solvent-less epoxy system. It is wonderful to adhere concrete substrate and FRP products. It has flexural strength of 55 MPa and flexural modulus of 1672 MPa under ASTM D790:01 standard (Master Builders Solutions España, 2021b).

The second one was Masterbrace ADH4000. It was used to bond web and flange connectors in adhesive configuration. Properties of the epoxy resin used is summarized in Table 12.

Table 12. Properties of the epoxy resin used to produce CFRP laminates for flange connection (Master Builders Solutions España, 2021a)

Property	Test method	value
Elongation (%)	ISO 527-3	3
Tensile Strength (MPa)	ISO 527-3	27
Tensile Modulus (MPa)	ISO 527-3	1350
Compressive Strength (MPa)	ISO 604	65

The third one was Loctite 3425. It was used to bond steel plates to the lower flange of GFRP pultruded profiles in the hybrid panel in order to restrain its transversal movement by fixing the steel plates to an external rigid steel frame. The physical property of Loctite 3425 is represented in Table 13.

Table 13. Mechanical properties of Loctite Hysol 3425 (Henkel - Loctite, 2020)

Property	Test method	value
Elongation (%)		2.9
Tensile Strength (MPa)	ASTM D882	27.2
Modulus (MPa)		1350

3.3 Testing methodology & specimen's definition

Three types of tests were conducted in order to characterize the interaction between components: GFRP-GFRP connection test, GFRP-Mesh connection test and Mesh-mortar connection test.

3.3.1 GFRP-GFRP connection test

The GFRP-GFRP connection test is a type of experimental testing performed to evaluate the behavior and performance of the connection between two GFRP elements. This test is typically conducted on a small-scale specimen that simulates the actual connection detail used in a larger structure. The production procedure for a GFRP-GFRP test involves several steps, including the preparation of the specimen, fabrication of the GFRP elements, and assembly of the connection detail. Figure *32* shows the procedure of making FRP connection.

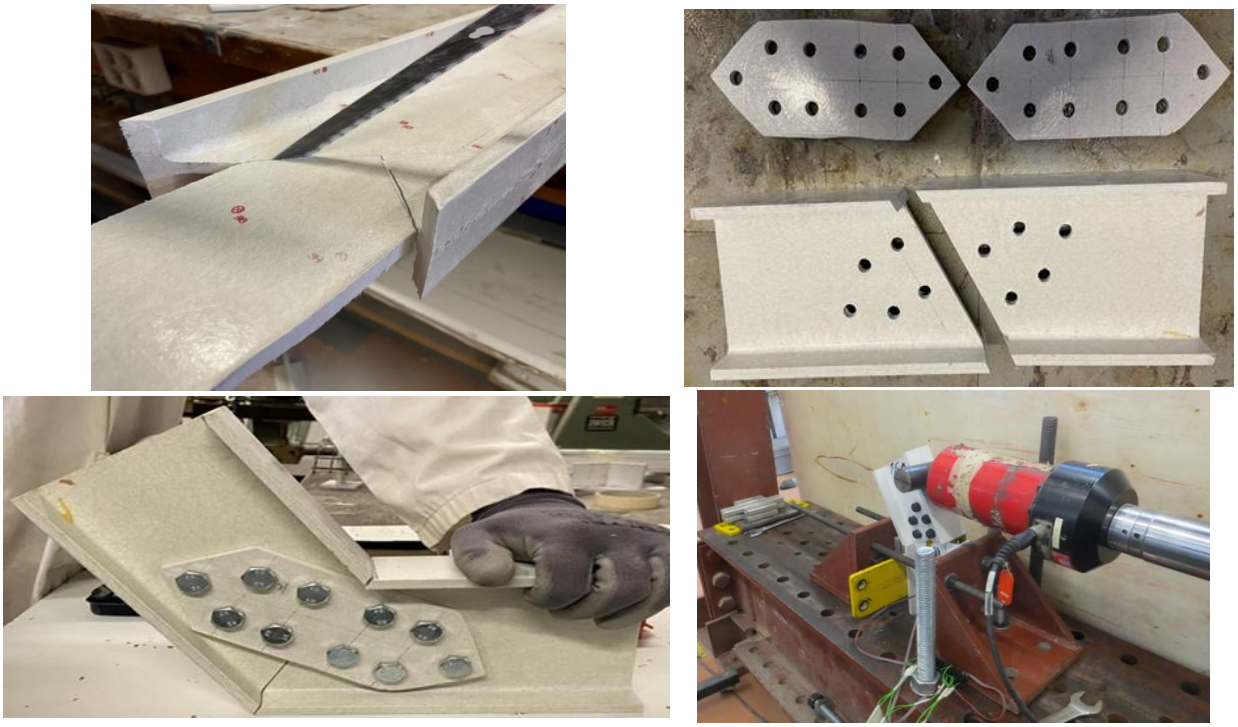

Figure 32. The procedure of making FRP connections

Specimen's description

The experimental study aimed to investigate the structural behavior of bolted and adhesively bonded connections between glass fiber reinforced polymer (GFRP) pultruded I-profile. A total number of 9 specimens were fabricated and tested. To label experimental specimens, the format 'abcd' is defined, where 'a' shows the angle between the two parts of GFRP profile: 120˚ or 160˚ defined as the extreme values of the suitability range to produce arched structures which was the final application aim of a larger research program this particular connection study belongs to, 'b'

indicates where the connection was placed: web-W or web&flange-WF, 'c' defines the type of connection: bolted-B connection or adhesively-A connection.

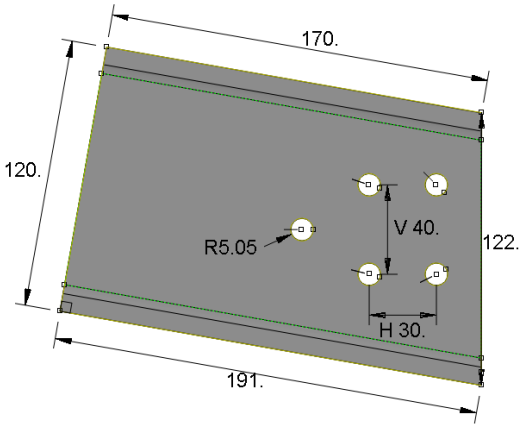

FRP Part (for angle of 160˚)

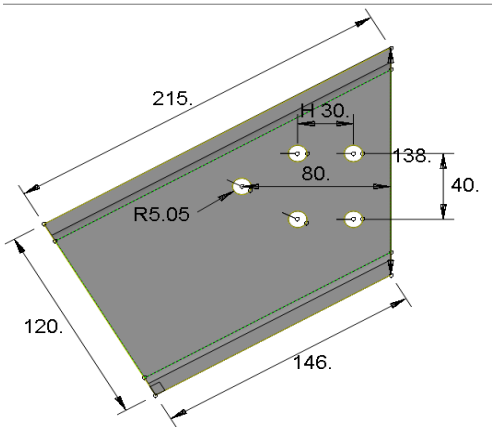

FRP Part (for angle of 120˚)

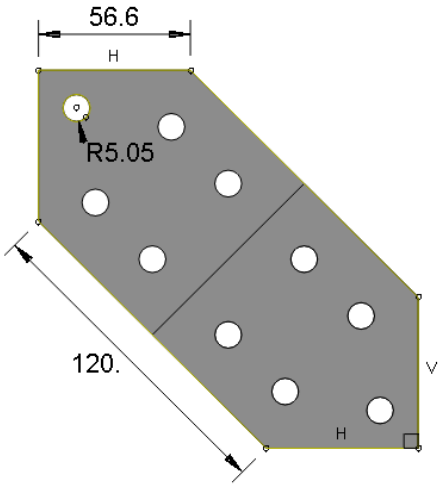

Connection part

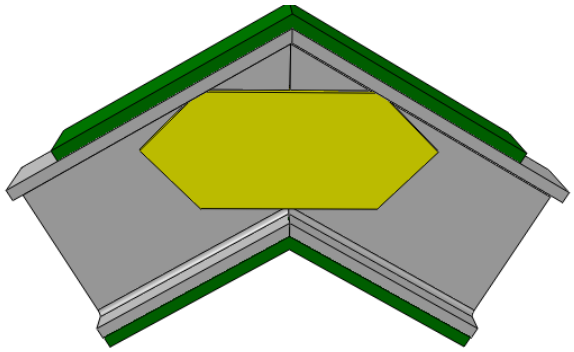

120WFAO specimen

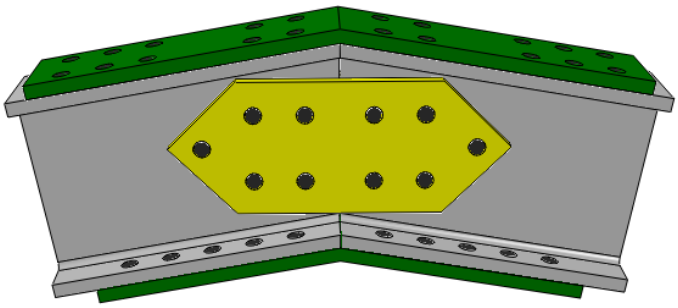

160WFBO specimen

Figure 33. The geometry of the specimens (dimensions in mm)

It was expected that bolted connection had more deformability but better durability in high moisture environment respect to adhesive connection, so assessing the stiffness of bolted vs. adhesive connection was required. Finally, 'd' shows the direction the load was applied: as per open-O the angle of the joint or to close-C it. One specimen 120WFBO was duplicated (120WFBO-2) in order to check the repeatability of the producing and testing procedures. Table 14 presents the specimens details. It shows the all details of the geometry of the parts used to mount the specimens. Table 14 shows the geometry of the specimens.

Table 14. Details of the FRP connection specimens

Specimen	Angle (º)	Connection position	Connection type	Force direction
120WAO	120	web	Adhesive	open
120WBO	120	web	Bolt	open
120WFAO	120	web & flange	Adhesive	open
120WFBO	120	web & flange	Bolt	open
120WFBO-2	120	web & flange	Bolt	open
160WBC	160	web	Bolt	close
160WBO	160	web	Bolt	open
160WFBC	160	web & flange	Bolt	close
160WFBO	160	web & flange	Bolt	open

Testing procedure

One of the two halves of each specimen was completely fixed to an external restraining structure, whereas the other halve was free to move and it was only restrained by the studied joint. Force was applied horizontally at 50mm in vertical from the free edge of the non-constrained halve. A hydraulic actuator with a 100 kN of force range was used. A steel cylinder coupled to the hydraulic actuator was used as lineal loading tool. Test was displacement controlled and the load was indirectly applied through an imposed horizontal displacement at 1 mm / min. A rosette strain gage (3 strain gages of 120Ω at 45º and 90º connected with 3 wires and temperature-compensated for glass composites) was placed on the central point of the joint (web connector of one side of the connection) so to determine the main strain values and their directions.

Test was displacement controlled and the load was indirectly applied through an imposed horizontal displacement. Figure 34 presents an overview of the GFRP-GFRP connection tests.

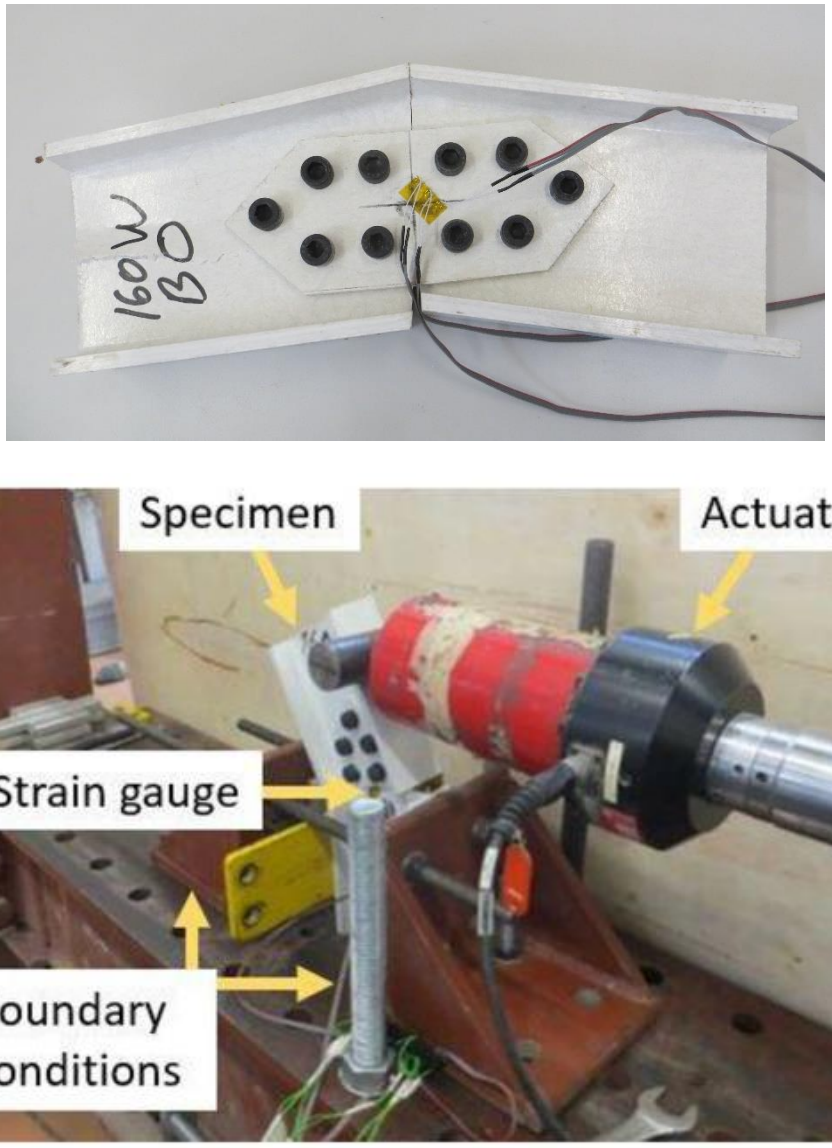

Figure 34. GFRP-GFRP connection tests used

Results and discussion

Table 15 summarizes the main experimental results including maximum load-bearing capacity (F_{max}), horizontal displacement of the load application point at the maximum force (d_{max}), maximum and minimum principal strain values in the central point of the web connector at the maximum force (ε_1 and ε_2) and orientation of this strain vector with respect to the longitudinal symmetry axe of the connection plate (θ_1). Finally, the failure mode is also included in Table 15. All bolted specimens failed because of local web-to-flange shear failure (see Figure 35b) whereas all bonded specimens failed because of debonding of the web connection plate (see Figure 35a).

Table 15. Main experimental results

Specimen	F_{max} (kN)	d_{max} (mm)	ε_1 (x10-6)	ε_2 (x10-6)	θ_1 (º)	Failure mode
120WAO	1.53	10.36	152	-237	77.6	Debonding failure
120WBO	13.01	34.56	1610	-1516	7.7	Local failure
120WFAO	2.76	13.22	10.3	-1	97.0	Debonding failure
120WFBO	12.36	33.15	577	-185	4.1	Local failure
120WFBO-2	12.48	20.25	394	36	9.7	Local failure
160WBC	14.00	43.63	1660	-1945	36.4	Local failure
160WBO	11.88	28.77	1533	-1051	40.1	Local failure
160WFBC	15.01	55.52	182	-579	82.3	Local failure
160WFBO	14.96	35.52	1711	-1719	38.8	Local failure

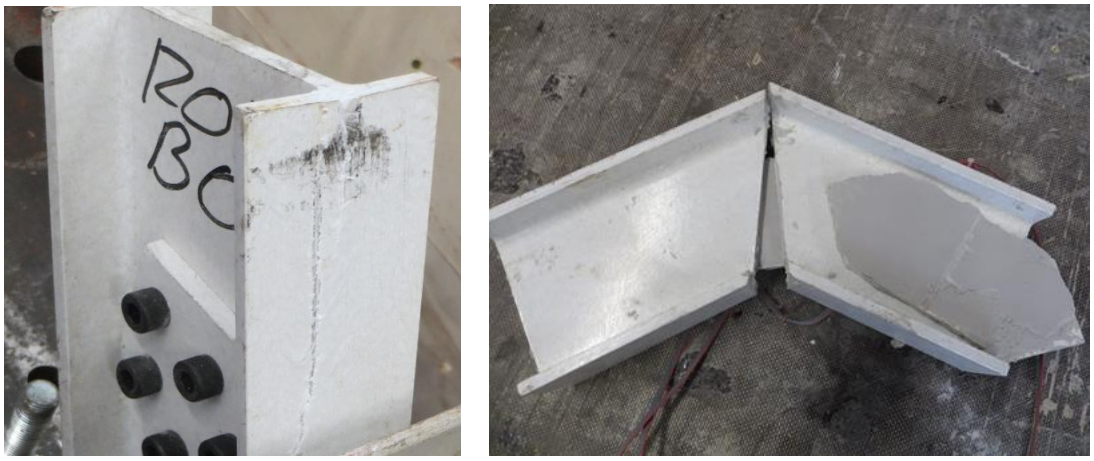

(a) **(b)**

Figure 35. Failure modes (a). Local failure (b). Debonding failure

The first qualitative experimental result was that the load-bearing capacity of adhesively connected joints was far lower than bolted ones around five times for the tested specimens. The second observation showed there was no clear influence of adding the flange connection to the web one in terms of load-bearing capacity, although flanges-connected specimens were stiffer.

Figure 36 represents the force-displacement plots of all specimens. It can be seen that all the graphs had an uptrend. Some cases (120WBO, 160WBC and 160WBO) showed continuous saw-like curve associated with the progressive settling of bolted connection with imperfect holes that allowed certain punctual sliding that was traduced into a force decrease that was automatically restored to the previous force because the rest of the bolts bore the released force. This phenomenon is supported by the fact that no external additional displacements were recorded during these responses. The maximum load-bearing capacity was reached by the 160WFBC specimen (15.01 kN) and the 120WAO specimen reached the lowest ultimate load (1.53 kN).

Figure 37 shows the first principal strain-displacement plots for all specimens. Observing the plots, it is clear that the connection plate played its role assuming and transmitting increasing stresses between the two halves of the connection during mechanical testing.

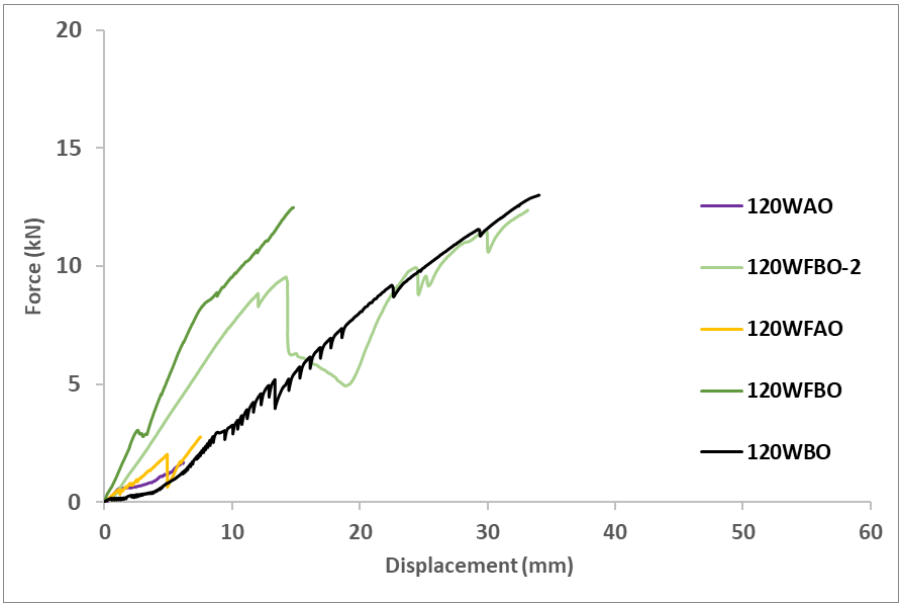

(a)

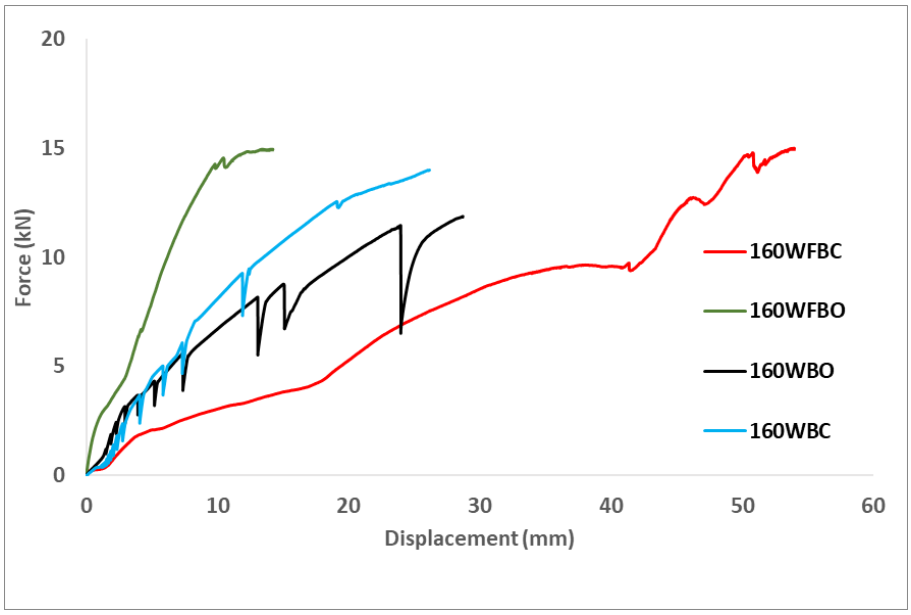

(b)

Figure 36. Force-displacement plots (a): specimens with the angle of 120˚ (b): specimen with the angle of 160˚

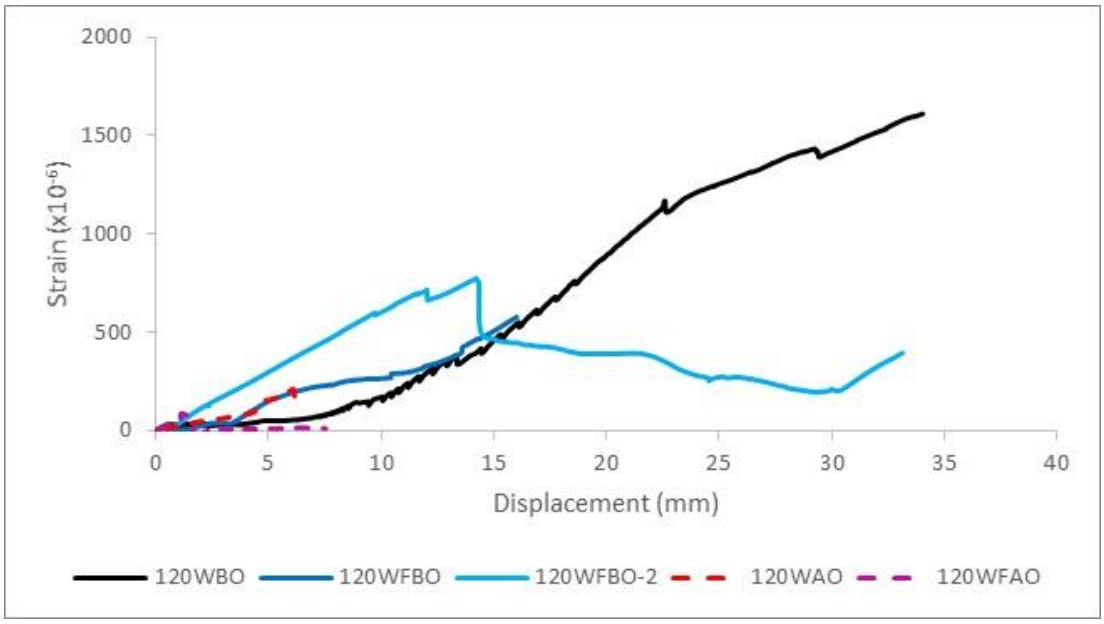

(a)

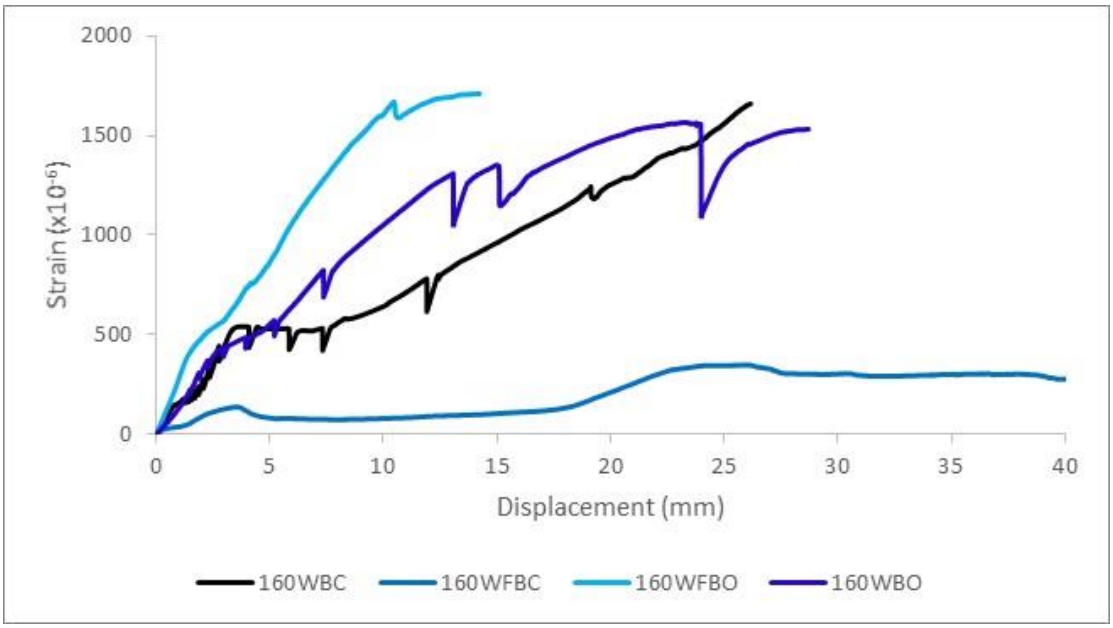

(b)

Figure 37. Strain-displacement plots (a): specimens with the angle of 120˚ (b): specimens with the angle of 160˚

3.3.2 GFRP-Mesh connection test

Specimen's description

Once the connection between profiles has been experimentally characterized, we proceed to describe the testing method to study the adherence between FRP profiles and mesh.

First of all, GFRP profiles are connected to mesh with two methods:

- Use of adhesive, resin.
- Use of mechanical joint, screws.

Only glass fiber mesh was considered for these tests according with the results on FRCM specimens, reported later on. Details of the two connection methods are included in the next subsections:

a. Adhesive connection

Six specimens were produced. Three of them were tested without any further modification but the other three were subjected to high temperature. To produce these specimens, GFRP profiles were cut into a length of 60mm so the upper part and the base of the specimen had dimensions of: 6 x 6 cm. The mesh piece was made up of 3 strands duly trimmed, in order to avoid possible threads loose that could alter the development of the test. Masterbrace P3500 resin was applied on the top part of GFRP profile piece and the mesh was bonded to it. Later, the free ends of the piece of mesh were encapsulated with the same resin and fiberglass chopped short fibers that produced an FRP that allowed to clamp the mesh without producing damage on the fiberglass tows. The specimens were tested by pulling the mesh from the encapsulated end until sliding or breaking.

b. Mechanical connection

The same procedure than for adhesive connections was followed to produce mechanical connections specimens except for the fact that the position of screws was limited by the geometry of the profile: the proximity to the web of the profile or to the edge of the flange could alter its behavior, either tilting the screws or not allowing their proper fit.

For this reason, the mechanical components used in the test had to respect safety margins with respect to the core of the I-profile, following the criteria established in the steel standard by analogy (Ministerio de Fomento, 2012). Thus, according to the standard, the components that should have been used to obtain correct mechanical adhesion of the mesh are from M6 series, resulting in 40mm interaxle separation.

Thus, according to the standard, the components that should have been used to obtain a correct mechanical adhesion of the mesh are:

- Metric 6 screws properly spaced.
- Metric 6 washers for top of face.
- Metric 6 washers for bottom of face.
- Metric 6 nuts for the bottom of the face

The scheme is shown in Figure 38, based on what is specified in the standard, the following scheme is obtained:

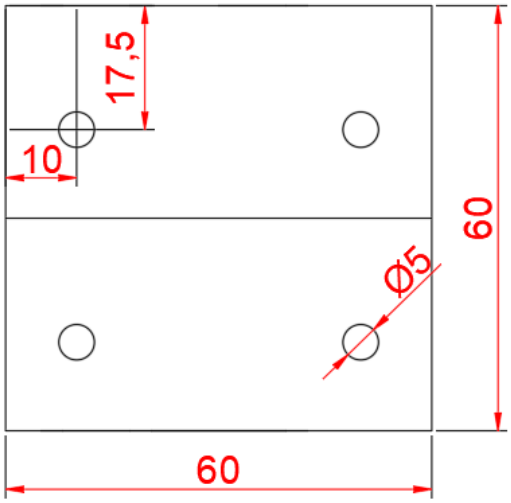

Figure 38. Position of the screws in the mechanical connection seen from the top floor (all dimensions in mm)

Figure 39 Shows specimens for both connection types.

The nomenclature of GFRP-Mesh connection specimens is the following:

- MPR: resin bond
- MPR-F: bond with heat-treated resin
- MPM: mechanical joint
- MPM-F: heat treated mechanical joint

Figure 39. Specimens with mechanical connection (left) and adhesive connection (right)

Testing procedure

Test configuration followed the characteristics of a pull-out test. During the test, it is necessary to transmit the forces of the meshes to the profiles, ensuring good adhesion between these two components and determining the optimal connection method. To carry out these tests, FRP profiles with a length of 6 cm have been used to connect to the 20 cm long pieces of mesh.

Apart for the pull-out tests on pristine specimens, these tests were repeated after imposing high temperature conditions (200ºC for 4 h) to assess the influence of temperature increase on this connection.

To perform the test, GFRP profile pieces were fixed and the free encapsulated end of the mesh was clamped with the clamps of 100kN range hydraulic actuator. Meshes were pulled at a constant speed of 1mm/min and force and displacement were simultaneously recorded at 50Hz.

Figure 40 shows GFRP-mesh test configuration.

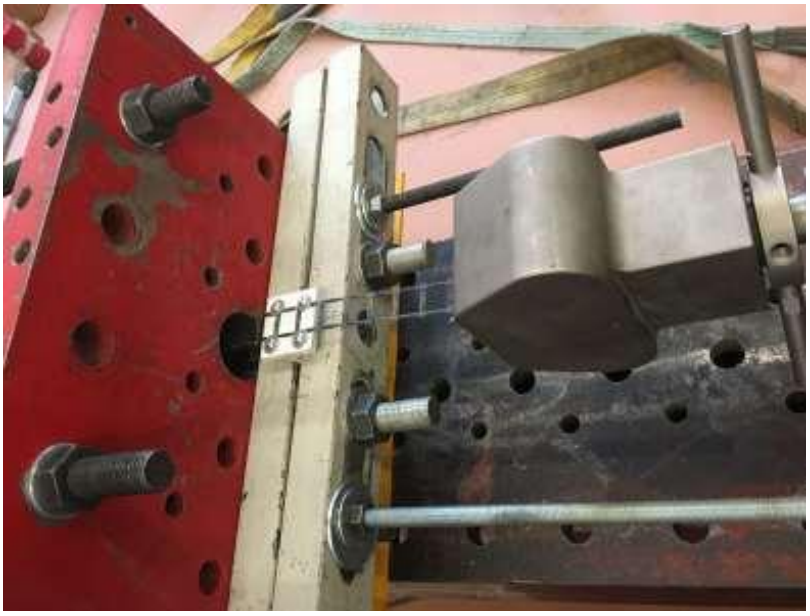

Figure 40. GFRP-mesh test configuration

Result and discussion

Once the test has been explained, the results obtained are analyzed and discussed as follows:

The failure mode was the same in all MPR cases, being a failure of mesh breakage. In the MPM cases, the sliding between the two materials occurred.

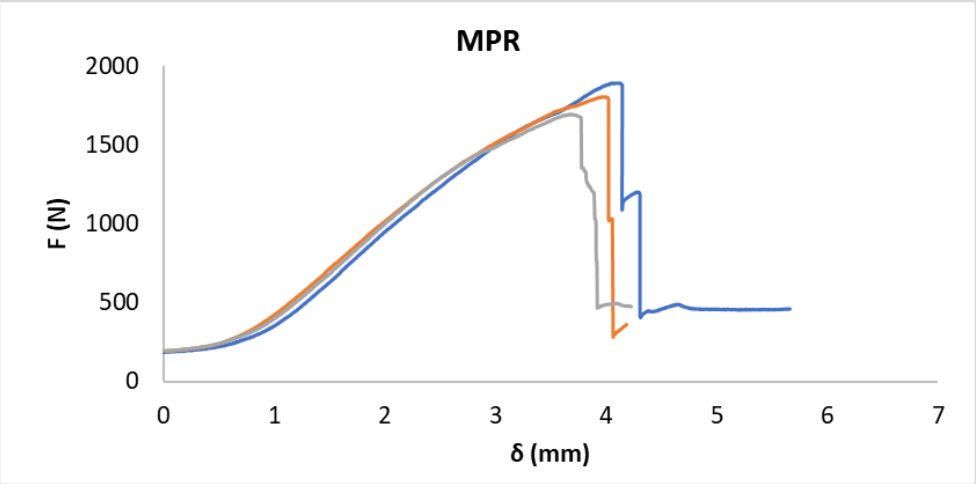
MPR
2000
1500
1000
500
0
F (N)
0
1
2
3
4
5
6
7
δ (mm)

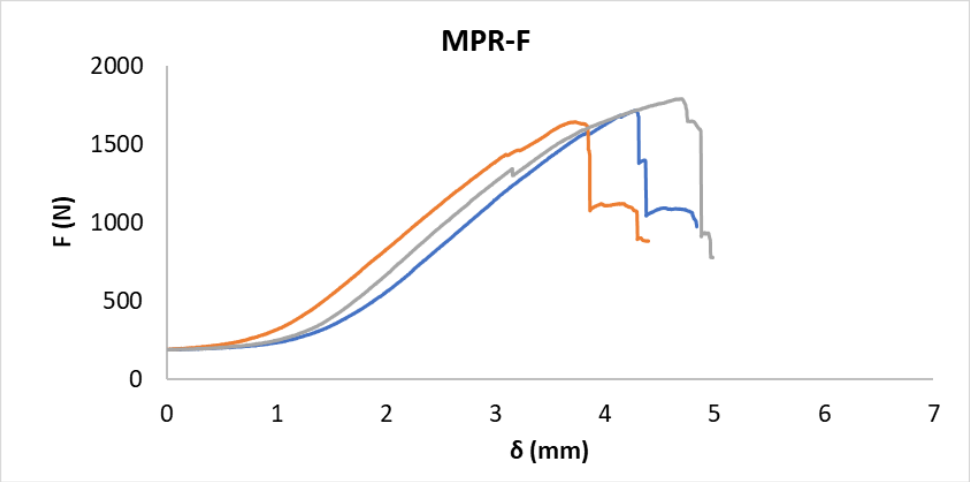
MPR-F
2000
1500
1000
500
0
F (N)
0
1
2
3
4
5
6
7
δ (mm)

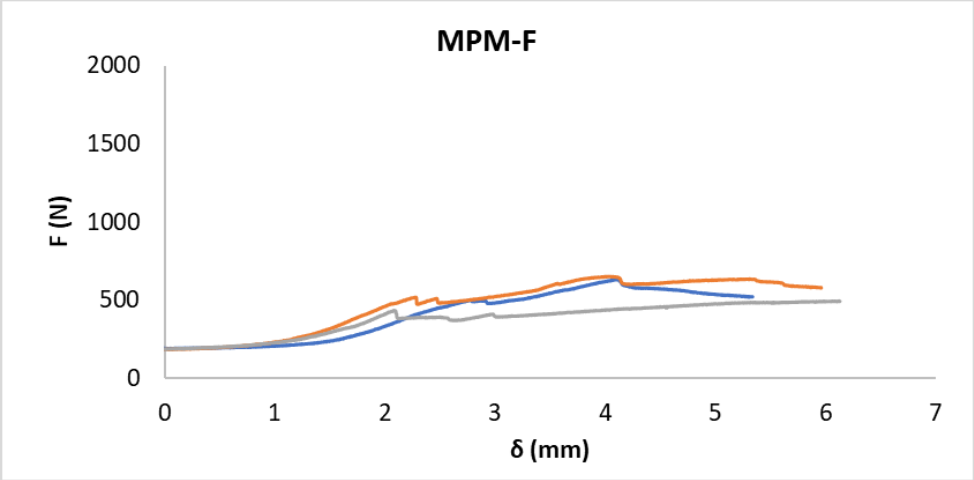
MPM-F
2000
1500
1000
500
0
F (N)
0
1
2
3
4
5
6
7
δ (mm)

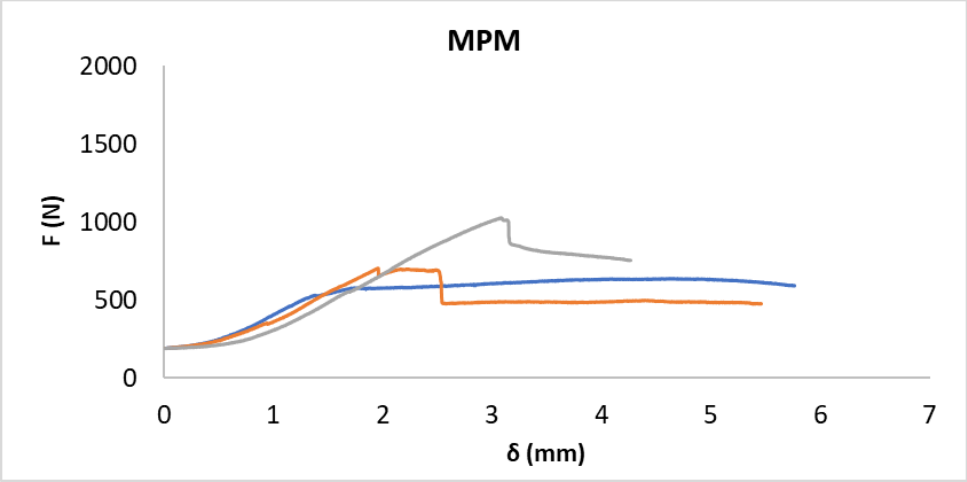

Figure 41. Force-Displacement curve for GFRP-Mesh connection specimens

It can be seen in Figure 41 that an initial displacement occurs that has not been taken in account in the post-processing due to the fact that it is a repositioning of the profiles until fixing the specimen completely. On the other hand, a difference is observed in the behavior of the two types of joints: in the case of resin, it has a linear behavior until breakage where it cannot bear any load, while in the mechanical joint the constant force is maintained due to sliding between the mesh and the bolt.

Table 16. Results of GFRP-Mesh connection test

Specimen	No.	Maximum force f_{max} (N)	Young's modulus E (MPa)
MPR	3	1800.1 (5.6%)	513.2 (0.6%)
MPR-F	3	1717.5 (4.3%)	540.6 (1.1%)
MPM	3	789.9 (26.5%)	335.3 (0.9%)
MPM-F	3	594.0 (14.4%)	221.1 (2.4%)

(%) = Coefficient of variation

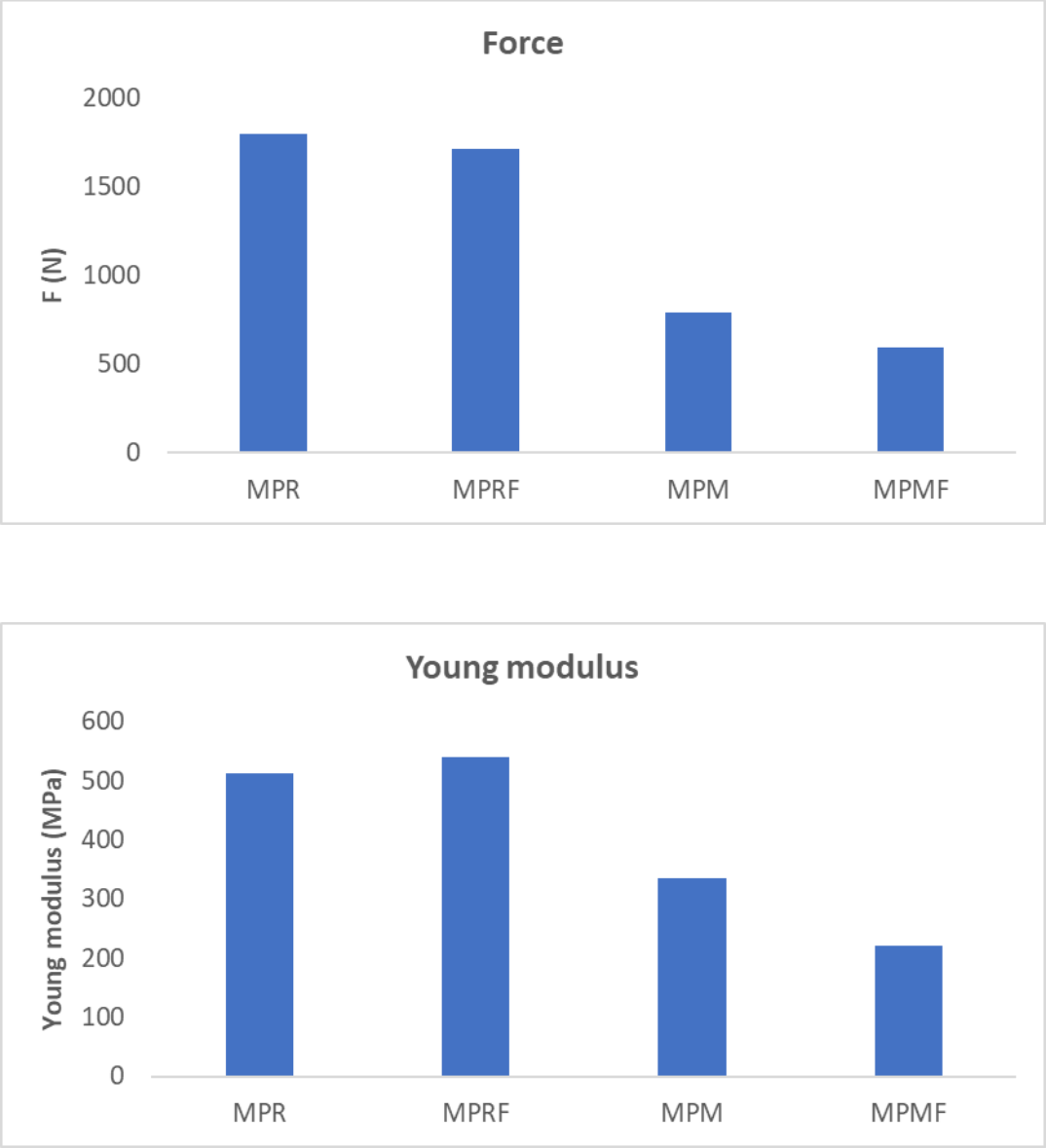

Figure 42. Comparative graph of the maximum F and E for GFRP-Mesh connection specimens

Table 16 and Figure 42 compare maximum force and young's modulus for each specimen. From the results it is obtained that the best type of union is by means of resin, being able to resist 227% with respect to mechanical bonding. On the other hand, the temperature element in the case of resin does not reduce its properties significantly, 4.6% less in the case of maximum force, although in the case of the modulus of elasticity increases 5.2%.

3.3.3 Mesh-Mortar connection test

Specimen's description

Four types of FRCM specimens, with different mesh-mortar combinations, were produced following the procedure that was previously implemented in previous researches (Bernat-maso *et*

al., 2018) but with some specific changes to integrate the externally projected/dropped mortar. Specimens were designed with the aim of determining FRCM mechanical response through tensile tests. These specimens were 400 × 50 × 9 mm. Additionally, 4 specimens of the combination which showed the best results were subjected to high temperature to assess the influence of this phenomena. The particularity of the FRCM specimens tested in the current research is that mesh was previously subjected separated from the bottom of the mold and mortar was "projected" on it. Detailed production procedure was as follows:

1) Preparing the wooden molds with the free available space to produce the specimens.
2) Fixing the reinforcement mesh to the mold so it stands at 5mm from the bottom surface.
3) Mixing the mortar.
4) Dropping the mortar from 1m height respect to the base of the mold to simulate the projection technique.
5) Remove the excessive mortar and assure a plain surface at the endings.
6) Cure for one week covered by plastic at indoor laboratory conditions with daily moistening of the surface by water spraying.
7) Removing from the mold and left it two cure for three more weeks.
8) During these three weeks curing, four steel plates were bonded on the endings of the specimen (two per ending with a contact length of 100mm) to generate the subjection tooling. Loctite 3425 was used to bond these plates. Figure 43 shows the placement of support plates. These plates left 200mm of free length of FRCM to be tested.

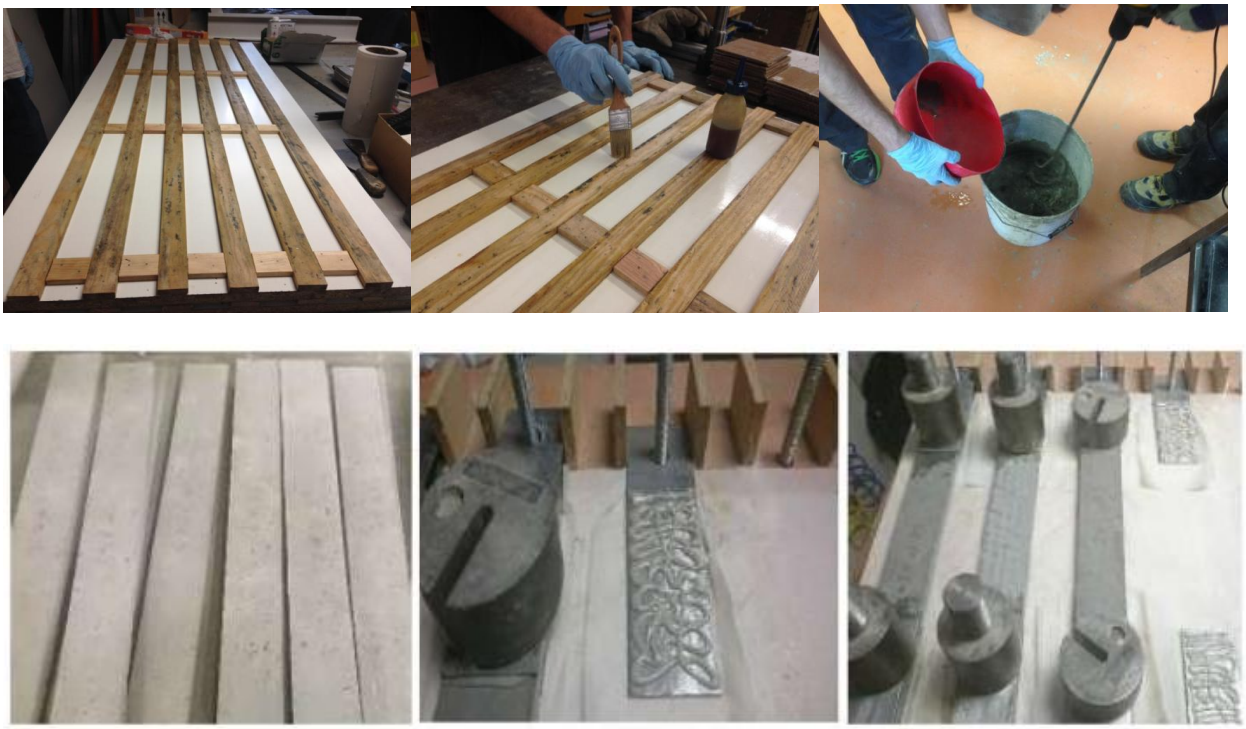

Figure 43. Top: production. Bottom: placement of support plates

After 28 days of curing, the specimens were tensile tested. For these tests, an electromechanical press of 10 KN capacity was used, as shown in Figure 44 .Specimens were connected to the testing machine by double hinged connection to assure that the stress transfer mechanism between the specimen and the plates was performed by tangential stress. This system was chosen for this study because it reproduces the behavior that FRCM materials present in the field, as it allows the mesh to slide, while contrary to a clamp system, where mesh slippage is limited by the compression of the mechanical grippers.

Testing procedure

The FRCM specimens were tested taking as reference the procedure described by AC434-0213-R1(ICC Evaluation Service Inc., 2016). Tests were conducted by displacement control at a ratio of 5 mm/min. An extensometer (25mm range) was placed on a movable system attached to the support plates via two magnets, that allowed to measure the deformations in the area located between the edges of the support plate of the test, so with a base length of 200mm. Force, displacement of the press and displacement of the extensometer were recorded at 5Hz.

Figure 44. Tensile test setup configuration

Result and discussion

The obtained results were processed and analyzed, with calculation tools (Excel). The data recorded from the tensile tests were the applied force on the specimens and the displacements measured by the extensometer associated with these. From these data it was possible to make the stress-strain curve and also identify the ultimate stress and the peak deformation.

The ultimate tension was calculated with the equation:

$$\sigma_u = \frac{F_u}{A_{Mesh}} \quad \text{Eq 6}$$

And the peak deformation was obtained:
Where:

$$\varepsilon_{pic} = \frac{\Delta L_u}{L} \quad \text{Eq 7}$$

F_u: maximum load
A_{mesh}: Cross section of the mesh
ΔL_u: extensometer displacement at breaking
L: Initial length of the extensometer

The fluidity of the Axton mortar allowed a better coating of the glass fabrics, but in the case of the carbon, the small size of the fabric squares did not allow an effective coating.

Due to the projected application (dropped) of the mortars, the specimens showed a certain curvature, which implied that the strain measurements with the extensometer were not precise because of sliding of this measurement tool. Because the deformations measured with the electromechanic press were significantly higher than real ones but proportional, a relationship between the deformations measured with the extensometer and with the press was carried out for previous specimens produced without dropping mortar. This approach made it possible to obtain displacements and strains that were more consistent with the strains of the tufts of the meshes. Selected Sika mortar could not be projected (dropped) efficiently.

The FRCM specimens subjected to fire failed due to a premature loosening of the mortar, which was greatly affected by the fire.

Figure 45 shows the failure modes of tested specimens. To more precise, the left picture shows bad penetration of sika mortar between mesh. The center picture presents the tooling used for extending the range of the extensometer so to capture the average strain of the full sample and finally, the right picture demonstrates multiple cracking of an Axton-glass sample that worked properly.

Figure 46 shows the stress-strain curve for each specimen in Mesh-Mortar connection test and

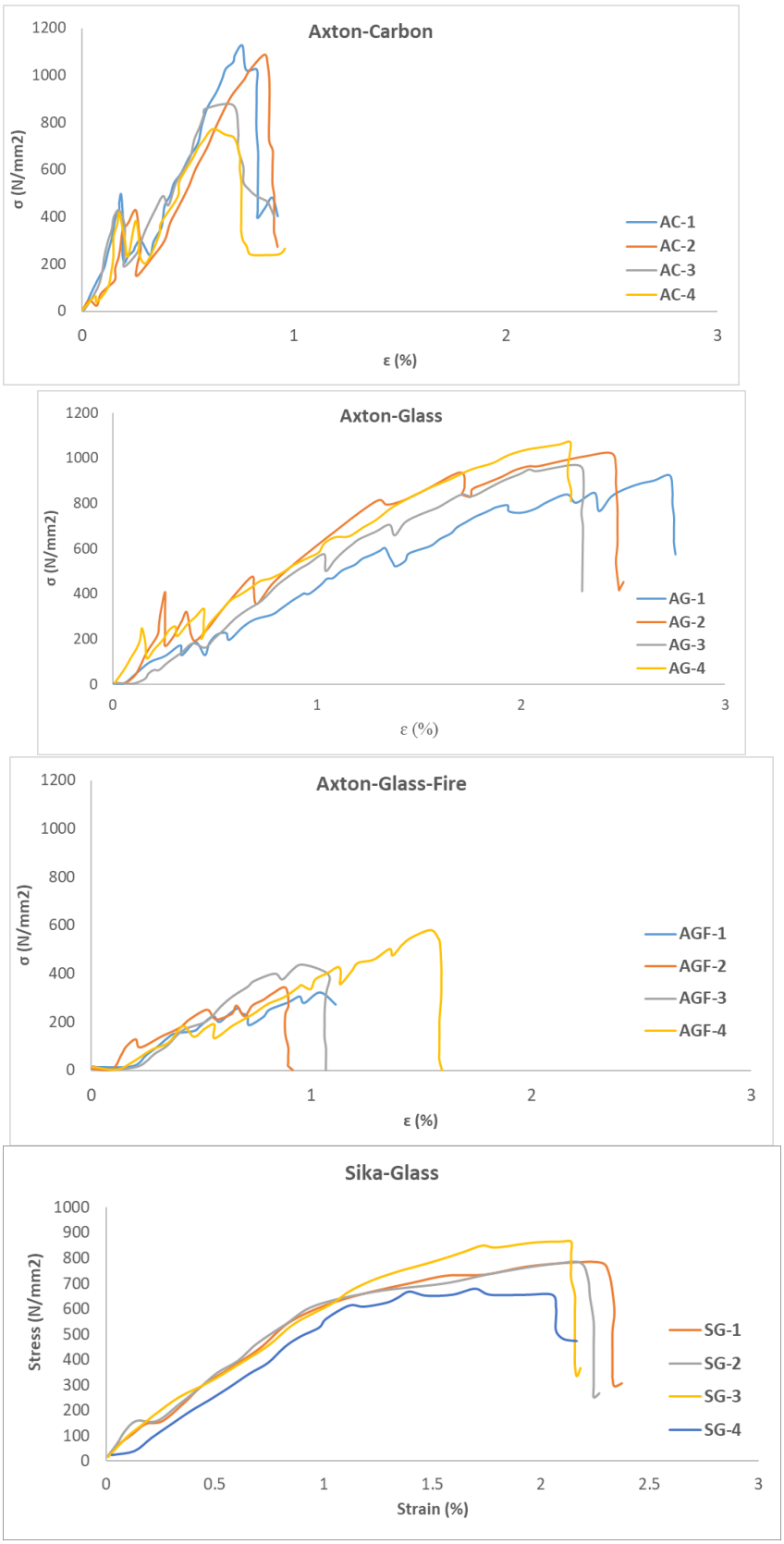

Figure 46. Stress-strain graph for the tested specimens

Table *17* summarizes the results of Mesh-Mortar connection tests and the average of maximum stress is shown for each specimen type. Maximum stress is obtained between the carbon meshes and glass, however, glass displacements are greater. For this reason and that the geometry of the glass mesh allows the mortar to be projected more easily due to the larger holes, the glass mesh was selected to perform the following specimens. In the case of mortar, comparing the ones made of glass mesh, better results were obtained with Axton. Finally, the influence of durability due to temperature is very noticeable, decreasing by 54% the tensile strength and 50% the ultimate displacement. This large decrease in properties can become a problem in the event of fires, requiring an insulating surface protection and fire retardant.

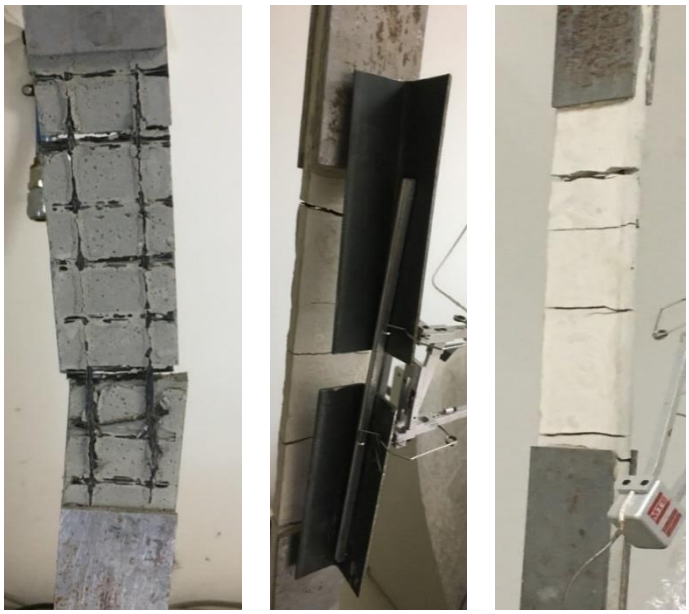

(a) **(b)** **(c)**

Figure 45. The failure modes of tested specimens

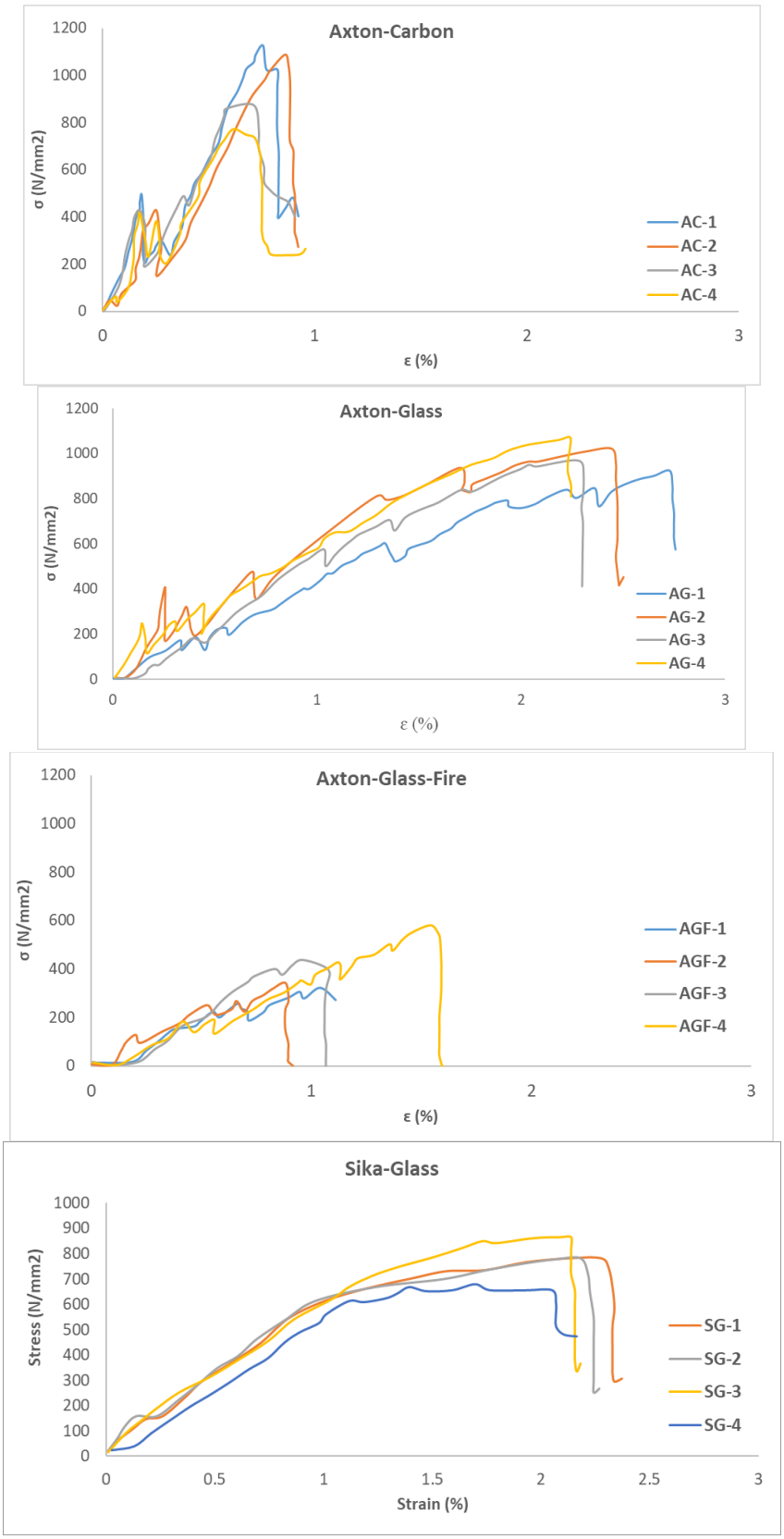

Figure 46. Stress-strain graph for the tested specimens

Table 17. The result of Mesh-Mortar connection tests. Coefficient of variation in brackets.

Specimen	Area of tissue (mm^2)	σ_{max} (MPa)	$\varepsilon_{h,\,pick}$ (%)
Axton-Carbon	2.35	1137.45	0.76
		1098.30	0.86
		893.62	0.71
		777.02	0.64
		976.6 (15%)	(11%)
Axton-Glass	2.1	931.90	2.74
		968.57	2.04
		938.10	2.04
		1037.14	2.04
		968.93 (14%)	2.21 (14%)
Axton-Glass-Fire	2.1	350.48	1.05
		370	0.88
		461.90	0.97
		599.05	1.54
		445.36 (22%)	1.11 (23%)
Sika-Glass	2.1	770.95	2.04
		771.90	2.03
		860.95	2.03
		662.38	1.69
		766.55 (9%)	1.95 (8%)

4

Experimental characterization of hybrid panel

4.1 Introduction

The current study shows the experimental investigation of hybrid FRP-FRCM structural elements composed of pultruded GFRP profiles, glass fiber mesh and projected mortar, together with the interactions between these components. There are not available publications about hybrid FRP-FRCM systems as per author knowledge.

This chapter describes the experimental research carried out to study hybrid FRP-FRCM superficial structural elements made of arched structures of straight pultruded glass fiber-reinforced polymer (GFRP) profiles that are connected to FRCM panels to provide a thin plate solution. The developed structural system can be applied for tunneling sustainment because of benefitting from FRCM deformability capacity and GFRP durability, light-weight and reduced cost.

All the tests have been performed by the author at the Laboratory for the Technological Innovation of Structures and Materials (LITEM) which is part of CATMech – TECNIO research group. It is located in Universitat Politècnica de Catalunya – Campus de Terrassa.

4.2 Material

All materials used in these experiments were reported in the previous chapter and are fully described in the section 3.2.

4.2.1 Specimen's description

Once the behavior between the different parts was characterized, test on two representative elements of the proposed hybrid GFRP pultruded profile – projected FRCM were conducted.

The experimental program consisted of two hybrid panels with different geometry (see Figure 47). Both panels were made of IPE 120 GFRP profiles and FRCM composed by fiber glass mesh and

mortar. Steel bolts were used to connect GFRP profiles among them. The angles between GFRP profiles (120˚ and 130˚) were selected to fall into the range of 120˚-160˚, which was set to cover possible arched sustainment solutions of real some sections.

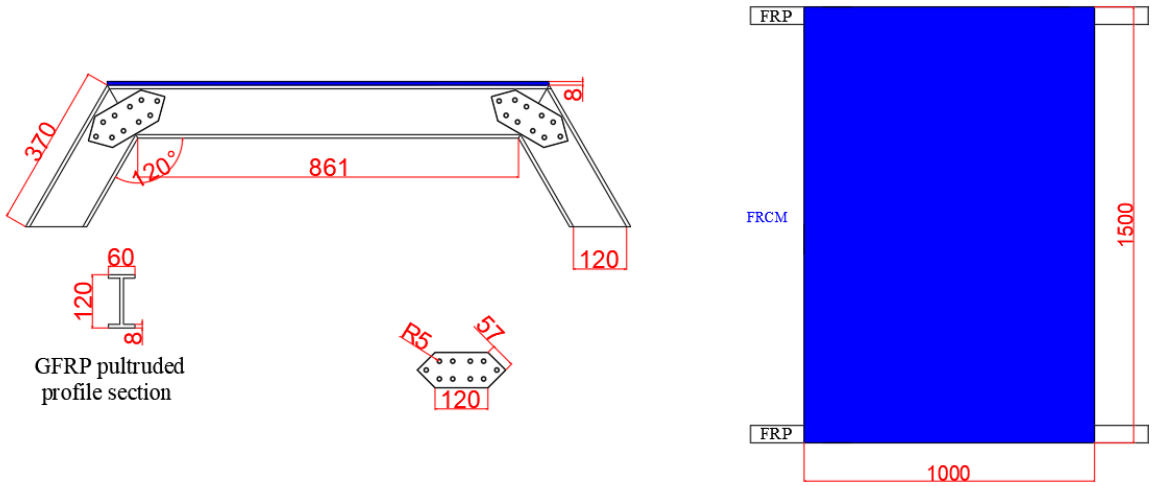

Lateral view **Top view**

Specimen "HP1"

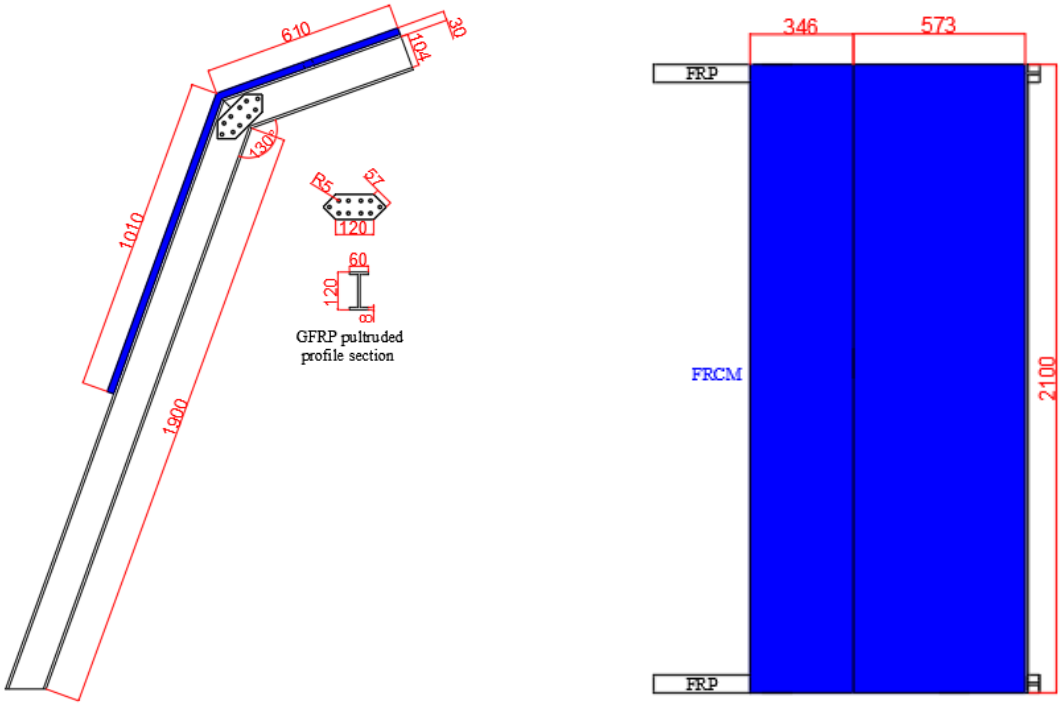

Lateral view **Top view**

Specimen "HP2"

Figure 47. The geometry of the hybrid panel (dimensions in mm)

The manufacturing process consisted of the following steps:

a. Cutting GFRP profiles to the desired length and angle, drilling the holes for the connection. Repeating the process for the connection plates.
b. Connecting GFRP profiles with a bolted connection including a connection plate at both sides of the web. Fixing GFRP profiles to the external reaction frame.
c. Bonding the fiber fabric onto the top part of the top flange of the corresponding GFRP profiles to the desired length.
d. Installing a wooden formwork (HP1) or a foam back surface (HP2) to support the production of the FRCM plate.
e. Casting (HP1) or spraying (HP2) mortar over the fiber grid to produce the FRCM plates.
f. Curing mortar for 28 days with daily superficial water spraying during the first week.

HP1 case

Primely, the test aimed to investigate the real behavior of the hybrid structures, as well as to determine the weaker connection. Although it was not intended to test the full number of mechanisms that may contain a future final application of large tubular-like structures, a significant sample including all previous tested mechanism was defined. The test consisted of two separate arched beams (GFRP pultrude profiles) joined by properly overlapped meshes, which were embedded into projected mortar.

In order to build the experimental specimens, the best configuration was selected based on the characterization carried out in the previous tests, which corresponded to the following characteristics:

- GFRP-GFRP bolted web connection at 120º
- GFRP-Mesh adhesive connection.
- FRCM composed by Axton mortar and Mapegrid G220 mesh.

The prototype dimensions were 1.5m between the edges of the FRP ribs and 1m width of the FRCM par. The height between the lower part of the web and the ground was delimited at 20 cm so that the sensors could be positioned correctly during the test. GFRP profile connection is shown in Figure 48.

Once the two ribs were made, steel plates were placed in the lower part of the web by means of the two-component epoxy resin, Loctite 3425. The function of these plates was to restrain the horizontal displacement of the GFRP profiles in transversal to the rib's direction. Then, ribs were presented in their final position and the mesh was placed. However, as both upper beams were 1 meter long, the mesh was not wide enough to join them, resulting in a discontinuity in the material solved by defining 20 cm overlap between meshes, which also allowed to study this particular case of mesh overlapping. To ensure that the meshes were tensioned during the drying of the resin that connected them to the top part of GFRP profiles, various weights were placed in the extremes.

Figure 48. GFRP rib joint

Figure 49. Placement of the plates

(a) **(b)**

Figure 50.(a)Placing the plate support, (b) Tension load on Mesh

To project the mortar, a wooden form was made so the mortar would not come off by the sides. The mortar was projected in the same way as described in section 3.3.3 forming a 16 mm thick

layer with the fiberglass mesh in the center. After 7 days the mold was removed, and after 30 days from the production date, specimen was tested. The process of making hybrid panel is presented in Figure 51.

Metal spacers and Glass mesh

Pouring mortar

Mortar in curing phase

Figure 51. The process of making hybrid panel

The structural characterization test consisted of applying an imposed displacement and registering the reaction force and the structure deformation at 50Hz.

Specimen HP1 was simply supported on thin rubber pads that restrained horizontal displacements of the supporting endings. In addition, it was longitudinally restrained by fixing the horizontal GFRP profiles to the external load frame (see Figure 55). For testing specimen, a hydraulic actuator (250kN of force range) was used to apply the displacement at midspan of the FRCM plate at a rate of 1mm/min. This action was distributed along the width of the specimen with a loading beam (HEM 200) that had an aluminum profile and a bar under it so as to concentrate the applied load in a line that was precisely placed at the desired position (see Figure 55).

The displacement of the actuator was measured with an internal LVDT of 250mm range and 0.2% linearity. In addition, there were 7 sensors which were used to monitor the test in specimen "HP1". 6 potentiometer sensors (10 cm range and 0.02% accuracy) were spread under the FRCM plate: 3 sensors were placed along each side edge at 8 cm apart from the edge (see Figure 55) and separated 25cm among them in the longitudinal direction with the central one centered under the displacement imposition line. In the longitudinal direction one LVDT with a 20 mm range and 0.02% accuracy was placed in contact with one of the horizontal GFRP profiles, at its central position, to control the effectiveness of the longitudinal fixation of the specimen to the loading frame.

HP2 case

The goal of the testing second hybrid panel (HP2) was to study the mechanical behavior of the hybrid structures with different shape. The test comprised of two distinct arching beams (GFRP pultrude profiles) linked by suitably overlapping meshes embedded in projected mortar.

In order to construct the experimental specimens, the optimal configuration was chosen based on the previous tests' characterization, which matched to the following features:

- GFRP-GFRP bolted web connection at 130º. Figure 52 depicts a GFRP profile connection.
- GFRP-Mesh adhesive connection.
- FRCM composed by Sika mortar and Mapegrid G220 mesh.

The prototype's sizes were 2.1m between the FRP rib edges and 2m height. The structure had 2 FRCM sections corresponding to the two plain surfaces. These were continuously produced so there was complete mesh and mortar continuity among them.

Glass fiber mesh was placed on top of the FRP profiles and adhesive was placed to bond it. Loctite 3425 was applied with the help of a brush, so the adhesive was better distributed between the profile and the mesh. Everything followed by baking paper to avoid the bonding to the tolling required to apply pressure on the bonded connection during curing time, which were applied with a sheet of rubber to uniform stress distribution and wood pieces fixed with F-clamps, as shown in Figure 53. Over it, polystyrene pieces were placed to simulate the background on which the mortar was going to be projected and a plastic cover was finally placed to prevent spreading mortar out of the working area (see Figure 53).

Figure 52. GFRP rib joint for HP2

Figure 53. Porexpan plates placed on the fiberglass meshes

The projection of mortar began with the preparation of the mixture in the concrete mixer, which were three batches of mixing. the first mix, it was made up of 3.5 sacks of mortar, 12 liters of water and 75 ml of accelerator for each liter of water. The second for 4.5 sacks of mortar, 14 liters of water and 75 ml of accelerator for each liter of water. And the last one for 2.5 bags of mortar, 12 liters of water and 75 ml of accelerator for each liter of water. Before emptying each mix from the concrete mixer, the technician in charge of the mortar spraying machine, empirically assessed if the consistency of the mortar was the correct one to project it. The projection was carried out in three batches, one for each mixture. Throughout the process, only one problem had to be solved, which was assuring that the mortar projected on the upper part will (upside-down position) sticked to the polystyrene and covered the mesh completely, since it came off under its own weight for thicker layers. To do this, while a person projected the mortar, another one compacted the mortar with a trowel. All producing and manufacturing processes of mortar are presented in Figure 54.

The curing phase of the mortar lasted a total of 28 days. During that time the background plastic protection and the structure supporting the polystyrene were removed. Polystyrene could not be

separated from the FRCM, due to sticking to it. This issue problem did not affect the study of the structure, since its rigidity is negligible against the mechanical properties of FRCM. Also, during this time, the FRCM was wept moist daily with a sprayer filled with water, in order to prevent cracks from appearing in the curing process of the mortar.

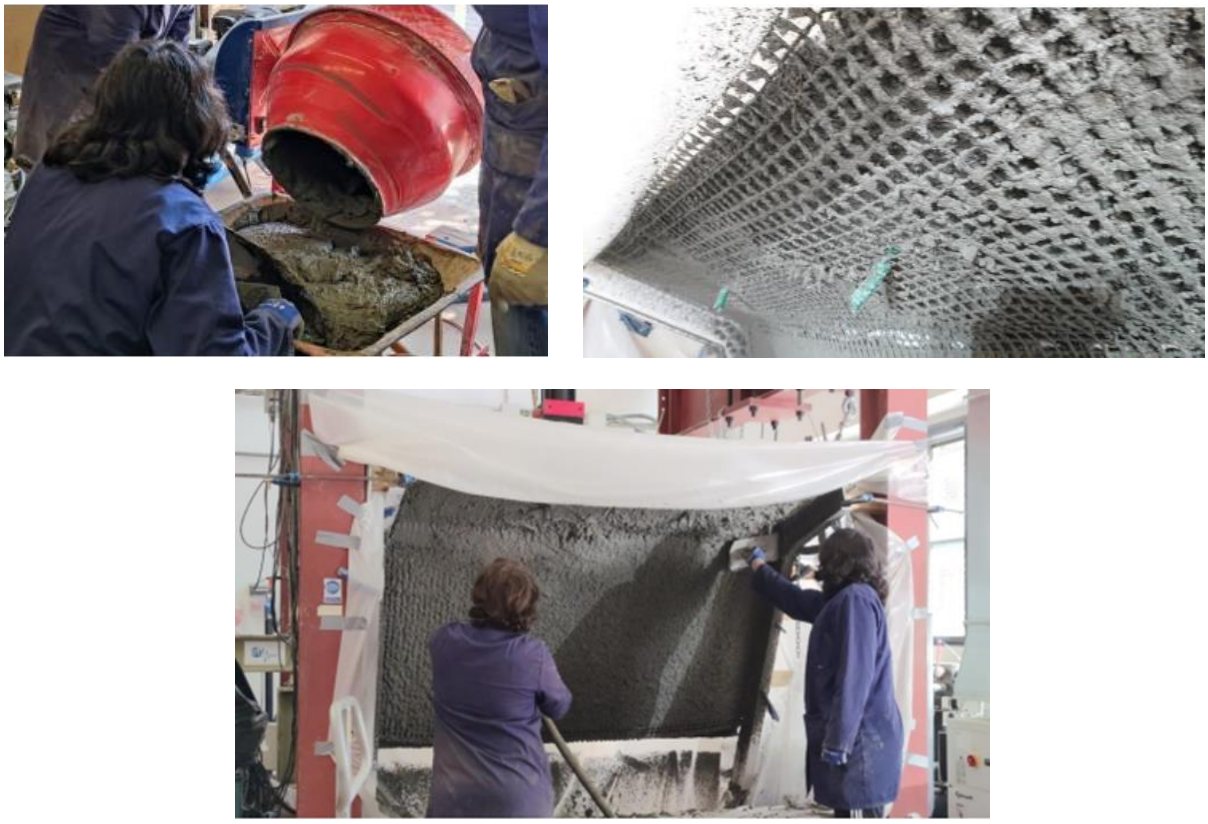

Figure 54. producing and manufacturing processes of mortar

Specimen HP2 was completely fixed at the lower part of the vertical-like GFRP profiles by bolting them to the external loading frame. In addition, the horizontal-like GFRP profiles were horizontally and vertically restrained with steel chains (see the sketch in Figure 55). The load was indirectly applied as an imposed displacement at two 150mm square areas placed at thirds of the length and at the transversal midspan of the top FRCM plate.

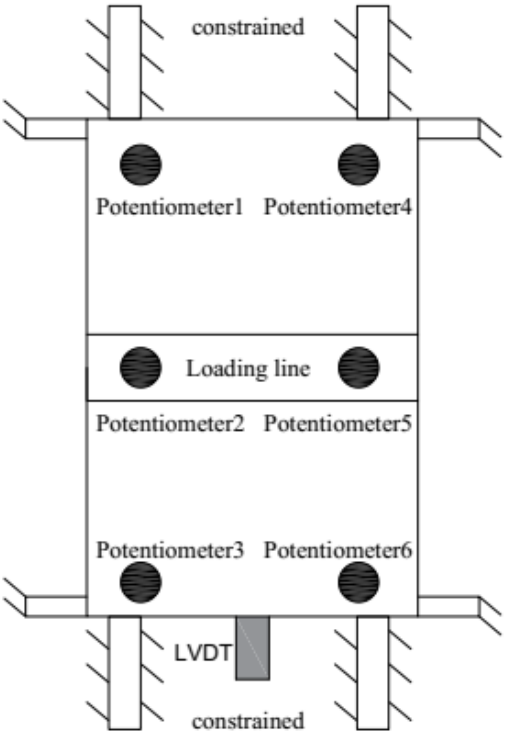

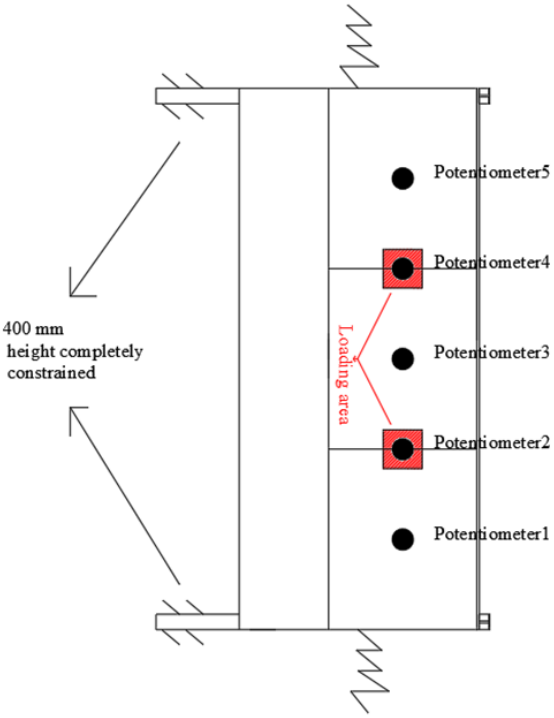

Figure 55. Setup of the monitoring and loading test for the hybrid structures.

This displacement was manually applied through tensioners that act on steel plates placed at the extrados of the structure. These tensioners were fixed to a reaction beam of the rigid loading frame through hinges. The direction of the applied displacement/load was orthogonal to the top FRCM

plate. The applied load at both areas was simultaneously measured (load cells with 10kN range), recorded and manually balanced by alternating the tensioners to be activated. Five potentiometers (10 cm range and 0.02% accuracy) were placed in line at a sixth of the length of the specimen, all at the same distance from each other. 2nd and 4th potentiometers were placed as close as possible to the load application position. All potentiometers measure the vertical displacement.

4.3 Result and discussion

Experimental results in terms of Force-Displacement curves are presented in Figure 56. The experimental response of the HP1 test is plotted in two parts. The first one (solid) shows the recorded force versus the average displacement of the potentiometer sensors placed below the loading line. Connected to this first part, the second part (thicker dotted line) represents the applied force versus the displacement of the actuator after correcting this last one according to the difference between the potentiometers during the first part of the test. This change is required because the deformation of the specimen was over the measuring range of the installed potentiometers.

HP1 response was characterized by a first initial lineal response in which the observed deformation of the specimen corresponded to two opposite edges fixed plate. This stiffer behavior was maintained up to the crack of the mortar along the two edges defined by the FRP-FRCM connection. From this point and on, the observed deformation corresponded to the typical parabolic description of a plate that is simply supported at two edges. Progressive cracking of the FRCM moved the mechanical qualitative response from a plate-like case to a membrane-like case in which the mortar contribution may be neglected and the wires of the glass fiber grid bore the load up to the final failure in which some of the wires broke in tension causing the last sudden load decrease (see Figure 57).

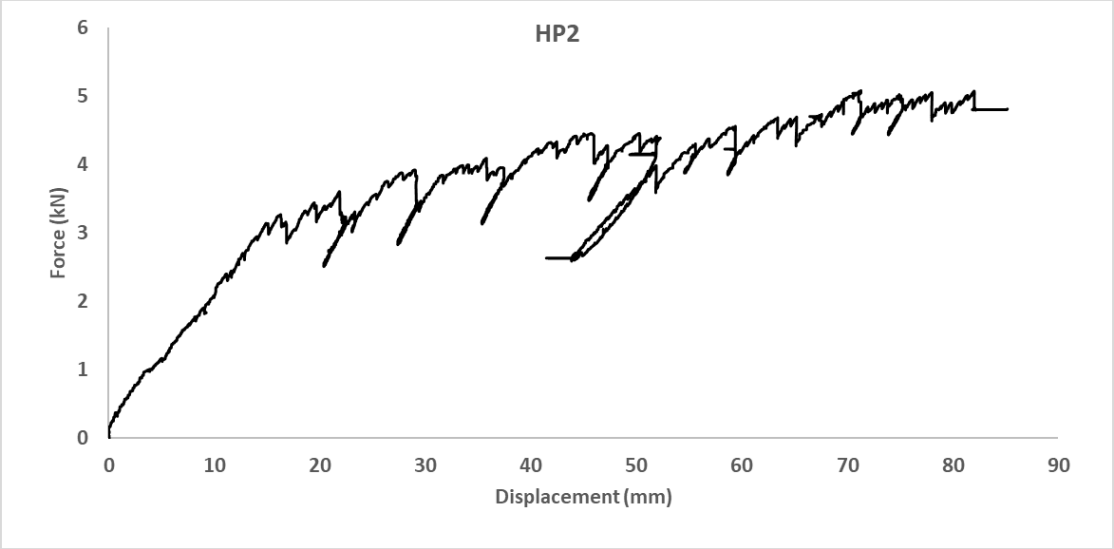

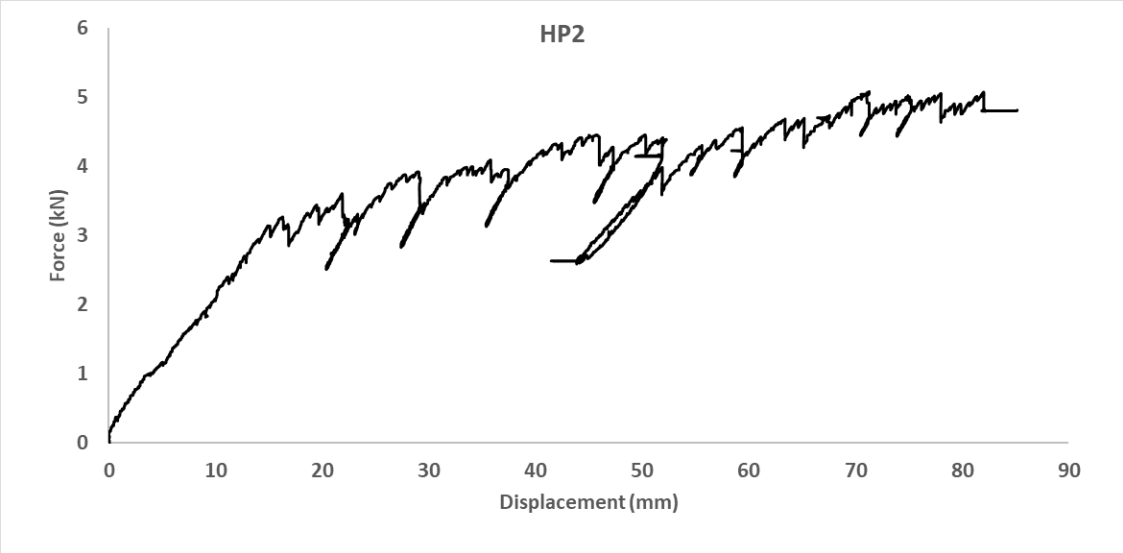

Figure 56. Force vs. displacement plot for experimental specimens

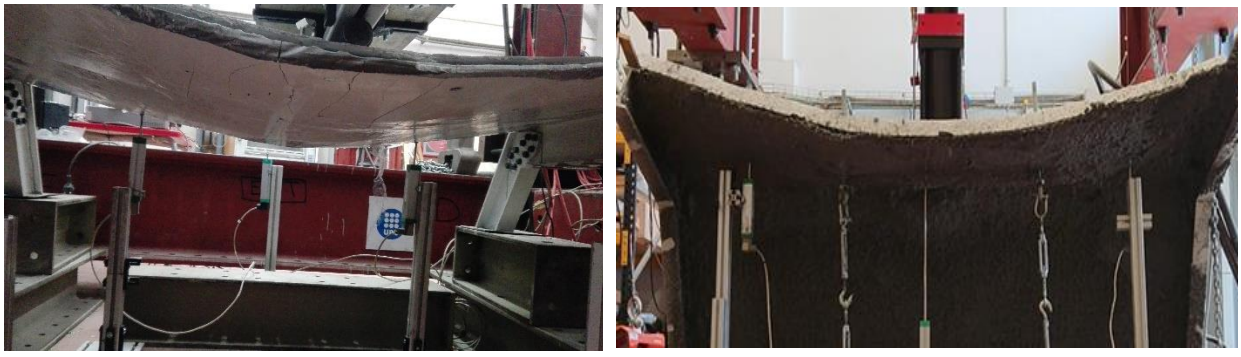

HP1 ***HP2***

Figure 57. Failure modes in the tests

Hence, the FRP-FRCM connection manufactured by adhesive bonding of FRCM mesh to the FRP profile before mortar casting was effective enough to support the loading process up to the FRCM tensile failure. In addition, no significant deformations or damage was observed in the FRP-FRP bolted connection of the specimen. Hence, it is concluded that the part that had the most influence on the mechanical response of the tested hybrid FRP-FRCM specimen was the FRCM plate. This observation proved the effectiveness of the FRP-FRP and FRP-FRCM connections proposed in this novel technology and turns the analysis far from the FRP-concrete connection typically analyzed for current hybrid structures (see, for example, the large plastic bolt deformations found in the load–slip curves by Di et al. (Di, Cao and Han, 2020) and Rajchel et al. (Rajchel, Kulpa and Siwowski, 2020) or the load–slip curves of FRP form-concrete elements by Gong et al. (Gong, Zou and Xia, 2019)). Finally, comparing the experimental observations of the specimen test with the idealization of the shear behavior of the FRP- flexible mesh-concrete connection presented in (Mahboob *et al.*, 2021a), which is the closest case to the novel tested technology, it is concluded that the FRP-FRCM connection worked in the elastic range during all test of the HP1 specimen.

HP2 mechanical response is also plotted in Figure 56. This plot represents the vertical displacement of the displacement sensors placed closest to the loading areas (average value of Potentiometer 2 and Potentiometer 4 in Figure 55) versus the load recorded by the individual load cell installed in each tensioner. The test of the HP2 specimen finished when the maximum deformation of the tensioners (over 80mm) was reached. HP2 behavior included a first lineal branch followed by multiple cracking formations. After reaching the maximum load (around 5 kN for a vertical deformation of 70mm), the cracking process continued and the load was kept almost stable with a slight decrease.

Comparing HP1 and HP2 specimens, it is clear that membrane formation previously observed in HP1 was not reached for HP2 case. Thus, an idealization of the HP2 response should consider the FRCM part as a flexible plate that did not reach to develop the membrane response because of insufficient damage to the mortar matrix. In fact, observed cracks in the HP2 case were located around the loading areas but these did not extend up to the FRCM-FRP connection edges (see Figure 57) keeping the plate-like structural response.

Again, like in the HP1 case, no damage or large deformation was observed in the FRP-FRP connections in the HP2 case. Moreover, the fiber grid was kept completely bonded to the FRP profiles during all the HP2 tests. Thus, it is also concluded for this case that the component part that most significantly controlled the mechanical response of this hybrid panel was the FRCM.

5

Numerical models for representing the interfaces between hybrid panel components

5.1 Introduction

The finite element method turns the mechanical problem into a system of algebraic equations. This method obtains the estimated values of the unknown parameters (displacements, from which strains, stresses, etc. derive) for a number of distinct points within the problem definition range. Finite element method is oriented to divide large problems into smaller, simpler sections called finite elements. Several numerical studies have been done on characterization of material interactions.

The numerical model described herein is oriented to characterize the interactions between the components of the hybrid FRCM-FRP system including GFRP-GFRP connections and Mesh-Mortar connections. Mesh-FRP interaction was not represented because it was experimentally proved that these materials were completely bonded up to the mesh tensile failure.

It was intended to describe all steps of modeling in a concise and practical manner. It should be emphasized that the modeling was done using the ABAQUS 2020 program.

5.2 GFRP-GFRP connection

5.2.1 Experimental specimens

The mechanical behavior of adhesively and bolted joints for pultruded Glass FRP connections have been investigated with experimental and numerical methods. A total number of nine specimens with different configurations (bolted joints, adhesively joints, web joint, web and flanges joints and two different angles between profiles) were fabricated and tested as presented in section 3.3.

5.2.2 Model's geometry construction

Regarding the geometric definition of the model, all parts were simulated using 3D elements. Screws were simplified as cylindrical parts and nuts and washers were not considered in the simulation.

Using the Part> Create path, model was created, as shown in Figure 58.

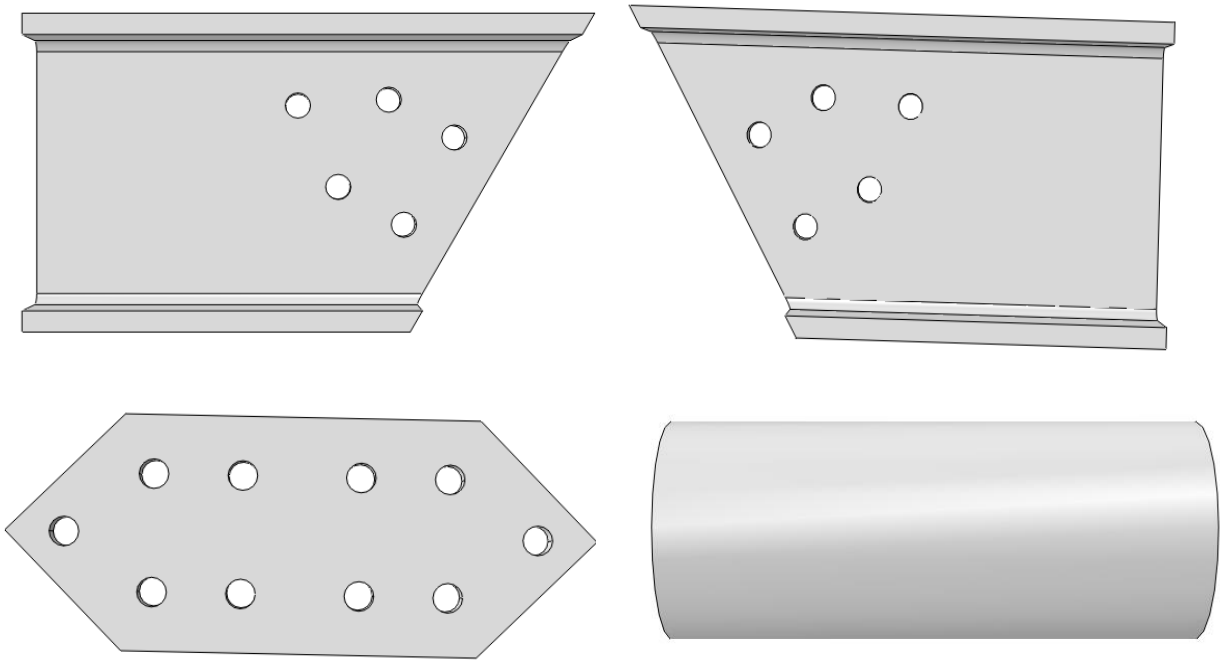

Figure 58. Model drawing steps in ABAQUS software

5.2.3 Materials' properties

Pultruded GFRP profile

The homogenous orthotropic linear-elastic characteristics of the glass fiber-reinforced polymer profiles were developed using the nine engineering constants. A composite material with transverse isotropy (see Figure 59) has five independent elastic parameters: longitudinal and transverse elastic modulus; in-plane longitudinal shear modulus; and two Poisson's ratios. All constants for GFRP profile are shown in Table 18.

Table 18. The mechanical properties of GFRP profile (Neagoe, 2016)

E_1 (GPa)	$\nu_{12}= \nu_{13}$	ν_{23}	$G_{12}= G_{13}= G_{23}$ (GPa)
10.77	0.27	0.33	3.98

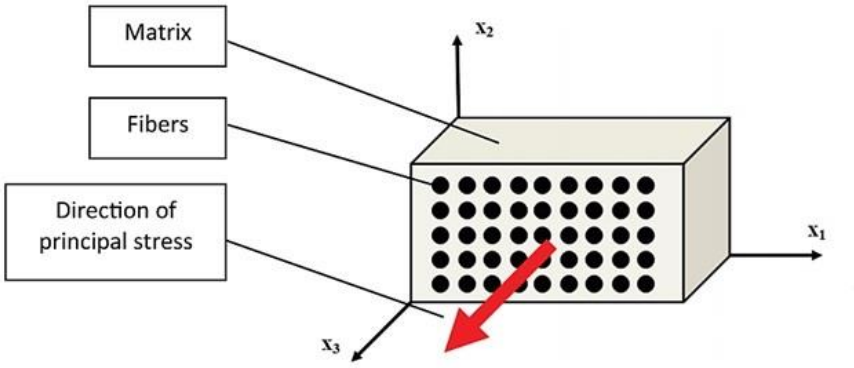

Figure 59. Composite material with transverse isotropy (Petrů and Novák, 2018)

Steel

The steel of the bolts was modeled as a homogeneous elastic-plastic material. The material property data acquired from standard testing were used to define the stress–strain relationship of steel bolts. Steel materials exhibit initial elasticity until they reach their yield points, beyond which they undergo additional yielding or strain hardening before fracture. Table 19 represents the mechanical property of steel.

Table 19. Mechanical properties of steel and CFRP

Material	Characteristics	Value
Steel	Young's Modulus (GPa)	210
	Poisson's rate	0.29
	Yield stress (MPa)	1100
	Plastic strain	0
CFRP	Young's Modulus (GPa)	227
	Poisson's rate	0.26

CFRP

Handmade carbon fiber laminate was simulated as a linearly-elastic homogeneous and the considered properties to be introduced in the numerical model are summarized in Table 19.

5.2.4 Meshing

The pultruded GFRP profiles and connection plates, the CFRP flange connection plates and the bolt pieces were defined as deformable solid elements in a three-dimensional finite element model. Through analyzing several different meshes with different mesh sizes, the size of element was selected. All FRP elements were meshed as 3D solid elements (C3D10) quadratic tetrahedron with

the size of 10 mm. 6-nodded linear hexahedron prism elements (C3D6) with the size of 5mm were used to model the bolts. Figure 60 shows the mesh of the numerical model.

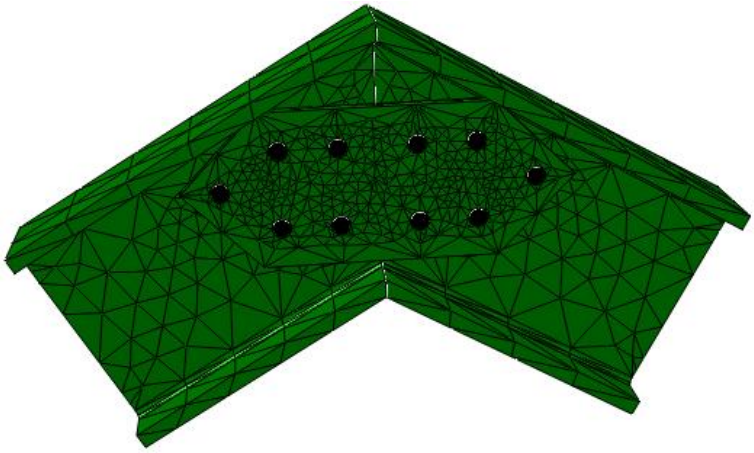

Figure 60. Meshing of all parts

A mesh convergence analysis was performed through analyzing a specific case (160WBO) with two different mesh sizes: 15 mm and 7.5 mm. Compared results in terms of force-displacement curves are shown in Figure 61. Maximum stress values had a variation below 10%. In conclusion, the mesh size of 15 mm was accepted as a balanced option between simulation accuracy and computational cost, which was also limited to a maximum calculation time of 8 h on in an Intel®CoreTM i7-7500 CPU @ 3.8 GHz with 16 GB RAM memory running Windows10.

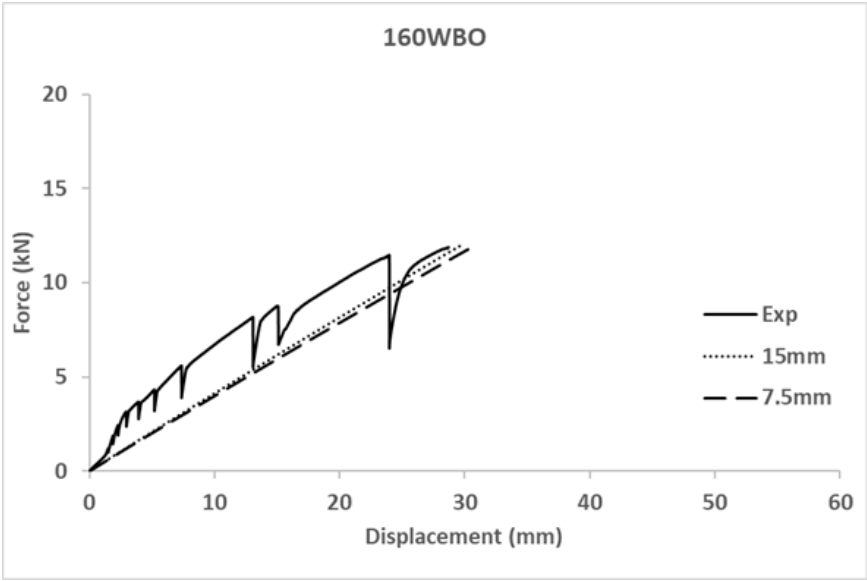

Figure 61. Mesh-convergence analysis on numerical result

5.2.5 Interactions and constraints

All parts may contact each other. In interaction module, the surface-to-surface contact that defined the bolted connections considered Coulomb friction model with a friction coefficient of 0.2 (see Figure 62) as previously proposed by other authors (Hyer, Klang and Cooper, 1987) (Mottram, Lutz and Dunscombe, 2004). On the other hand, tie constraint was used to modeling of adhering CFRP to flanges. A contact technology considering a cohesive behavior and damage was used to model the adhesive connections between GFRP profiles (see Figure 63).

Table *20* represents the used contact properties in detail. This last definition completely reflects experimental observations.

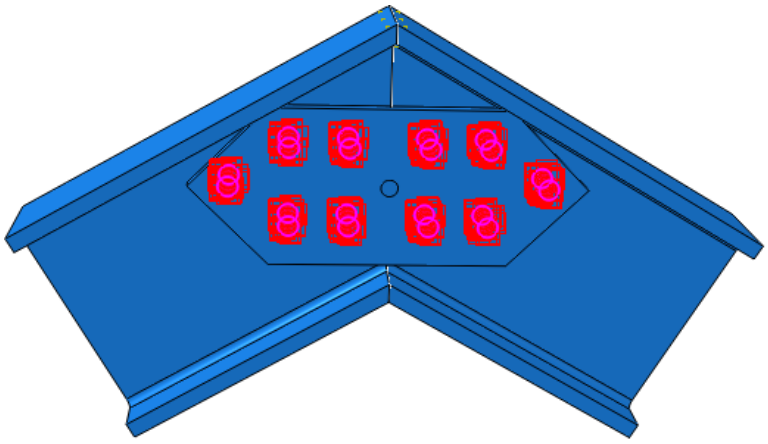

Figure 62. surface-to-surface contact definition for bolted connection

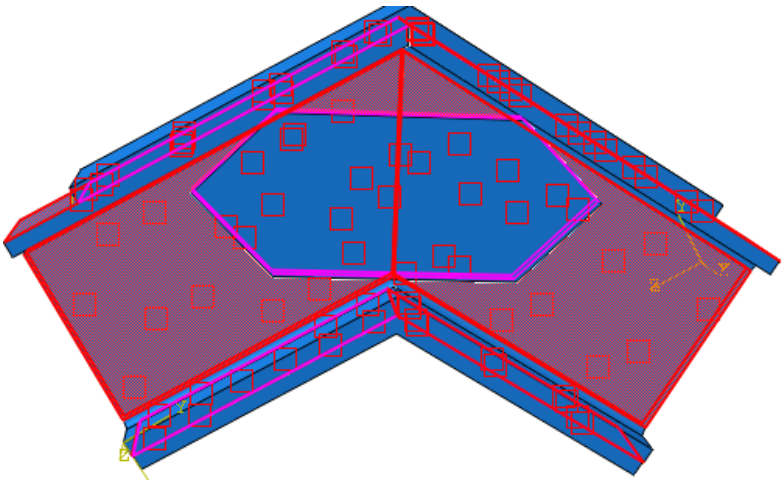

Figure 63. surface-to-surface contact definition for adhesive connection

Table 20. The used contact property for each connection

Connection type		Parameter
Adhesive connection	Cohesive behavior	$K_{nn}=K_{ss}=K_{tt}=1$
	Damage	Maximum nominal stress (Normal only, Shear-1 only, Shear-2 only) = 1 Total/Plastic Displacement=0.5
Bolted connection	Tangential behavior	Friction Coeff=0.2

5.2.6 Boundary and load conditions

All real boundary conditions and applied load were reproduced in the finite element model like experimental conditions. Real displacement restrains of the laboratory conditions were recreated in the numerical model by completely fixing the flanges of the restrained halve and applying the load as an imposed displacement in global horizontal direction. Figure 64 shows the boundary and load conditions for the finite element model.

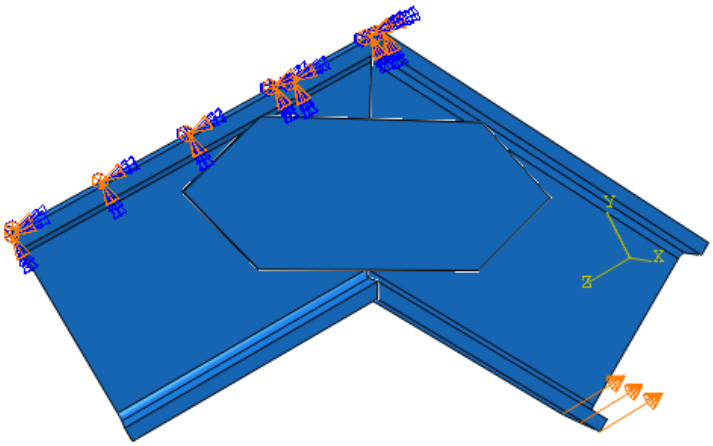

Figure 64. Boundary and load conditions for the finite element model

5.2.7 Analysis procedure and outputs

Static-General procedure was chosen to analyze the nonlinear behavior of the numerical models. The maximum number of increments was adjusted to 1000. The initial, minimum and maximum increment size were chosen 0.1, 1E-05 and 0.1 respectively. The time of analysis was 1 second. The direct method was used as an equation solver and full Newton was adjusted to solution technique.

The outputs include the load-displacement curve and failure mode. In this research, the numerical force-displacement plots were compared with experimental plots in order to evaluate the accuracy of the results.

5.2.8 Result and discussion

Figure 66 shows the force-displacement for all numerical models, comparing with experimental results. It can be seen that there is a good agreement between numerical model and experimental results in terms of stiffness, reaching an average difference between both studies below 10%. It shows the numerical model correctly captured the mechanical response of the connection. However, the maximum load-bearing capacity was not specifically calculated, but it may be justified on the base of the local web-to-flange failure of profiles that was experimentally observed and numerically (see Figure 65 a) represented by a shear stress over the range of 30MPa-50MPa, which were the maximum shear strengths reported by Neagoe (Neagoe, 2016) depending on the testing standard. These values were obtained for the same profiles used in the current research.

None of the profiles reached their tensile strength neither bolts reached their shear strength in any of the simulations, which proved the capacity of bolted joints.

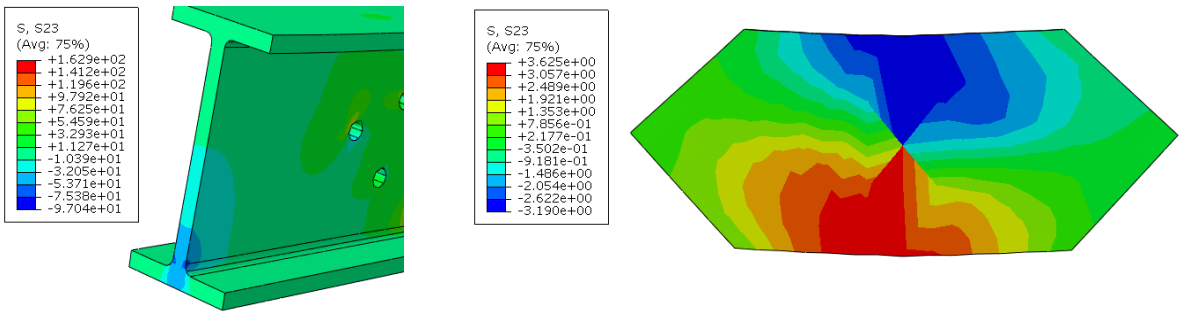

(a) **(b)**

Figure 65. Shear stress plots (a) Local web-to-flange shear failure for case 160WBC; (b) Shear stress distribution in the contact surface of the web connection plate of specimen 120WAO.

Regarding the numerical simulations, the model predicts in a more accurate way the mechanical response of the specimens which had flange connectors. Hence, adding a flange connector helps to uniform the manually executed web connection providing an experimental response closer to the theoretically expected one.

In addition, it has to be noticed that the results of the numerical model confirmed that bolts, connection plates and GFRP profiles reached stress levels far below their strength except for the weaker part of the GFRP profiles, which is the web-flange connection as previously reported by other researchers (Neagoe, 2016).

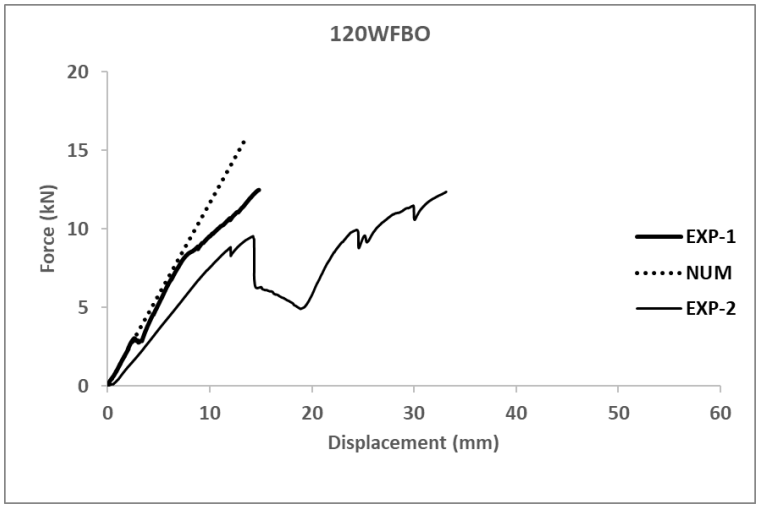

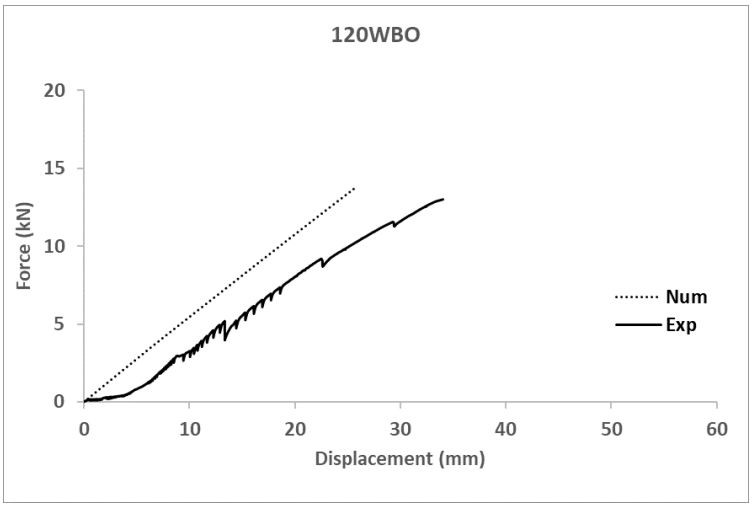
120WBO
Force (kN)
Displacement (mm)
Num
Exp

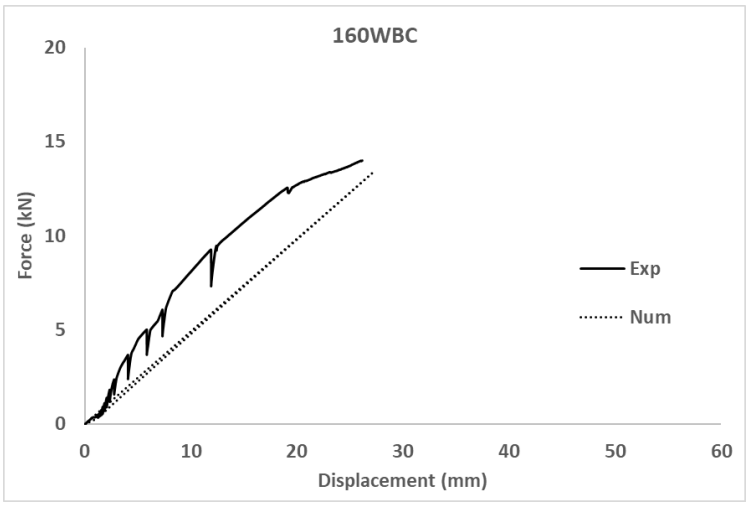
160WBC
Force (kN)
Displacement (mm)
Exp
Num

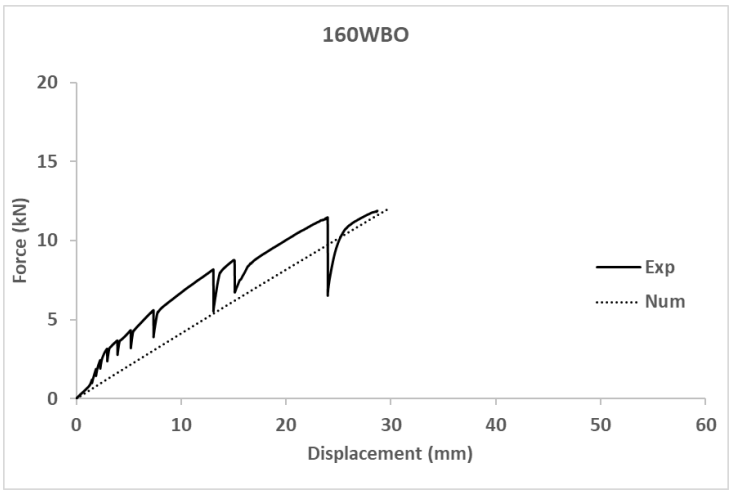
160WBO
Force (kN)
Displacement (mm)
Exp
Num

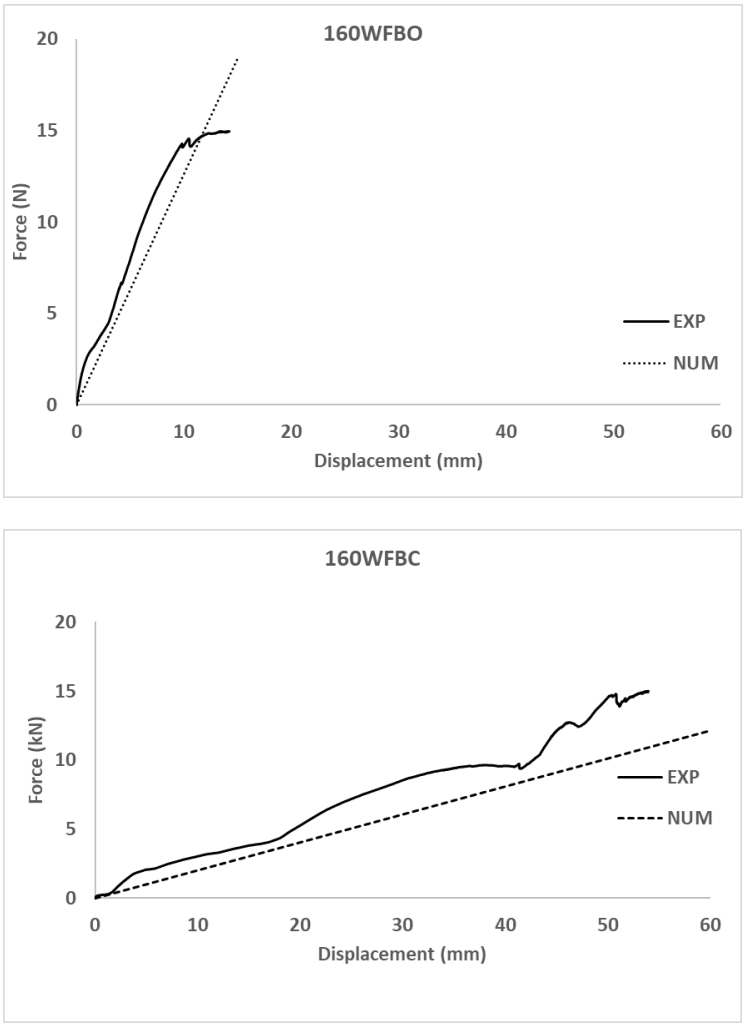

Figure 66. Force-displacement plots for all experimental and numerical models

Finally, the analysis of the simulations of the adhesive connections showed that a shear connection strength (see Figure 65 b) of 3.6 MPa was reached whereas the provider of the adhesive reported a shear strength between steel plates above 14MPa, see (Master Builders Solutions España, 2021a). Hence, it is concluded that the surface of the GFRP profiles was not properly prepared before the installation of the adhesive connection parts in the experimental campaign.

5.3 Mesh-mortar connection

5.3.1 Experimental specimens

There were 12 experimental FRCM specimens corresponding to three groups of four depending on the used materials: Axton mortar with glass fiber mesh, Axton mortar with carbon fiber mesh

and Sika mortar with glass fiber mesh. An electromechanic press was used to perform the tensile tests as presented in section 3.3.3. Figure 67 shows the failure mode of the specimens.

Figure 67. Mesh-mortar connection tests

5.3.2 Model's geometry construction

All parts were modeled as 3D objects; mortar as a 3D solid element and mesh as a 3D wire element. The used elements are shown in Figure 68.

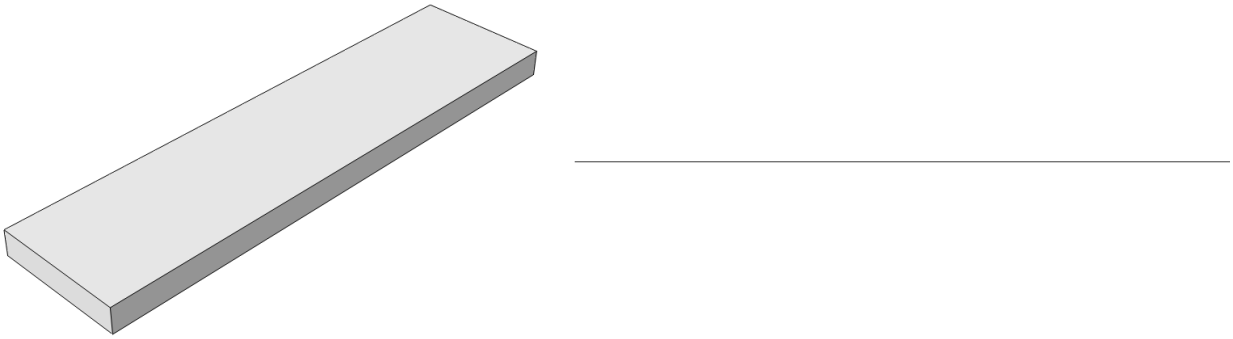

Mortar Mesh

Figure 68. 3D Model of all parts in mesh-mortar connection

5.3.3 Materials' properties

Mortar

A homogenous isotropic material with a coupled elastic-plastic constitutive curve was chosen for modeling the behavior of mortar. The elastic response was calculated using the calculated Young's

modulus and the standard Poisson's ratio for mortar. According to the experimental program, two types of mortar were used (Sika and Axton). The projection method for producing samples left far more voids than common procedures, resulting in lower mechanical properties. This value was chosen because it fits experimental results. Using a lower value of Young's modulus than the provider's data (see Table 4 and Table 5) is justified because the mortar bore tensile stresses in most of the test instead of compressive stresses was used to quantify this magnitude by the provider.

According to the provider's data (see Table 4 and Table 5), the Young's modulus and Poisson's rate of Sika mortar were considered 25GPa and 0.2 respectively and for Axton, these amount were 9.9GPa and 0.2 respectively. Poisson's rate was selected according general value of cementitious materials. Values different from those provided by the manufacturer in the technical sheet were used, because the planning method for producing samples creates much more voids than conventional methods and, as a result, has lower mechanical properties. This value was chosen because it is consistent with the experimental results.

Damaged plastic model of mortar represents the behavior of this material by expressing the separate behavior of concrete in compression and tension. This model can be used in static and dynamic calculations and includes the following assumptions:

- Ability to model mortar in different types of structural systems such as beam element, truss element, shell element and three-dimensional element.
- Ability to use reinforced concrete and non-reinforced concrete.
- Ability to use under uniform, oscillating and dynamic loads.
- Consider the effects of elastic stiffness recovery on periodic loads.
- Consider the sensitivity of the sample to the strain rate.
- Ability to use viscoelasticity in the basic equations to achieve better convergence in the softening section.

In the damaged plastic model of mortar, the two main failure mechanisms are:

- Tensile cracks.
- Compressive compression of concrete.

Failure level completion is controlled by hardening variables (ε_t^{pl} ، ε_c^{pl}) which are related to the failure mechanisms under compressive and tensile loads, respectively. These plastic strains are equivalent.

The stress-strain diagrams of concrete in uniaxial tension and compression are shown in Figure 69. Due to uniaxial tension, the stress-strain curve changes linearly to the failure point σ_{t_0}, which is associated with the onset and expansion of fine cracks in concrete. After passing this point, the failures become visible cracks, which are displayed as a softening curve in the stress-strain space.

Under uniaxial compression, the response will be elastic until the flow point σ_{c_0} is reached, and the behavior in the plastic region is generally expressed as the hardening curve, which eventually reaches the final stress point σ_{c_u}. The curves become softer. This model, despite its relative simplicity, satisfies the main properties of concrete (Wang *et al.*, 2020).

Stress-strain diagrams (see Figure 69) under uniaxial loading have the ability to convert plastic stress-strain curves, which is done automatically using given stresses and inelastic strains given by the user to the software.

Table 21 and Figure 70 represent the plastic behavior of mortar. This behavior of mortar has been simulated in Abaqus.

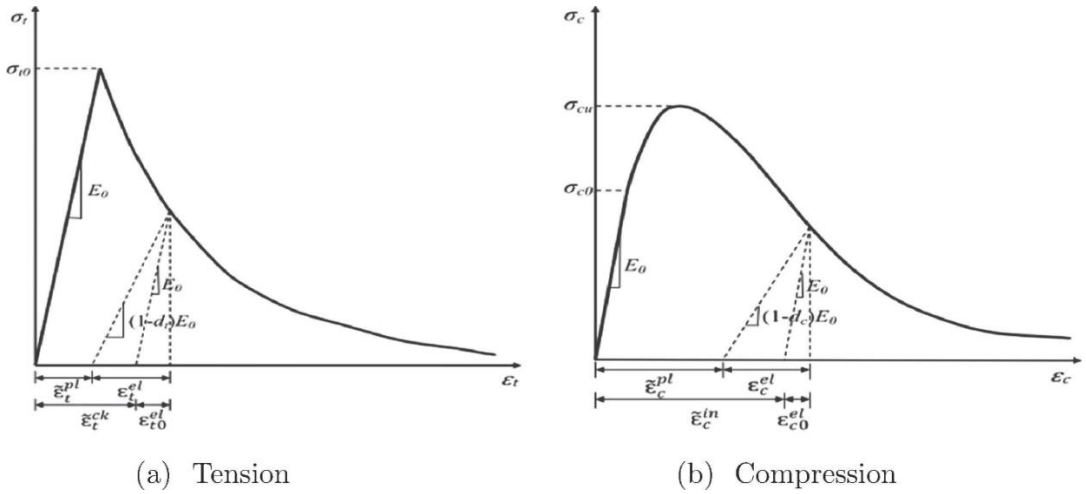

Figure 69. Uniaxial stress–strain curve with damage plasticity (Wang *et al.*, 2020)

Table 21. Mortar damage plasticity (Kent and Park, 1971)

Parameter	Dilation Angle	f_{b0}/f_{c0}	K	Viscosity Parameter
Value	31	1.16	0.67	5E-05

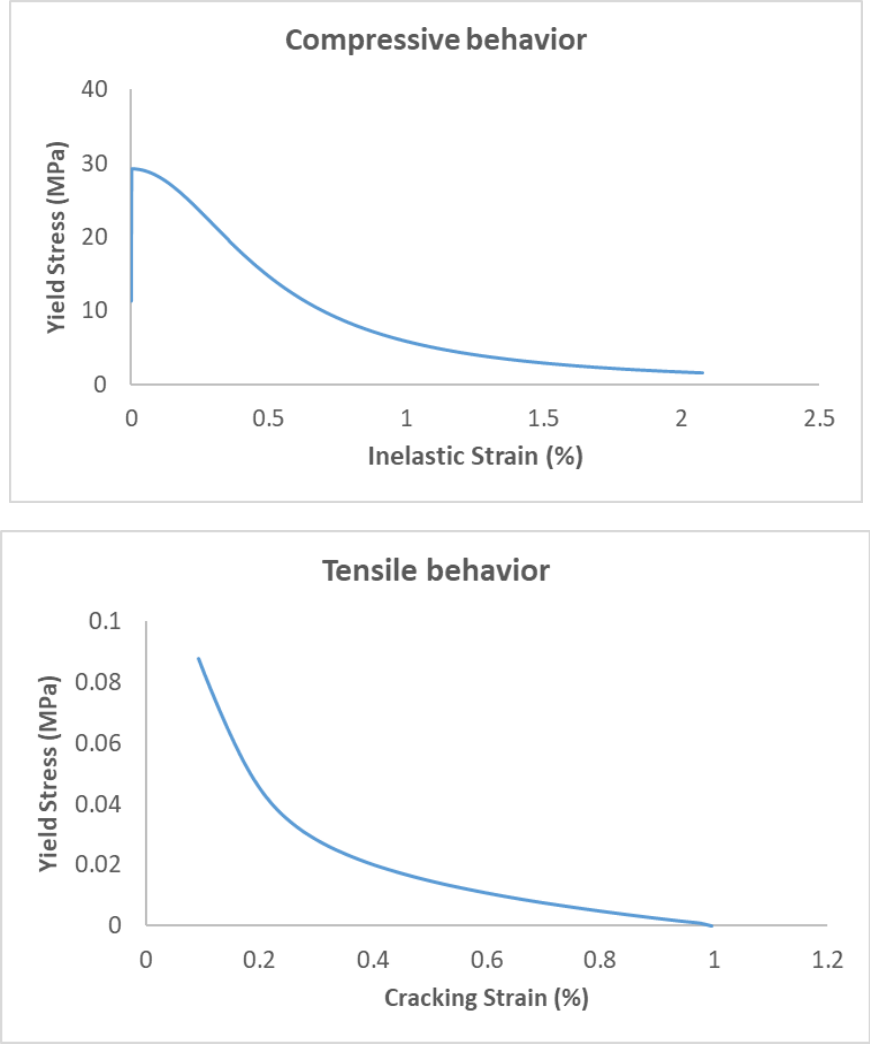

Figure 70.The compressive and tensile behavior of mortar

5.3.4 Meshing

In a three-dimensional finite element model, the mortar and glass fiber mesh were specified as deformable solid elements. The size of the element was determined by examining numerous distinct meshes with varying mesh sizes. Mortar was constructed as 3D solid elements (C3D8R) general purpose linear brick element, with reduced integration (1 integration point) with a 25 mm dimension. The glass fiber mesh was modeled using 2-node linear displacement (T3D2) with a size of 10 mm. Figure 71 depicts the numerical model's mesh.

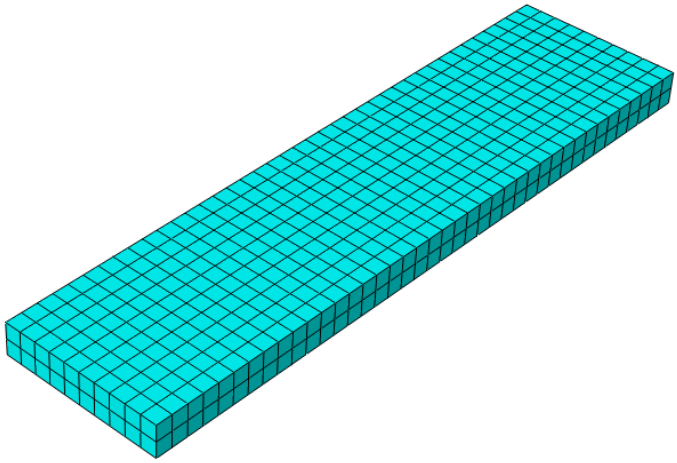

Figure 71. Meshing of all parts

5.3.5 Interactions and constraints

In this research, two parts are created. With a single interaction, the contact between several or all parts of the model can be defined. Glass fiber mesh can be defined as one-dimensional strain elements that can be used with embedded constrain in mortar. Their behavior is identical to that of an elastic-plastic material. Figure 72 shows the interaction between glass fiber mesh and mortar.

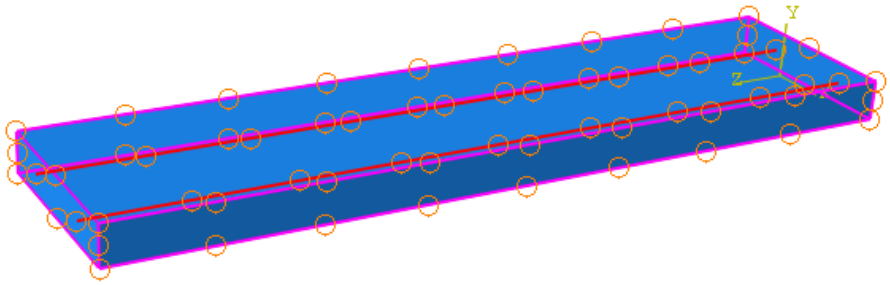

Figure 72. Using embedded region constraint for defining interaction between glass fiber mesh and mortar

5.3.6 Boundary and load conditions

According to experimental conditions, all boundary condition and load are simulated and also real displacement is defined in the numerical model by fixing one side of mortar (symmetry) and imposing the load in the other side of mortar. All the boundary and load condition are presented in Figure 73 for the finite element model of mesh-mortar connection test. Indirectly displacement-imposed loading was applied on the free transversal face of the mortar.

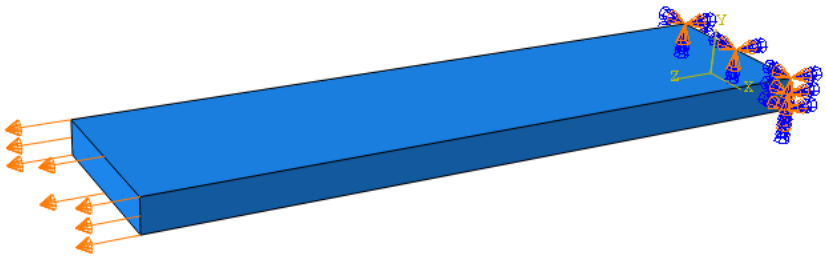

Figure 73. Boundary and load conditions for the finite element model

5.3.7 Analysis procedure and outputs

To analyze the nonlinear behavior of the numerical models, the Static-General approach is used. The maximum number of increments was increased to 100000. The increment sizes for the initial, minimum, and maximum increments were set to 0.01, 1E-09, and 1, respectively. As an equation solver, the direct approach is applied, and complete Newton is used as a solution strategy.

The load-displacement curve and failure mode fitted the results. In this study, computed force-displacement plots are compared to experimental plots to assess the correctness of the results, in the next section.

5.3.8 Result and discussion

Figure 74 compares stress-strain curves for all numerical models and experimental data. In terms of stiffness, it can be observed that the numerical models showed greater initial stiffness than experimental tests for all specimens. This may be due to an initial microcracking of experimental samples, which was not detected by naked eye but it is consistent with the production mode. After this first stage, there is a good agreement with an average discrepancy between the two experimental and numerical elastic modulus and ultimate load of less than 15%. It demonstrates that both numerical and experimental tests had a linear behavior during most of the loading range. This simplified approach is believed to be accurate enough to be implemented into the more complex simulations of hybrid structures, which was the final aim of this partial simulation of components. Hence, the proposed model is valid for its application to model hybrid structures in which FRCM is only one of the compounds.

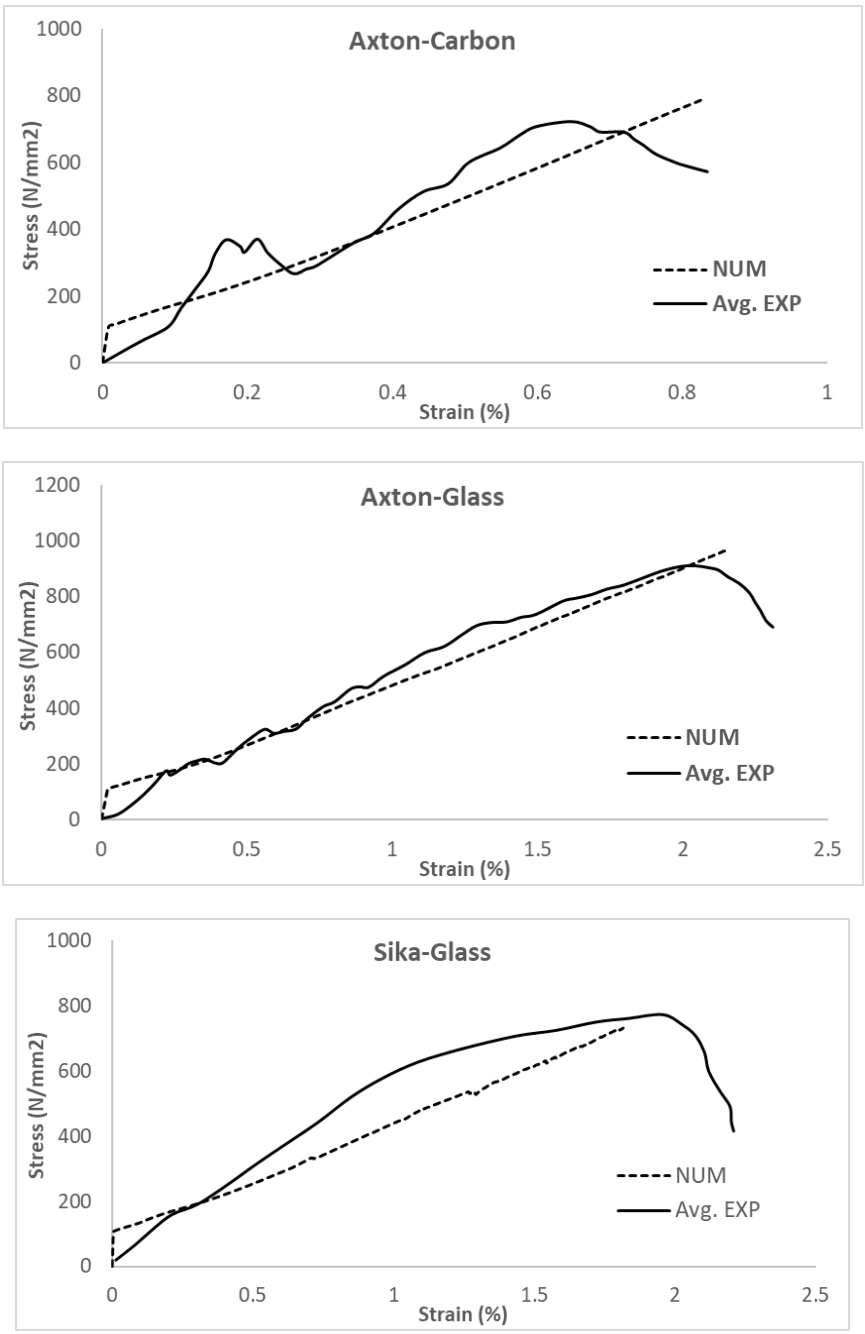

Figure 74. Stress vs. strain plot for experimental specimens and their numerical verifications

6

Numerical models for the characterization of the hybrid panels

6.1 Introduction

This chapter describes the creation of an integrated finite element model capable of capturing the fundamental behavior of full hybrid FRP-FRCM panels under different loading conditions. The material constitutive laws, geometry, mesh, interactions and constraints, boundary and load conditions, as well as the analysis settings and outputs, are all mentioned in the model descriptions. The simulation of the first full hybrid panel was used to calibrate the model and the simulation of the second one was used to validate the model with the experimental results.

6.2 Introduce experimental specimens

Two full hybrid panels were tested at CATMech-LITEM laboratory of UPC. The main aim was to characterize the structural behavior of FRP profiles-FRCM hybrid superficial elements. The tested geometries were proposed to cover bidimensional and three-dimensional application cases of the proposed technology. Details can be consulted in sections 4.2 and 4.3.

HP1 ***HP2***

Figure 75. Full hybrid panels carried out by Amir Reza Eskenati et. al

6.3 Model's geometry construction

All components of the model except mesh were simulated utilizing 3D elements in terms of geometric specification and Fiber glass mesh was modeled as a wire element. Only longitudinal wires were simulated to reduce computational cost. Figure 76 represents all used parts in this study.

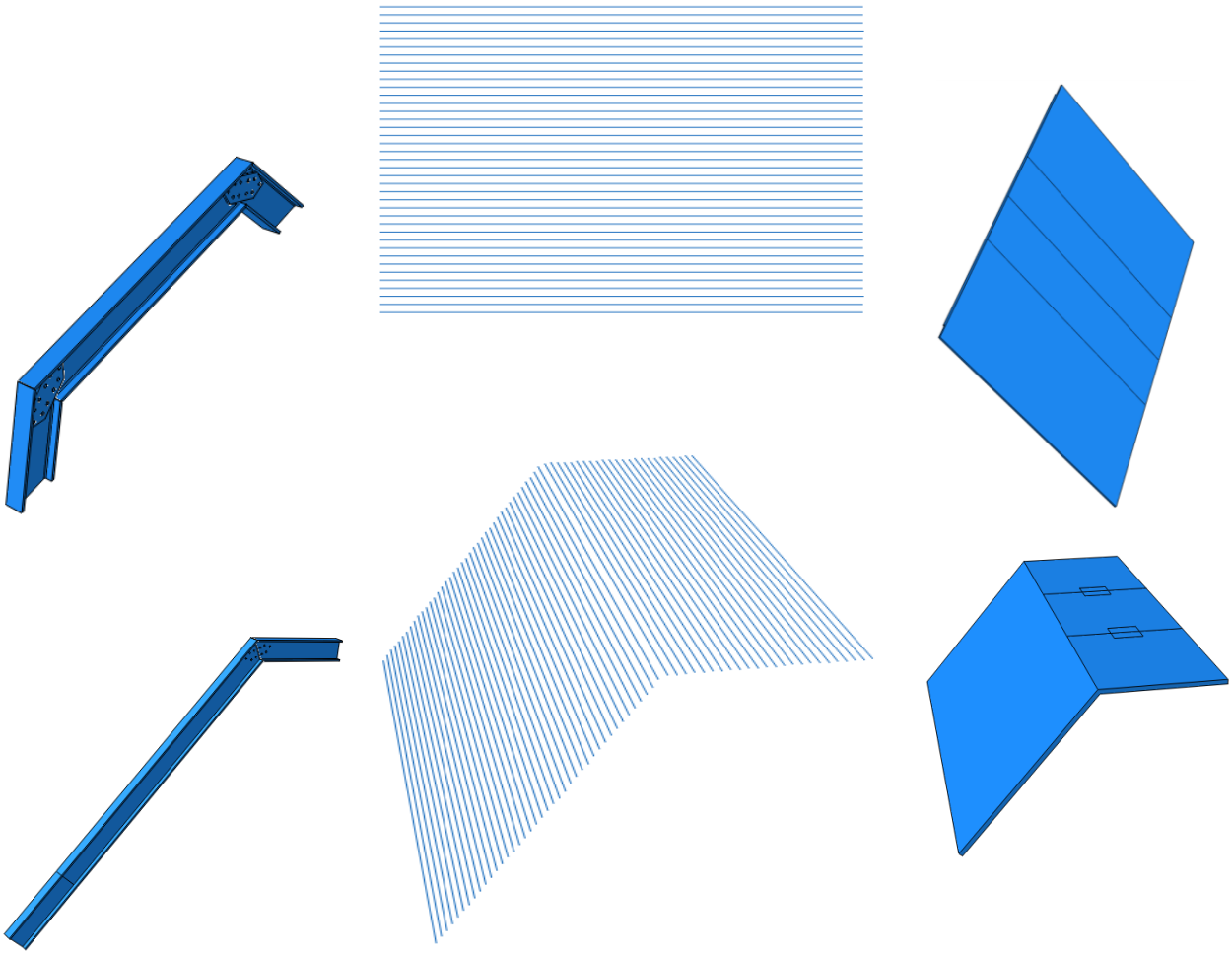

GFRP profile and bolt Fiber glass mesh Mortar

Figure 76. Model drawing steps in ABAQUS software

6.4 Materials' properties

In this study, the used materials include pultruded GFRP profile, steel, mesh and mortar. The material of pultruded GFRP profile, steel and mortar were described previously.

6.1.1 Fiber glass mesh

The glass fiber of the grid was defined as an elastic-perfect plastic material with a Young's modulus and Poisson's of 61250 MPa and 0.2 respectively. This fitted value of the young's modulus is in the range of the experimentally determined one (see Table 7). The yield stress was set to 676.8 MPa, which is the experimental value of the direct tensile test (Table 7). Finally, a softening response of the mesh after yielding (500 MPa of stress for a plastic strain of 0.1%) was defined to represent progressive tensile breaking of the mesh tows.

6.5 Meshing

The pultruded GFRP profile and bolt pieces were simulated as describe previously.

The mortar element was assigned the C3D8 linear hexahedral element type, which is a first-order, fully integrated 8-node linear brick with shear deformation and warping formulas. To mesh fiber glass wires T3D2 element was used. It is a two-nodes, 3-dimensional truss element. This was defined with a circular 1.05 mm^2 section in the principal loading direction. Orthogonal wires were not considered to simplify the model although it may be interesting to include them in future research in which three-dimensional response would be more relevant. In order to decrease the calculation time below 24 hours, the size of mesh for all parts was set to 110 mm. Figure 77 shows the meshed numerical model.

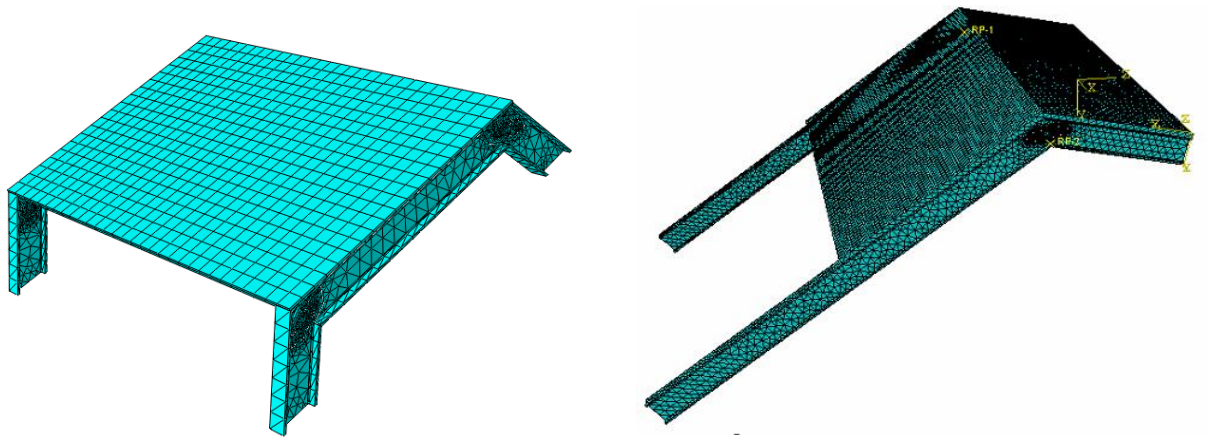

HP1 **HP2**

Figure 77. Meshing of all part in the model of full hybrid panel

6.6 Interaction and constraints

The contact region between bolts and GFRP parts was described previously. For the fiber glass mesh, an embedded region constraint (total compatibility of strains) was applied being the mortar the host region of the model. The connection between mortar and GFRP profiles was modelled with a tie constrain (total compatibility of strains). All used constraints are shown in Figure 78.

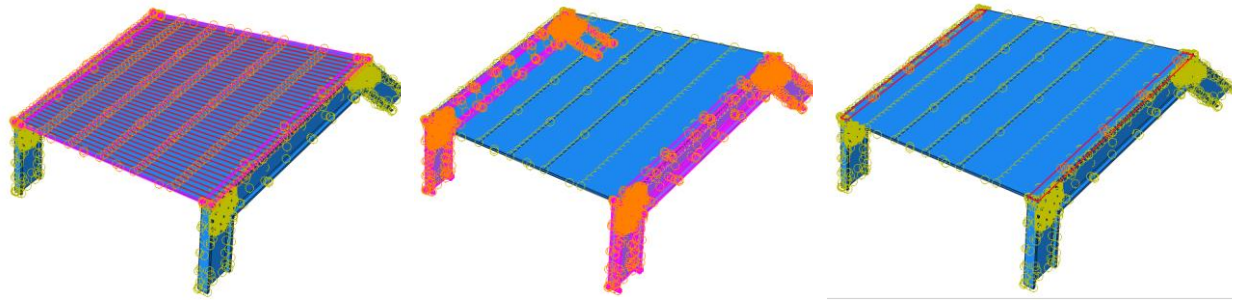

Embedded region Tie

Specimen "HP1"

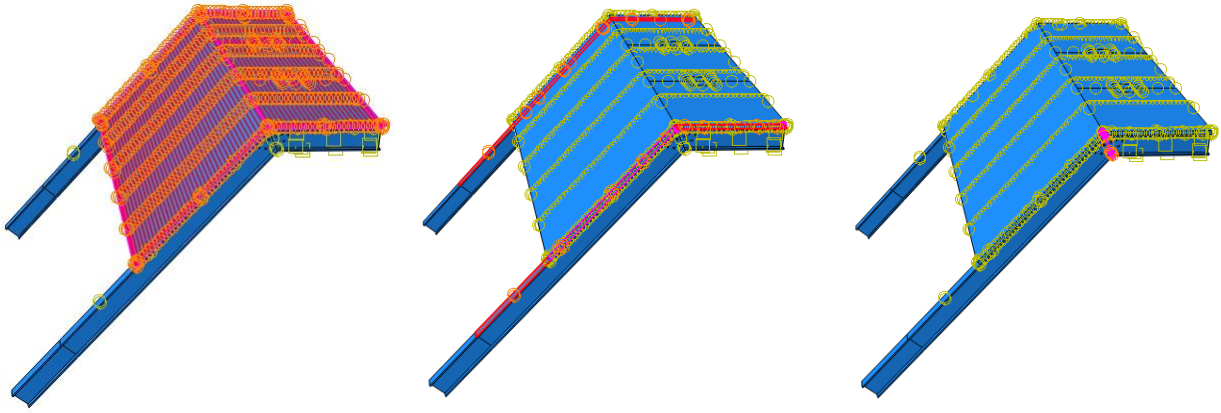

Embedded region Tie

Specimen "HP2"

Figure 78. All used constrains in modeling full hybrid panel

6.7 Boundary and load conditions

The bottom supports of the GFRP profiles were considered to be fixed in the simulation. The bending load was applied on the mortar in the same areas than in the experimental tests, being a line for HP1 case and two square surfaces in HP2 case. The representation of the loads and the boundary conditions can be observed in Figure 79.

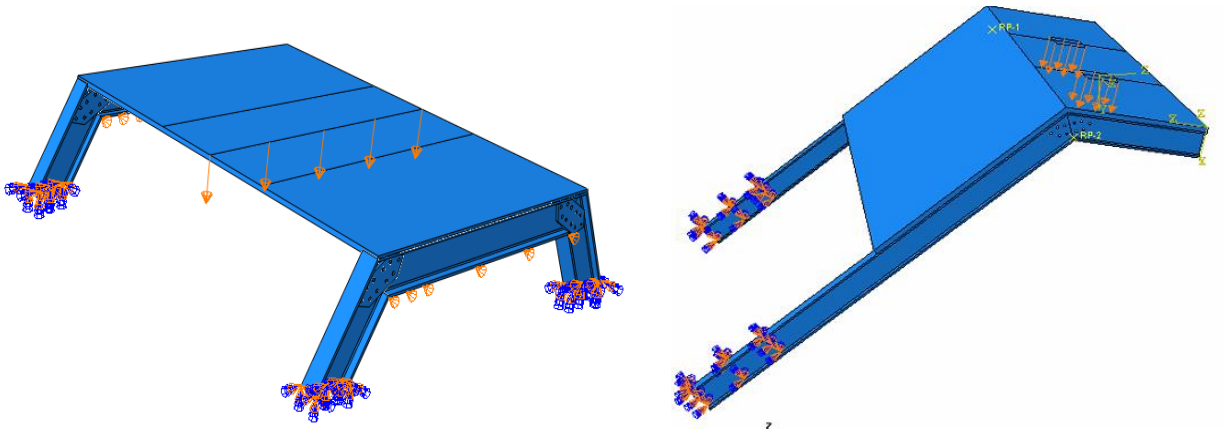

HP1 ***HP2***

Figure 79. Boundary and load conditions for the hybrid beam finite element model

6.8 Analysis procedure and outputs

The analysis was carried out utilizing the Static-General method in order to evaluate the nonlinear behavior of hybrid panel. The load-displacement curve, failure mode, Maximum principal stress distribution in maximum load for mortar and wire elements were chosen as relevant outputs to be analyzed.

6.9 Result and discussion

The force-displacement curves obtained from the numerical simulations are included in Figure 80, where the overlapping with experimental results can be observed. For both specimens, HP1 and HP2, the proposed numerical model successfully predicted the mechanical response of the experimental tests in terms of initial stiffness and maximum load.

As expected, the fitting of the calibration case (HP1) was better than the fitting of the validation case (HP2). For the former, initial stiffness, postcracking stiffness, maximum load and load sudden drop were accurately predicted. In contrast, the predicted cracking load of the case HP2 was slightly overestimated and the postcracking response was more conservative than the experimental output. Progressive cracking was not observed in simulations but it was clearly identified in experimental results. This fact is justified by the experimental imperfections that contribute to a progressive asymmetric cracking of the mortar and the possibility of partial failure of the mesh. In contrast, the perfectly symmetric definition of the numerical models caused a slight increase in the cracking load that required causing the local mortar failure at several areas simultaneously increasing the required external energy. Analyzing the failure modes (Figure 81) and the output results in terms of maximum principal stresses in mesh (Figure 82) and mortar (Figure 83), a clear difference between the two cases arose: the HP1 structure reached the complete cracking of the mortar under the load application edge whereas it was in progress at the end of the test of the HP2 case.

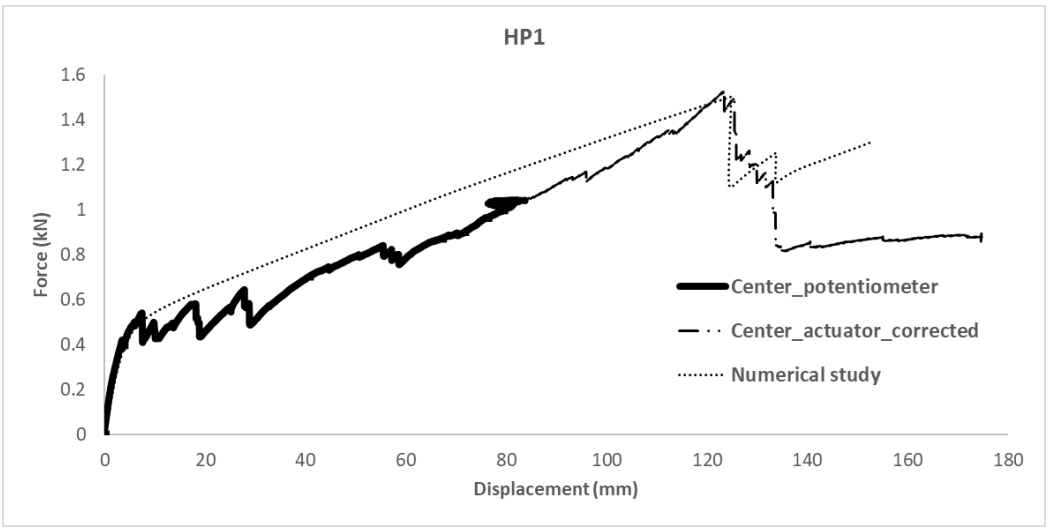

Figure 80. Force vs. displacement plot for experimental specimens and their numerical verifications

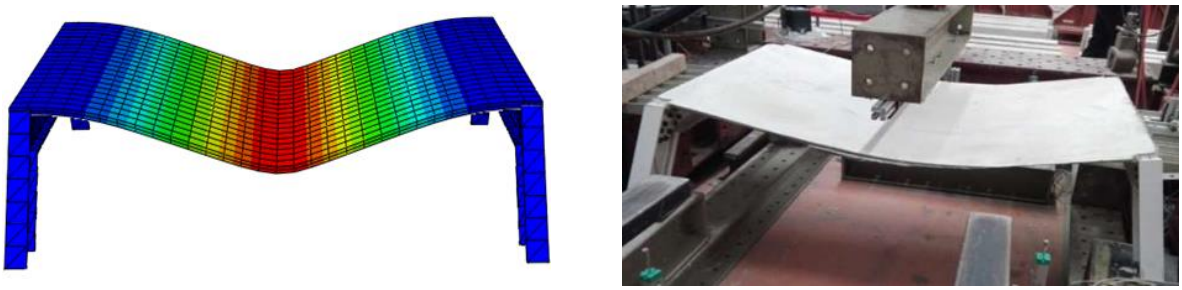

HP1

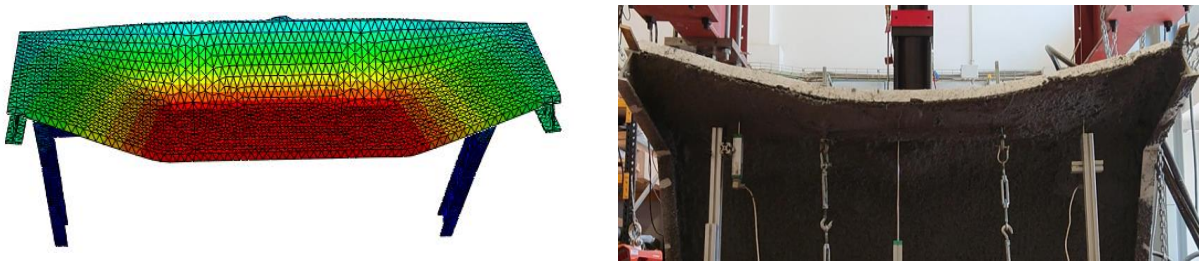

HP2

Figure 81. Failure mode in the experimental specimen and numerical model

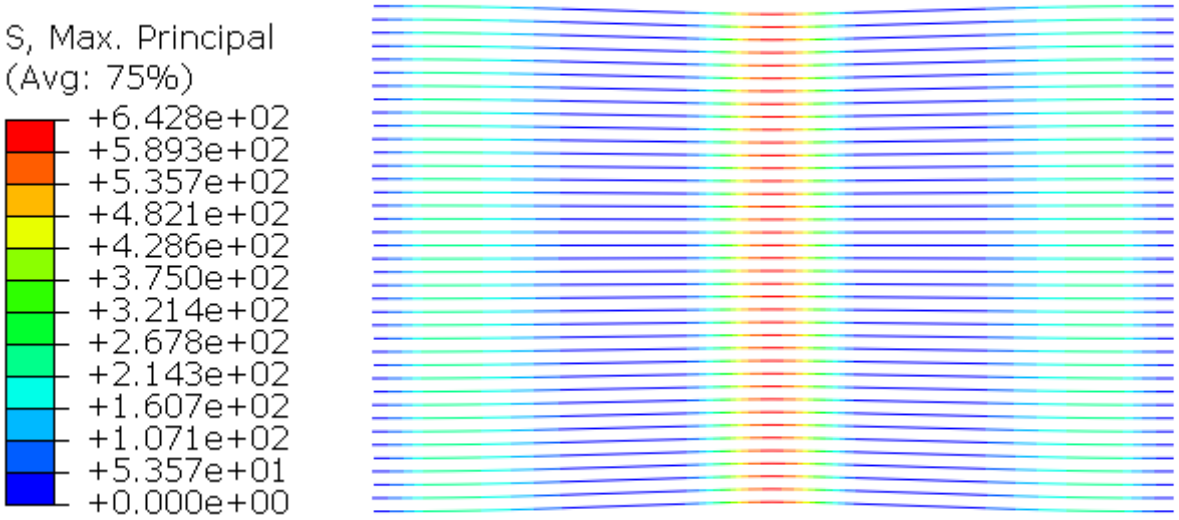

Specimen "HP1"

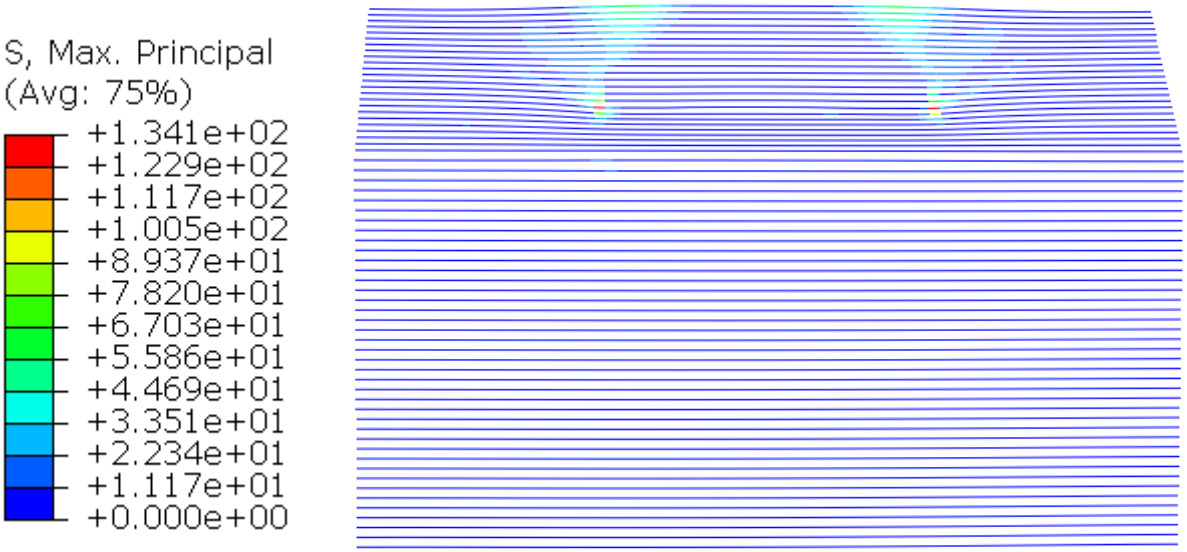

Specimen "HP2"

Figure 82. Stress distribution in the wire in the maximum load

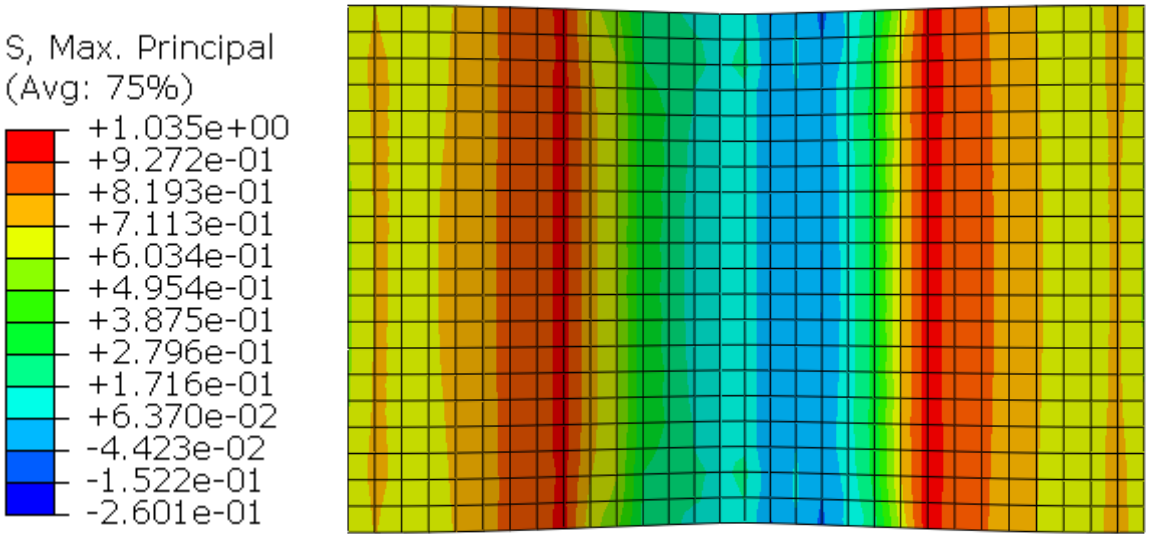

Specimen HP1

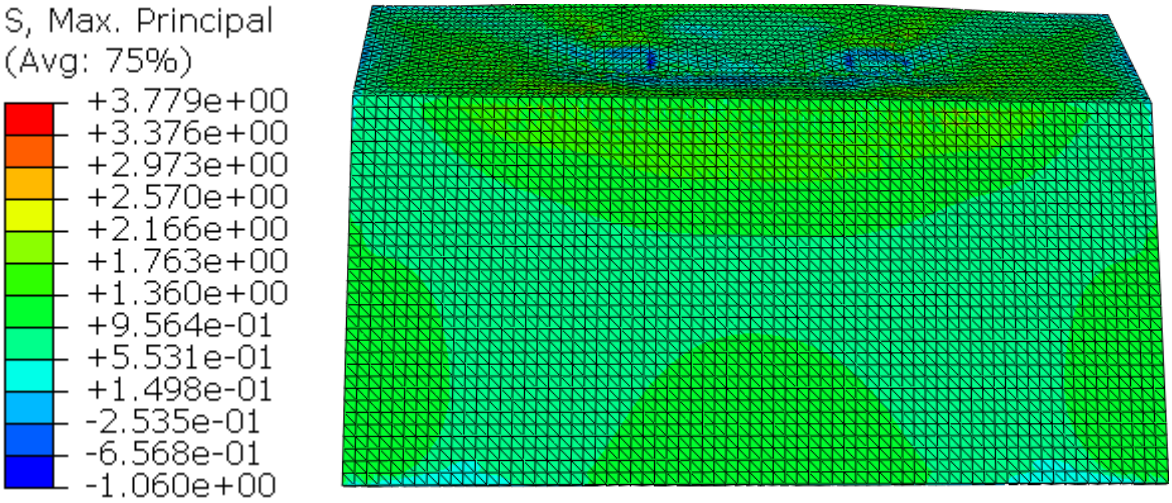

Specimen HP2

Figure 83. Stress distribution in mortar

Observing the experimental failure mode of the HP1 specimen (Figure 81) it was clear that the FRCM behaved as a membrane in the last part of the experiment and the FRP-FRCM connections acted as hinges. The membrane response was also modelled by the simulation through a more concentrated deformation describing a sharper shape than the typical parabolic flexural one

expected for plates. Regarding the calculated maximum principal stresses, it is clear that for the maximum load the mortar around the loading edge in HP1 had failed (see Figure 83); maximum stress values were not under the load application edge but displaced on both sides indicating that the mortar in the central area had broken because of reaching its tensile strength. In the maximum loading instant, the mesh bore the load as a membrane and the mortar just covered it so reaching lower stresses. In contrast, the stresses at the mesh (Figure 82) were concentrated at the midspan position reaching values of over 640MPa, that were close to the maximum strength value defined in Table 7, indicating its tensile failure.

Analyzing the HP2 case, it was observed that the model reproduced the deformation at maximum load, although experimental observations indicated a more evident plate-like response between the load application areas describing a parabola, whereas the numerical model predicted a flatter shape (Figure 81). This difference may indicate that the predicted mortar cracking is greater than the experimental observations. This would be a conservative approach. In fact, the stress level at mortar (see Figure 83) overpassed the mortar tensile strength and approached the flexural strength without reaching it. These outputs indicated that the flexural failure possibility, which was not experimentally observed because developed cracks had no continuity, was not reached even in the numerical model. Finally, the hypothesis that the HP2 case did not reach the point at which FRCM moves from behaving as a plate to behaving as a membrane was confirmed because the stresses in the mesh were far lower than its capacity (134 MPa vs. 676.8MPa in Table 7).

To continue with the analysis of the numerical results, it is observed that the maximum principal stresses in GFRP pultruded profiles and in the FRP-FRP connection areas did not reach significant values (85 MPa and 33MPa for HP1 and HP2 cases respectively, see Figure 84) in comparison with GFRP mechanical capacities (Table 3).

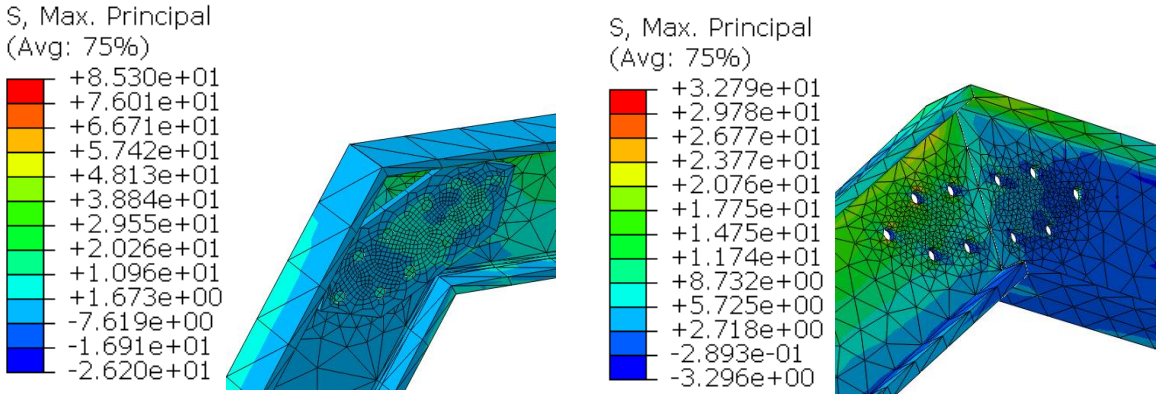

Specimen HP1 **Specimen HP2**

Figure 84. Stress distribution around connection area between FRP and FRP

To sum up, it is concluded that the proposed model properly represented the structural response of hybrid FRP-FRCM structures, including mortar cracking and the possible change of structural response of FRCM from plate to membrane. It also correctly captured the possibility of the tensile failure of the mesh and the mechanical contribution of the GFRP substructure through the accurate prediction of the load-displacement curves. Not considering the orthogonal mesh wires in the HP2 case, where slight bidimensional response is observed, may partially explain why not obtaining as good results as with the calibration HP1 case in which clear unidirectional response was registered.

Comparing the structural response of the two analyzed cases and considering that the free span of HP2 case was greater than the span of the HP1 case, but it was the HP1 case that resulted in more damaged even turning the response from plate to membrane. It is believed that two factors influenced this difference. First, the thicker mortar layer of the HP2 case (30mm against 10mm of the HP1 case) that contributed to extend the flexural load bearing capacity of the mortar matrix of FRCM. Second, the three-dimensional shape of HP2 specimen contributed to a stiffer response of the FRCM plate enhancing its performance as expected.

7

Conclusions and future research

7.1 Introduction

The current research was aimed at characterizing the structural behavior of novel FRP profiles - FRCM hybrid superficial elements. The initial idea was replacing the concrete of hybrid FRP-concrete structures with an FRCM composite, resulting in a combination of composite materials, where FRCM layer may work in flexural or tensile configuration. The investigation was focused on experimentally characterizing the different components and the interaction between them. Finally, numerical simulation models to represent this novel system and the interactions between its components is proposed and assessed.

The mechanical behavior of adhesively and bolted joints for pultruded Glass FRP connections have been investigated with experimental and numerical methods. A total number of nine specimens with different configurations (bolted joints, adhesively joints, web joint, web and flanges joints and two different angles between profiles) were fabricated and tested. Three-dimensional finite element analysis was also carried out.

The mechanical behavior of the connection between glass FRP profile and glass fiber mesh was experimentally assessed. There were six specimens with different connection: adhesive and bolted. Moreover, the effect of high temperature was also considered.

The composite response of FRCM specimens was experimentally determined through tensile tests on 12 specimens with different materials. The effect of high temperature was also investigated. Numerical simulations to represent the mechanical response of FRCM were implemented for 3 cases with the aim of using them as part of the numerical simulation of hybrid FRP-FRCM structures.

Two different prototypes of the hybrid FRP-FRCM superficial structural typology were tested to cover bidimensional and three-dimensional application cases of the proposed technology. A Finite element model was implemented, calibrated, and validated by comparing numerical data with experimental results of the two prototypes.

Following these methodologies, the goals of the research were achieved and the primary results and contributions to the state of the art for each one of the main parts of the work were included as conclusions. Finally, because the findings revealed areas where more research was needed, the thesis concludes with some possible research directions.

7.2 Conclusions

The main conclusion of the research is that it has been possible to characterize the interaction between the different components of the proposed hybrid FRP-FRCM structural system and their contribution to the overall response, as well as the performance of this new type of structures has been demonstrated and simulated with numerical tools. In particular, the following particular conclusions arise:

7.1.1 FRP-FRP connection

Nine GFRP joint specimens with different configurations (bolted joints, adhesive joints, web joints, web and flange joints, and two different angles between profiles) were experimentally tested and numerically simulated. The following conclusions were obtained:

- In general, flange connectors are more effective for larger angles between profiles. These are also more effective when the internal bending moment tends to widen the angle between profiles. It indicates that the mechanical stiffness of flange connectors increased when the loading configuration did not increase the initially existing curvature of the fibers.
- Flange connection increases joint stiffness by 7.6 times but only shows a slight improvement in load-bearing capacity, around 26%, when the failure is controlled by a local profile collapse.
- The inclusion of a flange connection redistributes stresses in the joint, promotes a more uniform joint response, and unloads the web connector as measured by strain gages. A significant part of the applied efforts is supported by the flange, reducing the stresses in the web. Flanges reduced the strain in web over 70% respect to the web-only connected cases.
- Adhesive connections were always associated with fragile debonding failure types in the current research.
- Numerical simulation accurately predicts the mechanical response in terms of force-displacement behavior, showing an average relative error between 10% and 20% when assessing the full testing curves. However, the current model is not able to capture the local web-to-flange shear failure in a direct way, but it may be assessed by comparing the corresponding results with the material strength values.

7.1.2 GFRP-Mesh connection

Four specimens with different connectors (resin connection, bolted connection) were tested and the conclusions obtained are:

- The best type of joint is resin adhesive one, which resisted over 200% more than bolted connection, preventing sliding process and assuring tensile failure of the mesh because of the good chemical compatibility of this joint.
- High temperature did not lead to reduce the resistance of the adhesive joint as previously, indicating that this connection typology may be useful in a wider range of applications than expected.

7.1.3 Mesh-Mortar connection test

Four types of FRCM specimens were tested under tensile configuration. The evidences led to conclude that:

- Glass fiber mesh is more compatible with the high deformability of projected FRCM samples, causing a greater performance in terms of ultimate load-bearing capacity and strain.
- Axton mortar had better results than Sika in terms of tensile strength because of the best penetration of Axton mortar through the fiber mesh. Hence, the possibility of penetrating the fiber mesh is a key factor when producing projected FRCM.
- High temperature exposure had a significant detrimental impact on the performance of FRCM because of its affectation on fiber-matrix interface as long as component materials showed no particular damage. This evidence was not expected an it opens the door to question about the supposed fire-resistant capabilities of FRCM.

7.1.4 Full hybrid panels

Experimental research and the corresponding numerical analysis for two tested specimens of FRP-FRCM hybrid superficial elements were carried out. Failure mode and structural-resistant configurations were analyzed by combining both experimental and numerical data. The experimental evidence matched the results of the implemented numerical model. Finally, the following conclusions may be presented:

- Hybrid FRP-FRCM structures behaved linearly up to initial mortar cracking. After that, FRCM behaved as a plate with no linear response up to the flexural mortar failure. From this point and on, the FRCM behaved as a membrane whose main resistance mechanism was the tensile response of mesh tows up to their strength. A ductile response and high mechanical capacity after mortar cracking were observed. The different structural-resistant

configurations that this novel system shows during its loading process have to be considered when designing structural applications.

- The three-dimensional design of FRP-FRCM hybrid elements contributed to increase the load-bearing capacity of the element. In the same line, increasing the thickness of the mortar matrix of the FRCM plate had a significant impact on the load-bearing capacity of FRP-FRCM hybrid elements.
- The proposed numerical model accurately represented the experimental response. The predicted failure modes were consistent with those experimentally observed in terms of the structural mechanisms involved in resisting the load at the comparison point.

Finally, the novel proposed FRP-FRCM structural system proved to be able to resist large deformation states by maintaining and even increasing the load-bearing capacity through mobilizing different resisting mechanisms including nonlinear bending of the FRCM plate with progressive cracking or the residual membrane response defined by mesh capacity.

7.3 Future lines of investigation

The research also identified prospective future study lines, which will be discussed in this section:

It is necessary to assess the influence of temperature on FRCM composites in exhaustive research on the topic.

Updating the numerical model to consider the complex web-to-flange shear failure using a more detailed material definition is necessary to completely reproduce the response of the mechanical connections between FRP profiles. A possible alternative in this line is including an additional material in the web-to-flange connection area that represents this weaker part of pultruded profiles by replacing the originally defined material. Setting the mechanical properties of this weaker part opens a significant future research line to achieve simplified simulation tools.

References

Al-Sunna, R. *et al.* (2012) 'Deflection behaviour of FRP reinforced concrete beams and slabs: An experimental investigation', *Composites Part B: Engineering*, 43(5), pp. 2125–2134. Available at: https://doi.org/https://doi.org/10.1016/j.compositesb.2012.03.007.

Alocci, C. and Valvo, P.S. (2019) 'Feasibility study of a hybrid FRP-steel cable-stayed pedestrian swing bridge', *Engineering Structures*, 189, pp. 359–372. Available at: https://doi.org/https://doi.org/10.1016/j.engstruct.2019.03.087.

Antonietta, A.M. and Luciano, O. (2002) 'Structural Performances of Concrete Beams with Hybrid (Fiber-Reinforced Polymer-Steel) Reinforcements', *Journal of Composites for Construction*, 6(2), pp. 133–140. Available at: https://doi.org/10.1061/(ASCE)1090-0268(2002)6:2(133).

Ascione, F. *et al.* (2017) 'Strength and stiffness of adhesively bonded GFRP beam-column moment resisting connections', *Composite Structures*, 160, pp. 1248–1257. Available at: https://doi.org/https://doi.org/10.1016/j.compstruct.2016.11.021.

Ascione, F. *et al.* (2018) 'Pseudo-ductile failure of adhesively joined GFRP beam-column connections: An experimental and numerical investigation', *Composite Structures*, 200, pp. 864–873. Available at: https://doi.org/10.1016/j.compstruct.2018.05.104.

Ascione, F., Feo, L. and MacEri, F. (2010) 'On the pin-bearing failure load of GFRP bolted laminates: An experimental analysis on the influence of bolt diameter', *Composites Part B: Engineering*, 41(6), pp. 482–490. Available at: https://doi.org/10.1016/j.compositesb.2010.04.001.

Ascione, L., De Felice, G. and De Santis, S. (2015) 'A qualification method for externally bonded Fibre Reinforced Cementitious Matrix (FRCM) strengthening systems', *Composites Part B: Engineering*, 78(April), pp. 497–506. Available at: https://doi.org/10.1016/j.compositesb.2015.03.079.

Bank, L.C. (2006) *Composites for Construction: Structural Design with FRP Materials*, *New Jersey: John Wiley & Sons, Inc*. Available at: https://doi.org/10.1002/9780470121429.

Bencardino, F., Condello, A. and Ombres, L. (2016) 'Numerical and analytical modeling of concrete beams with steel, FRP and hybrid FRP-steel reinforcements', *Composite Structures*, 140, pp. 53–65. Available at: https://doi.org/https://doi.org/10.1016/j.compstruct.2015.12.045.

Bernat-maso, E. *et al.* (2018) 'Mechanical properties of pre-stressed fabric-reinforced cementitious matrix composite (PFRCM)', *Construction and Building Materials*, 191, pp. 228–241. Available at: https://doi.org/10.1016/j.conbuildmat.2018.09.210.

British Standards Institution (1999) 'Textiles — Tensile properties of fabrics. Part 1: Determination of maximum force and elongation at maximum force using the strip method', *Bs Iso 13934-1* [Preprint].

Brózda, K., Selejdak, J. and Koteš, P. (2018) 'The GFRP profiles as stay-in-place formwork', in *E3S Web of Conferences*. Available at: https://doi.org/10.1051/e3sconf/20184900008.

Carozzi, F.G. *et al.* (2017) 'Experimental investigation of tensile and bond properties of Carbon-FRCM composites for strengthening masonry elements', *Composites Part B: Engineering*, 128, pp. 100–119. Available at: https://doi.org/10.1016/j.compositesb.2017.06.018.

Carozzi, F.G., Milani, G. and Poggi, C. (2014) 'Mechanical properties and numerical modeling of Fabric Reinforced Cementitious Matrix (FRCM) systems for strengthening of masonry structures', *Composite*

Structures, 107, pp. 711–725. Available at: https://doi.org/10.1016/j.compstruct.2013.08.026.

Carozzi, F.G. and Poggi, C. (2015) 'Mechanical properties and debonding strength of Fabric Reinforced Cementitious Matrix (FRCM) systems for masonry strengthening', *Composites Part B: Engineering*, 70, pp. 215–230. Available at: https://doi.org/10.1016/j.compositesb.2014.10.056.

de Carvalho Bello, C.B. *et al.* (2019) 'Experimental tests for the characterization of sisal fiber reinforced cementitious matrix for strengthening masonry structures', *Construction and Building Materials* [Preprint]. Available at: https://doi.org/10.1016/j.conbuildmat.2019.05.168.

Casacci, S. *et al.* (2019) 'Shear strengthening of masonry wallettes resorting to structural repointing and FRCM composites', *Construction and Building Materials* [Preprint]. Available at: https://doi.org/10.1016/j.conbuildmat.2019.02.044.

CEN 1999 (1999) 'EN 1015-11: Methods of test for mortar for masonry - Part 11: Determination of flexural and compressive strength of hardened mortar', *European Committee for standardization* [Preprint].

Chellapandian, M. and Suriya Prakash, S. (2021) 'Applications of Fabric Reinforced Cementitious Mortar (FRCM) in Structural Strengthening', in S.B. Singh, M.V.R. Sivasubramanian, and H. Chawla (eds) *Emerging Trends of Advanced Composite Materials in Structural Applications*. Singapore: Springer Singapore, pp. 201–233. Available at: https://doi.org/10.1007/978-981-16-1688-4_9.

CNR-DT (2018) 'Guide for the Design and CNR-DT 2015/2018. Construction of Externally Bonded Fibre Reinforced Inorganic Matrix Systems for Strengthening Existing Structures'. Rome, Italy.

Committee AEN/CTN 83 (2006) 'UNE-EN 1504-3:2006. Products and systems for the protection and repair of concrete structures - Definitions, requirements, quality control and evaluation of conformity - Part 3: Structural and non-structural repair'. Madrid: AENOR.

Corradi, M. *et al.* (2014) 'Shear strengthening of wall panels through jacketing with cement mortar reinforced by GFRP grids', *Composites Part B: Engineering*, 64, pp. 33–42. Available at: https://doi.org/10.1016/j.compositesb.2014.03.022.

D'Ambrisi, A., Feo, L. and Focacci, F. (2013a) 'Experimental analysis on bond between PBO-FRCM strengthening materials and concrete', *Composites Part B: Engineering*, 44(1), pp. 524–532. Available at: https://doi.org/https://doi.org/10.1016/j.compositesb.2012.03.011.

D'Ambrisi, A., Feo, L. and Focacci, F. (2013b) 'Experimental and analytical investigation on bond between Carbon-FRCM materials and masonry', *Composites Part B: Engineering*, 46, pp. 15–20. Available at: https://doi.org/https://doi.org/10.1016/j.compositesb.2012.10.018.

D'Antino, T. *et al.* (2014) 'Matrix–fiber bond behavior in PBO FRCM composites: A fracture mechanics approach', *Engineering Fracture Mechanics*, 117, pp. 94–111. Available at: https://doi.org/10.1016/j.engfracmech.2014.01.011.

Dalalbashi, A. *et al.* (2018) 'Fiber-to-mortar bond behavior in TRM composites : Effect of embedded length and fiber configuration', 152, pp. 43–57. Available at: https://doi.org/10.1016/j.compositesb.2018.06.014.

Di, J., Cao, L. and Han, J. (2020) 'Experimental study on the shear behavior of GFRP-concrete composite beam connections', *Materials*, 13(5). Available at: https://doi.org/10.3390/ma13051067.

De Domenico, D. *et al.* (2020) 'Bond behavior and ultimate capacity of notched concrete beams with

externally-bonded FRP and PBO-FRCM systems under different environmental conditions', *Construction and Building Materials* [Preprint]. Available at: https://doi.org/10.1016/j.conbuildmat.2020.121208.

Donnini, J., Spagnuolo, S. and Corinaldesi, V. (2019) 'A comparison between the use of FRP, FRCM and HPM for concrete confinement', *Composites Part B: Engineering*, 160, pp. 586–594. Available at: https://doi.org/https://doi.org/10.1016/j.compositesb.2018.12.111.

Ebead, U. and El-Sherif, H.E. (2019) 'Near surface embedded-FRCM for flexural strengthening of reinforced concrete beams', *Construction and Building Materials* [Preprint]. Available at: https://doi.org/10.1016/j.conbuildmat.2019.01.145.

Ebead, U. and Younis, A. (2019) 'Pull-off characterization of FRCM/Concrete interface', *Composites Part B: Engineering* [Preprint]. Available at: https://doi.org/10.1016/j.compositesb.2019.02.025.

Estevan, L. *et al.* (2020) 'Stone masonry confinement with FRP and FRCM composites', *Construction and Building Materials* [Preprint]. Available at: https://doi.org/10.1016/j.conbuildmat.2019.117612.

Falliano, D. *et al.* (2019) 'Improving the flexural capacity of extrudable foamed concrete with glass- fiber bi-directional grid reinforcement : An experimental study', *Composite Structures*, 209, pp. 45–59. Available at: https://doi.org/10.1016/j.compstruct.2018.10.092.

Feo, L., Marra, G. and Mosallam, A.S. (2012) 'Stress analysis of multi-bolted joints for FRP pultruded composite structures', *Composite Structures* [Preprint]. Available at: https://doi.org/10.1016/j.compstruct.2012.06.017.

FIDIA global services (2010) 'FIDBASALT GRID 300 C95'. Perugia: FIDIA s.r.l.

Francesca, F. and Salvatore, R. (2016) 'Structural Behavior of All-FRP Beam-Column Plate-Bolted Joints', *Journal of Composites for Construction*, 20(4), p. 4016004. Available at: https://doi.org/10.1061/(ASCE)CC.1943-5614.0000667.

Fu, M. and Mallick, P.K. (2001) 'Fatigue of hybrid (adhesive/bolted) joints in SRIM composites', *International Journal of Adhesion and Adhesives*, 21(2), pp. 145–159. Available at: https://doi.org/https://doi.org/10.1016/S0143-7496(00)00047-6.

Ge, W. *et al.* (2015) 'Flexural behaviors of hybrid concrete beams reinforced with BFRP bars and steel bars', *Construction and Building Materials*, 87, pp. 28–37. Available at: https://doi.org/https://doi.org/10.1016/j.conbuildmat.2015.03.113.

Gong, J., Zou, X. and Xia, P. (2019) 'applied sciences Experimental Investigation of the Natural Bonding Strength between Stay-In-Place Form and Concrete in FRP-Concrete Decks / Beams', pp. 1–16. Available at: https://doi.org/10.3390/app9050913.

Hall, J.E. and Mottram, J.T. (1998) 'Combined FRP reinforcement and permanent formwork for concrete members', *Journal of Composites for Construction* [Preprint]. Available at: https://doi.org/10.1061/(ASCE)1090-0268(1998)2:2(78).

Hart-Smith, L. (1987) 'Design of adhesively bonded joints', *Elsevier Applied Science Publishers Ltd, Joining Fibre-Reinforced Plastics*, pp. 271–311.

Hart-Smith, L.J. (1985) 'Bonded-bolted composite joints', *Journal of Aircraft*, 22(11), pp. 993–1000. Available at: https://doi.org/10.2514/3.45237.

Hawileh, R.A. (2015) 'Finite element modeling of reinforced concrete beams with a hybrid combination

of steel and aramid reinforcement', *Materials & Design (1980-2015)*, 65, pp. 831–839. Available at: https://doi.org/https://doi.org/10.1016/j.matdes.2014.10.004.

Henkel - Loctite (2020) 'Technical Data Sheet Hysol 3425'. Montornès del Vallès: LOCTITE. Available at: https://www.henkel-adhesives.com/es/es/producto/structural-adhesives/loctite_ea_3425.html.

Huang, L. *et al.* (2018) 'Flexural behavior of U-shape FRP profile-RC composite beams with inner GFRP tube confinement at concrete compression zone', *Composite Structures* [Preprint]. Available at: https://doi.org/10.1016/j.compstruct.2017.10.029.

Hyer, M.W., Klang, E.C. and Cooper, D.E. (1987) 'The Effects of Pin Elasticity, Clearance, and Friction on the Stresses in a Pin-Loaded Orthotropic Plate', *Journal of Composite Materials*, 21(3). Available at: https://doi.org/10.1177/002199838702100301.

ICC Evaluation Service Inc. (2016) 'AC434. Acceptance Criteria for Masonry and Concrete Strengthening Using Fabric-reinforced Cementitious Matrix (FRCM) Composite Systems'. Indiana. Available at: https://icc-es.org/acceptance-criteria/ac434/.

Kara, I.F., Ashour, A.F. and Köroğlu, M.A. (2015) 'Flexural behavior of hybrid FRP/steel reinforced concrete beams', *Composite Structures*, 129, pp. 111–121. Available at: https://doi.org/https://doi.org/10.1016/j.compstruct.2015.03.073.

Kelly, G. (2005) 'Load transfer in hybrid (bonded/bolted) composite single-lap joints', *Composite Structures*, 69(1), pp. 35–43. Available at: https://doi.org/10.1016/j.compstruct.2004.04.016.

Kent, D.C. and Park, R. (1971) 'Flexural Members with Confined Concrete', *Journal of the Structural Division*, 97(7), pp. 1969–1990. Available at: https://doi.org/10.1061/JSDEAG.0002957.

Khani, M.S. (2015) 'Connections in structural FRP', *Master of Science Thesis, Chalmers University of Technology, Göteborg, Sweden*, pp. 1–85.

Khodaii, A., Fallah, S. and Moghadas, F. (2008) 'Geotextiles and Geomembranes Effects of geosynthetics on reduction of reflection cracking in asphalt overlays', 27, pp. 1–8. Available at: https://doi.org/10.1016/j.geotexmem.2008.05.007.

Kim, J. *et al.* (2021) 'An experimental study on the mechanical behaviour of bonded and hybrid bonded-bolted composite joints using digital image correlation (DIC) technique', *Composite Structures*, 276, p. 114544. Available at: https://doi.org/https://doi.org/10.1016/j.compstruct.2021.114544.

Lau, D. and Pam, H.J. (2010) 'Experimental study of hybrid FRP reinforced concrete beams', *Engineering Structures*, 32(12), pp. 3857–3865. Available at: https://doi.org/https://doi.org/10.1016/j.engstruct.2010.08.028.

Lee, Y.G., Choi, E. and Yoon, S.J. (2015) 'Effect of geometric parameters on the mechanical behavior of PFRP single bolted connection', *Composites Part B: Engineering*, 75, pp. 1–10. Available at: https://doi.org/10.1016/j.compositesb.2015.01.015.

Liu, L. *et al.* (2021) 'Resistance and ductility of FRP composite hybrid joints', *Composite Structures* [Preprint]. Available at: https://doi.org/10.1016/j.compstruct.2020.113001.

Mahboob, A. *et al.* (2021a) 'Experimental and Numerical Study of Shear Interface Response of Hybrid Thin CFRP–Concrete Slabs', *Materials*, 14(18), p. 5184. Available at: https://doi.org/10.3390/ma14185184.

Mahboob, A. *et al.* (2021b) 'Flexible Fiber Fabric for FRP–Concrete Connection of Thin Hybrid Slabs', *Polymers*, 13(17), p. 2862. Available at: https://doi.org/10.3390/polym13172862.

Manalo, A.C. *et al.* (2012) 'Composite behaviour of a hybrid FRP bridge girder and concrete deck', in *Advances in Structural Engineering*. Available at: https://doi.org/10.1260/1369-4332.15.4.589.

MAPEI Spain (2018) 'Mapegrid G 220'. Santa Perpetua de Mogoda, Spain: MAPEI Spain S.A., pp. 1–4. Available at: https://www.mapei.com/es/es/productos-y-soluciones/lista-de-productos/detalles-del-producto/mapegrid-g-220.

Martins, D. *et al.* (2017) 'Development of a novel beam-to-column connection system for pultruded GFRP tubular profiles', *Composite Structures* [Preprint]. Available at: https://doi.org/10.1016/j.compstruct.2017.03.049.

Master Builders Solutions España (2021a) *MasterBrace ADH 4000, MasterBrace ADH 4000 - Ficha técnica*. Available at: https://assets.master-builders-solutions.com/es-es/masterbrace-adh-4000.pdf (Accessed: 3 February 2022).

Master Builders Solutions España (2021b) *MasterBrace P 3500, MasterBrace P 3500 - ficha tecnica*. Cornellà de Llobregat. Available at: https://assets.master-builders-solutions.com/es-es/masterbrace-p-3500.pdf (Accessed: 3 February 2022).

Meng, W. and Khayat, K.H. (2016) 'Experimental and Numerical Studies on Flexural Behavior of Ultrahigh-Performance Concrete Panels Reinforced with Embedded Glass Fiber-Reinforced Polymer Grids', *Transportation Research Record*, 2592(1), pp. 38–44. Available at: https://doi.org/10.3141/2592-05.

Mercedes, L., Bernat-maso, E. and Gil, L. (2020) 'In-plane cyclic loading of masonry walls strengthened by vegetal-fabric- reinforced cementitious matrix (FRCM) composites', *Engineering Structures*, 221(June), p. 111097. Available at: https://doi.org/10.1016/j.engstruct.2020.111097.

Mercedes, L., Bernat-Maso, E. and Gil, L. (2020) 'In-plane cyclic loading of masonry walls strengthened by vegetal-fabric-reinforced cementitious matrix (FRCM) composites', *Engineering Structures*, 221, p. 111097. Available at: https://doi.org/10.1016/j.engstruct.2020.111097.

Ministerio de Fomento (2012) 'Instrucción de Acero Estructural', *https://www.fomento.gob.es/AZ.BBMF.Web/documentacion/pdf/RE2360.pdf*, pp. 1–658.

Mosallam, A.S. (2011) 'Design guide for FRP composite connections', *ASCE Manuals and Reports on Engineering Practice* [Preprint]. Available at: https://doi.org/10.1061/9780784406120.

Mottram, J.T., Lutz, C. and Dunscombe, G.C. (2004) 'Aspects On The Behaviour Of Bolted Joints For Pultruded Fibre Reinforced Polymer Profiles', *Advanced Polymer Composites for Structural Applications in Construction: ACIC 2004*, pp. 384–391. Available at: https://doi.org/10.1016/B978-1-85573-736-5.50043-1.

Mottram, J.T. and Zheng, Y. (1999) 'Further Tests of Beam-to-Column Connections for Pultruded Frames: Flange-Cleated', *Journal of Composites for Construction*, 3(3), pp. 108–116. Available at: https://doi.org/10.1061/(ASCE)1090-0268(1999)3:3(108).

Napoli, A. and Realfonzo, R. (2020) 'Compressive strength of concrete confined with fabric reinforced cementitious matrix (FRCM): Analytical models', *Composites Part C: Open Access*, 2(June), p. 100032. Available at: https://doi.org/10.1016/j.jcomc.2020.100032.

Neagoe, C.A. (2016) *Structural performance of FRP-concrete hybrid beams with flexible shear connection*. Universitat Politècnica de Catalunya, BarcelonaTECH.

Neagoe, C.A., Gil, L. and Pérez, M.A. (2015) 'Experimental study of GFRP-concrete hybrid beams with low degree of shear connection', *CONSTRUCTION & BUILDING MATERIALS*, 101, pp. 141–151. Available at: https://doi.org/10.1016/j.conbuildmat.2015.10.024.

Nguyen, H., Mutsuyoshi, H. and Zatar, W. (2014) 'Push-out tests for shear connections between UHPFRC slabs and FRP girder', *COMPOSITE STRUCTURE*, 118, pp. 528–547. Available at: https://doi.org/10.1016/j.compstruct.2014.08.003.

Nordin, H. and Täljsten, B. (2004) 'Testing of hybrid FRP composite beams in bending', *Composites Part B: Engineering* [Preprint]. Available at: https://doi.org/10.1016/j.compositesb.2003.08.010.

Olivito, R.S., Codispoti, R. and Cevallos, O.A. (2016) 'Bond behavior of Flax-FRCM and PBO-FRCM composites applied on clay bricks: Experimental and theoretical study', *Composite Structures* [Preprint]. Available at: https://doi.org/10.1016/j.compstruct.2016.03.004.

PermaStruct (2020) 'PermaStruct® FRP Structural Design Guide', *https://www.permacomposites.com/wp-content/uploads/2021/06/PermaStruct-FRP-Structural-Design-Guide-V.0320.pdf*, pp. 1–54.

Petrů, M. and Novák, O. (2018) 'FEM Analysis of Mechanical and Structural Properties of Long Fiber-Reinforced Composites', in *Finite Element Method - Simulation, Numerical Analysis and Solution Techniques*. InTech. Available at: https://doi.org/10.5772/intechopen.71881.

PROPAMSA S.A.U. (2020) 'PASTA NIVELADORA 10 mm'. Sant Vicenç dels Horts, Spain: AXTON.

Qureshi, J. (2022) 'A Review of Fibre Reinforced Polymer Structures', *Fibers*, 10(3), p. 27. Available at: https://doi.org/10.3390/fib10030027.

Qureshi, J. and Mottram, J.T. (2013) 'Behaviour of pultruded beam-to-column joints using steel web cleats', *Thin-Walled Structures*, 73, pp. 48–56. Available at: https://doi.org/10.1016/j.tws.2013.06.019.

Rajchel, M., Kulpa, M. and Siwowski, T. (2020) 'Experimental Study on a Novel Shear Connection System for FRP-Concrete Hybrid Bridge Girder', *Materials*, 13(9). Available at: https://doi.org/10.3390/ma13092045.

Reichenbach, S. *et al.* (2021) 'A review on embedded fibre-reinforced polymer reinforcement in structural concrete in Europe', *Construction and Building Materials*, 307, p. 124946. Available at: https://doi.org/10.1016/j.conbuildmat.2021.124946.

Ruredil (2013) 'X Mesh C10'. Milano: Ruredil S.P.A.

Si Larbi, A. *et al.* (2007) 'Static behaviour of steel concrete beam connected by bonding', *Engineering Structures* [Preprint]. Available at: https://doi.org/10.1016/j.engstruct.2006.06.015.

SIKA AG (2018) 'Sika MonoTop -612'. Alcobendas: Sika AG. Available at: https://esp.sika.com/content/dam/dms/es01/i/sika_monotop_-612.pdf.

Smith, S.J., Parsons, I.D. and Hjelmstad, K.D. (1999) 'Experimental Comparisons of Connections for GFRP Pultruded Frames', *Journal of Composites for Construction*, 3(1), pp. 20–26. Available at: https://doi.org/10.1061/(ASCE)1090-0268(1999)3:1(20).

Sneed, L. (2013) *Fiber Reinforced Cementitious Matrix (FRCM) Composites for Reinforced Concrete Strengthening*.

Turvey, G.J. and Wang, P. (2008) 'An FE analysis of the stresses in pultruded GRP single-bolt tension joints and their implications for joint design', *Computers and Structures* [Preprint]. Available at: https://doi.org/10.1016/j.compstruc.2007.04.026.

Vallée, T. *et al.* (2013) 'Dimensioning method for bolted, adhesively bonded, and hybrid joints involving Fibre-Reinforced-Polymers', *Composites Part B: Engineering*, 46, pp. 179–187. Available at: https://doi.org/https://doi.org/10.1016/j.compositesb.2012.09.074.

Vedernikov, A. *et al.* (2020) 'Pultruded materials and structures: A review', *Journal of Composite Materials*, 54(26), pp. 4081–4117. Available at: https://doi.org/10.1177/0021998320922894.

Wang, J. *et al.* (2020) 'Experimental and numerical investigation of mortar and ITZ parameters in meso-scale models of concrete', *Theoretical and Applied Fracture Mechanics*, 109, p. 102722. Available at: https://doi.org/https://doi.org/10.1016/j.tafmec.2020.102722.

Weitzenböck, J. and McGeorge, D. (2011) 'Science and Technology of Bolt-Adhesive Joints', in *Hybrid Adhesive Joints*, pp. 177–199. Available at: https://doi.org/10.1007/8611_2011_54.

Wenjun, Q., Xiaoliang, Z. and Haiqun, H. (2009) 'Flexural Behavior of Concrete Beams Reinforced with Hybrid (GFRP and Steel) Bars', *Journal of Composites for Construction*, 13(5), pp. 350–359. Available at: https://doi.org/10.1061/(ASCE)CC.1943-5614.0000035.

Van Wingerde, A.M., Van Delft, D.R.V. and Knudsen, E.S. (2003) 'Fatigue behaviour of bolted connections in pultruded FRP profiles', *Plastics, Rubber and Composites*, 32(2), pp. 71–76. Available at: https://doi.org/10.1179/146580103225009103.

Wood, J. (1996) 'Structural design of polymer composites eurocomp design code and handbook', *Composite Structures* [Preprint]. Available at: https://doi.org/10.1016/s0263-8223(96)00058-x.

Ye, Y.-Y. *et al.* (2021) 'Recyclable LRS FRP composites for engineering structures: Current status and future opportunities', *Composites Part B: Engineering*, 212, p. 108689. Available at: https://doi.org/10.1016/j.compositesb.2021.108689.

Younis, A., Ebead, U. and Shrestha, K.C. (2017) 'Different FRCM systems for shear-strengthening of reinforced concrete beams', *Construction and Building Materials* [Preprint]. Available at: https://doi.org/10.1016/j.conbuildmat.2017.07.132.

Yuan, J. (2017) 'Flexural behaviour of composite beams reinforced with GFRP I- section Doctor of Philosophy From University of Wollongong , Australia'.

Zhang, Y., Vassilopoulos, A.P. and Keller, T. (2009) 'Environmental effects on fatigue behavior of adhesively-bonded pultruded structural joints', *Composites Science and Technology*, 69(7–8), pp. 1022–1028. Available at: https://doi.org/10.1016/j.compscitech.2009.01.024.

Zhang, Z.J., Bai, Y. and Xiao, X. (2018) 'Bonded Sleeve Connections for Joining Tubular Glass Fiber–Reinforced Polymer Beams and Columns: Experimental and Numerical Studies', *Journal of Composites for Construction*, 22(4), p. 04018019. Available at: https://doi.org/10.1061/(ASCE)CC.1943-5614.0000853.

Zhou, B. *et al.* (2020) 'Modeling of tensile behavior of hybrid GFRP-steel reinforced concrete chords', *Composite Structures*, 236, p. 111853. Available at:

https://doi.org/https://doi.org/10.1016/j.compstruct.2019.111853.

Zhou, B. *et al.* (2021) 'A general numerical model for predicting the flexural behavior of hybrid FRP-steel reinforced concrete beams', *Engineering Structures*, 239, p. 112293. Available at: https://doi.org/https://doi.org/10.1016/j.engstruct.2021.112293.

Zoghi, M. (2013) *The international handbook of FRP composites in civil engineering, Assessment*. CRC Press.

Zou, X. *et al.* (2021) 'A review on FRP-concrete hybrid sections for bridge applications', *Composite Structures*, 262, p. 113336. Available at: https://doi.org/https://doi.org/10.1016/j.compstruct.2020.113336.

Zou, X., Feng, P. and Wang, J. (2018) 'Bolted Shear Connection of FRP-Concrete Hybrid Beams', *Journal of Composites for Construction*, 22(3). Available at: https://doi.org/10.1061/(ASCE)CC.1943-5614.0000845.